CHARACTERISATION AND STATIC BEHAVIOUR OF THE DMLS Ti-6Al-4V FOR BIO-MEDICAL APPLICATIONS

MAKHABO KHABISO ELLEN RAMOSOEU

20203047

Dissertation Submitted In Fulfilment of the Requirements for the Degree

MAGISTER TECHNOLOGIAE: ENGINEERING: MECHANICAL

in the

Department of Mechanical and Mechatronics Engineering

Faculty of Engineering & Information Technology

at the

Central University of Technology, Free State

BLOEMFONTEIN

Supervisor: Mr G. Booysen, M-Tech

Co-supervisor: Mr T. N. Ngonda, M-Eng

February 2015

DECLARATION OF INDEPENDENT WORK

DECLARATION WITH REGARD TO INDEPENDENT WORK

I, MAKHABO KHABISO ELLEN RAMOSOEU, identity number 7504021263086 and student number 20203047, do hereby declare that this research project submitted to the Central University of Technology, Free State (CUT,FS) for the MAGISTER TECHNOLOGIAE DEGREE ENGINEERING: MECHANICAL, is my own independent work; and complies with the code of Academic integrity, as well as other relevant policies, procedures, rules and regulations of the Central University of Technology, Free State; and has not been submitted previously to any institution by myself or any other person in fulfilment of the requirements for the attainment of any qualification.

SIGNATURE OF STUDENT.....DATE.....

ACKNOWLEDGEMENTS

I am grateful to my supervisors, Mr G. Booysen of Central University of Technology, Free State (CUT, FS) and Mr T. N. Ngonda of Cape Peninsula University of Technology (CPUT) for their valuable suggestions and relentless efforts which have made this work possible. I would like to express deep gratitude and appreciation to the following institutions and people who assisted me in one way or another during the course of my research; The Centre of Rapid Prototyping and Manufacturing (CRPM) for supplying the titanium test specimen, especially Mr J. Els and Mr D. Mosimanyane.

I acknowledge the assistance rendered by Dr H. Chikwanda and the staff of the Metal and Metal Processing Department at the Council for Scientific and Industrial Research (CSIR). Ms G. Lesejane, Dr C. Machio and Dr S. Chikosha are acknowledged for their assistance with the metallographic analysis and Mr C. McDuling for his assistance in mechanical testing. It has been a great pleasure collaborating with the CSIR team.

I thank the staff of the School of Mechanical Engineering at CUT, FS for their constant words of encouragement, as well as their companionship and contributions.

I acknowledge the support of the following institutions for providing funding: Light Metals Development Network (LMDN) and CUT, FS for funding the general needs of the research; CRPM for subsidising the manufacturing of specimens and the mechanical tests costs, while the CSIR subsidised the metallographic analysis costs.

To my family, especially my husband, Lebohang, thank you for your love, prayers and constant support during the course of this hard work. I would also like to thank my son, Relebohile for his understanding and encouragement throughout this research project.

The greatest of all is my thanksgiving to God Almighty for giving me the strength and perseverance throughout the course of this study.

ABSTRACT

The Centre for Rapid Prototyping and Manufacturing (CRPM) at the Central University of Technology, Free State (CUT) manufactures implants using Electro Optical Systems (EOS) titanium Ti-6Al-4V alloy powder (further referred to as EOS Ti64 powder) by means of Direct Metal Laser Sintering (DMLS) process on the EOSINT M 270 machine. For this reason, there is a need to characterise and acquire knowledge of the basic properties of direct metal laser sintered EOS titanium Ti-6Al-4V alloy samples (further referred to as DMLS Ti64 samples) under static tensile loading in order to provide the CRPM with engineering design data. The first objective of this Master's study is to acquire the characteristics of EOS Ti64 powder in order to ascertain its suitability in the DMLS process. Secondly, the study aims to assess tensile properties and elastic constants of DMLS Ti64 samples produced from the set process parameters of EOSINT M 270 machine. Thirdly, it is to investigate microstructures of DMLS Ti64 samples subjected to different heat treatment techniques which will eventually assist in the determination of a suitable heat treatment technique that will yield higher ductility. Finally, the study aims to validate the static behaviour of DMLS Ti64 samples subjected to the static tensile loading up to a yield point in order to determine failure due to yielding.

The samples were manufactured at CRPM Bloemfontein. The metallographic examinations, heat treatment and the determination of mechanical properties were done at the CSIR in Pretoria. Optical Microscope (OM) and Scanning Electron

Microscope (SEM) were used to determine microstructures of DMLS Ti64 samples while Energy Dispersive X-Ray (EDX) analyses were performed using SEM. The samples were heat treated at temperatures of 700, 1000 and 1100°C respectively, and subsequently either cooled with the furnace, air or were water quenched. The mechanical property tests included tensile, hardness and determination of elastic constants. The static behaviour of DMLS Ti64 samples under static tensile load up to a yield point was predicted and verified using ABAQUS^{TM} Finite Element Analysis (FEA). The stress-strain curves from ABAQUS^{TM} were interpreted using MDSolid program. The point of interest was Von Mises yield stress at 0.2% offset, in order to determine failure due to yielding.

EOS Ti64 powder particles were spherical in shape and the alpha and alpha+beta phases were identified. As-laser sintered samples possess a very fine and uniform alpha case with islands of martensitic plates; samples were brittle and showed low levels of ductility with an average elongation of 2.6% and an area reduction of 3.51%. Ultrasonic test results showed that DMLS Ti64 samples have Young's modulus of 115 GPa, Shear modulus of 43 GP, a bulk modulus of 109 GPa and Poisson's ratio of 0,323 while the density was 4.4 g/cm^3. Slow cooling of DMLS Ti64 samples from 1000 and 1100^{o}C resulted in a microstructure constituted more by the alpha phase of lower hardness than those from 700^{o}C and as-laser sintered samples. High hardness was obtained by water quenching. The water quenched samples showed martensitic transformation and high hardness when compared to furnace cooled samples. Beta annealing tailored a microstructure of as-laser sintered samples into a lamellar structure

with different lath sizes as per cooling rate. Beta annealing improved ductility levels up to 12.67% elongation for samples furnace cooled for 4 hours and even higher to 18.11% for samples furnace cooled for 34 hours, while area reduction increased to 25.94% and 33.39%, respectively. Beta annealing conversely reduced yield strength by 19.89% and ultimate tensile strength was reduced by 23.66%.

The calculated maximum Von Mises stresses found were similar to the FEA interpreted results. The average percentage error, without the stress concentration factor, was approximately 8.29%; with the stress concentration factor included, it was 0.07%. The small reaction forces induced in both x-axis and z-axis contributed to this error of 0.07% between the calculations and ABAQUS^{TM} FEA results. Samples that were not heat treated fell outside the Von Mises criterion and failed due to yielding. This justified the brittleness found in the tensile test results where elongation and area reduction were 2.6% and 3.51% respectively. However, all samples that were heat treated fell within the Von Mises criterion.

The objectives of this study were achieved; the mechanical properties were similar to those of standard specification for wrought annealed Ti-6Al-4V alloy for surgical implant applications and EOS GmbH manufacturer's material data sheet. DMLS Ti64 samples must be beta annealed in order to attain higher levels of ductility. A recommendation was made to further investigate the effect of heat treatment on the other mechanical properties. Furthermore, detailed results of basic properties of DMLS Ti64 samples are provided in the appendices in chart format and were written on a CD disc.

THE CD DISC IS HANDED IN TOGETHER WITH THE DISSERTATION BOOK.

Key words: EOS Ti64 powder, DMLS Ti64 samples, heat treatment, metallographic examinations, ductility, 0.2% proof Von Mises yield stress, ABAQUS^{TM} FEA.

TABLE OF CONTENTS

LIST OF FIGURES

LIST OF TABLES

LIST OF EQUATIONS

GLOSSARY

3D-CAD	Three Dimensional-Computer Aided Drawing
AC	Air Cooled
BCC	Body Centred Cubic
CPUT	Cape Peninsula University of Technology
CRPM	Centre for Rapid Prototyping and Manufacturing
CSIR	Council for Scientific and Industrial Research
CUT, FS	Central University of Technology, Free State
DMLS	Direct Metal Laser Sintering
EOS	Electro Optical Systems
FC	Furnace Cooled
FEA	Finite Element Analysis
FE-SEM	Field-Emission Scanning Electron Microscope
HCP	Hexagonal Close-Packed
HV	Hardness Vickers
OM	Optical Microscope
RBED	Robinson Backscatter Electron Detector
SEM	Scanning Electron Microscope
SEM-EDX	Scanning Electron Microscope-Energy Dispersive X-Ray
WQ	Water Quenched
XRD	X-Ray Diffraction

NOMENCLATURE

(Symbols are defined in the sequence as in which they appear in the text)

Ti	Titanium
Al	Aluminium
V	Vanadium
α	Alpha
β	Beta
α + β	Alpha + Beta
N	Nitrogen
O	Oxygen
H	Hydrogen
Fe	Iron
P	Density
V	Poisson's Ratio
G	Shear Modulus
E	Young's Modulus
K	Bulk Modulus
σ_y	Yield Stress
σ_o	Materials Constant for the Starting Stress for the Dislocation Movement (or the Resistance of the Lattice to Dislocation Motion)
K	Strengthening Coefficient (a Constant Unique to Each Material)
d_g	Average Grain Diameter

$\rho_{material}$	Density of the Material
$V_{material}$	Volume of Material
M_{dry}	Measured mass dry
ΔL	Displacement
L_o	Initial Length of the Specimen
F	Force
A_o	Initial Area of the Specimen
σ	Engineering Stress
ε	Engineering Strain
σ_{true}	True Stress
ε_{true}	True Strain
$\varepsilon_{plastic}$	Plastic Strain
$\sigma_{vm(normal)}$	Normal Von Mises Stress
$\sigma_{vm(maximum)}$	Maximum Von Mises Stress
K_t	Stress Concentration Factor
D	Large Diameter of Circular bar
d	Small Diameter of Circular bar
R	Fillet Radius of Circular bar

Chapter 1. INTRODUCTION

1.1 Background

Direct Metal Laser Sintering (DMLS) is one of the Additive Manufacturing (AM) technologies developed by EOS GmbH of Munich, Germany. A new EOSINT M 270 sintering machine was introduced in 2003. The EOSINT M 270 machine is based on a solid-state, dual focus 200 Watt ytterbium fibre laser. It has the scan speed of up to 7.0 metres per second, and the available focus diameter of 100-500 micro-metres. The layer thickness depends on the material and ranges between 20-60 micro-metres. (Hänninen 2002: 33-36; Simachi & Pohl 2003: 120-123; EOS Gmbh-Material Data Sheet 2011: 1-4).

The CRPM at Bloemfontein received the EOSINT M 270 sintering machine in May 2007. The CRPM mainly uses this machine to manufacture titanium products for the medical industry. DMLS technology enables surgical and medical prostheses to be manufactured directly from Three Dimensional-Computer Aided Drawing (3D-CAD) designs (Ghany & Moustafa 2006: 88-90; Ning et al. 2004: 185-190).

Medical science has developed the ability to implant devices into human bodies to replace fractured, damaged or degenerated bones. The artificial device or part is known as the bone prosthesis. In medical applications, bone prostheses are

generalised and made for any individual; thus, many implants are being manufactured in mass production using conventional manufacturing technologies, such as forging, casting and machining. However, the disadvantage of generalising the shape is that the human anatomy is not uniform. Some individuals require customised shapes for their implants, especially on the complex topographies such as the bones in the knee, elbow or hip joints (Ghany & Moustafa 2006: 88-90; Mahesh et al. 2004: 124-131; Ning et al. 2004: 185-190).

Using conventional manufacturing technologies to produce an individual prosthesis is time consuming, expensive and complex. These methods require artisans with extraordinary skills. The DMLS method can also be used in manufacturing bone replacement prostheses. The DMLS process is very advantageous as it enables the designer to produce part geometries that have complex shapes and allows for the fabrication of parts with a high degree of geometric freedom, high individuality, as well as few processing steps (Bertol et al. 2010: 3982–3986; Ghany & Moustafa 2006: 88-90; Mahesh et al. 2004: 124,131; Ning et al. 2004: 185-190). The DMLS process produces parts directly from 3D CAD data; no tooling is required. This process can combine what would have been several parts into one, thus saving manufacturing costs, and reducing assembly time. DMLS process offers more potential in the manufacturing of implants. Conversely, the parts produced by this process on the EOSINT M 270 machine showed lower levels of ductility than required. Moreover, implants need to indicate or show a warning that it will break when subjected to load; for this reason the yield point of the material must be considered as an important design

factor. At present, the DMLS process is suitable for low volume production. More work still has to be done to investigate the process quality, capability and the repeatability of parts. Industry needs to be convinced that the DMLS process can produce functional parts; thus, investigating the fundamental behaviour of parts produced by DMLS technology is a prerequisite. Therefore, this research focuses on investigating the basic mechanical properties and microstructures of DMLS Ti64 samples manufactured by DMLS process on the EOSINT M 270 machine. The study will include the alteration of ductility.

1.2 The Aim of the Project

The main purpose of this Master's engineering project is to acquire knowledge of the basic properties of DMLS Ti64 samples and to provide CRPM with engineering design data that meet the required standards.

The objectives of these projects are as follows:

1. To acquire the characteristics of EOS Ti64 powder in order to ascertain its suitability in the DMLS process.
2. To assess tensile properties and elastic constants of DMLS Ti64 samples produced from the set process parameters of the EOSINT M 270 machine.
3. To investigate metallographic examination of DMLS Ti64 samples subjected to different heat treatment techniques which will eventually determine a suitable heat treatment technique that will yield higher ductility.

4. Finally, to validate the static behaviour of DMLS Ti64 samples subjected to the static tensile loading up to a yield point in order to determine failure due to yielding. The outcomes of this prediction will be used to verify the ductility found in both as-laser sintered and in all sets of heat treated samples.

1.3 The Scope of the Project

The research work will firstly include acquiring the characteristics of EOS Ti64 powder; exploring different heat treatments thereafter; determining the hardness values and then a metallographic examination of DMLS Ti64 samples, which will later assist in the tailoring of the desired tensile properties. In addition, the fundamental characteristics of DMLS Ti64 samples under static tensile loading and the investigation of elastic constants will also be done; secondly, based on the outcomes of the first investigations, the heat treatment will be done together with a tensile test and metallographic examination. Thirdly, predicting the static behaviour of the DMLS Ti64 samples under static tensile load up to a yield point using the ABAQUS^{TM} Finite Element Analysis (FEA) program, will be conducted.

1.4 Research Methodology

The research has been conducted as follows:

1. The literature has been reviewed relating to the mechanical properties of titanium Ti-6Al-4V alloy and its microstructures; the material failure due to

yielding; the application of titanium Ti-6Al-4V alloy in the biomedical environment; and the manufacturing processes of bone prostheses.

2. Metallographic examination which incorporates macro hardness, Optical Microscope (OM), Scanning Electron Microscope (SEM), Scanning Electron Microscope-Energy Dispersive X-Ray (SEM-EDX) and X-Ray Diffraction (XRD) analyses were conducted to investigate the relationships between the microstructure and the mechanical properties on EOS Ti64 powder and DMLS Ti64 samples.
3. Mechanical tests on DMLS Ti64 samples, such as an ultrasonic test which was employed to investigate elastic constants, a tension test which was conducted to acquire tensile behaviour, while post-sintering heat treatment was performed to alter ductility.
4. The simulation of the tensile test using ABAQUS^{TM} FEA program was conducted to validate the tensile properties and analyse failure due to yielding of DMLS Ti64 samples.

1.5 Expected Contributions

The mechanical properties of DMLS Ti64 samples will be compared to those of the standard specification for wrought annealed Ti-6Al-4V alloy for surgical implant applications (ASTM F1472-08$^{\varepsilon 1}$ Standards) and EOS GmbH manufacturer's material data sheet (EOS Gmbh-Material Data Sheet 2011) in order to ascertain the required standard. The expected outcome of this study will be recommendations on:

1. The empirical tensile properties, microstructures, the elastic constants and density of DMLS Ti64 samples manufactured on a vertical orientation which will be presented to CRPM in the form of charts.
2. The heat treatment technique of DMLS Ti64 samples, particularly where high ductility is of interest and where failure due to yielding is considered.

1.6 An Overview of the Dissertation

The overview of this research is elaborated as follows:

- The first chapter introduces the research.
- The second chapter will then review the literature that has been consulted in relation to the research.
- Experimental procedures and the results of the characterisation of EOS Ti64 powder, the elastic constants of DMLS Ti64 samples, the characterisation of both as-sintered and heat treated DMLS Ti64 samples under tensile loading, as well as the static behaviour predicted on ABAQUS^{TM} FEA program are outlined in chapters three and four, respectively.
- A discussion of the results will be addressed in chapter five, while both the conclusion and the recommendations will be presented in chapter six.

Chapter 2. LITERATURE REVIEW

2.1 Introduction

This chapter presents a summary of the literature on the mechanical properties and the microstructure of titanium Ti-6Al-4V alloy (further referred as Ti64 alloy); material failure due to yielding; some of the biomedical applications of Ti64 alloy, as well as the manufacturing processes of bone prostheses. Titanium alloys are used in the biomedical application due to their biocompatibility. The titanium Ti-6Al-4V alloy, commonly known as Ti64 alloy and described as the 'work horse' of the titanium industry, offers a combination of high strength, light weight and resistance to corrosion (Matthew & Donachie 2000: 43-45; Carpenter technology 2011: 1).

2.2 The Mechanical Properties of Ti64 Alloy and its Microstructures

2.2.1 Ti64 Alloy Powder

Aspects, such as the particle size and distribution, as well as the particle shape are powder characteristics that ultimately influence the properties of the DMLS sintered part. Narrow particle size distribution with a small average particle size and a regular

particle shape are better as powder characteristics. Powders of this kind have small inter-particle friction and good flowability, as well as density which enable good deposition in the form of thin layers during the DMLS process (Simchi 2006:148-158). The powder analysis on EOS Ti64 powder was done to identify phases present in the powder, particle size and shape, as well as the chemical composition. The EOS Ti64 powder was optimised for processing on the EOSINT M 270 machine (EOS Gmbh-Material Data Sheet 2011: 1). Thus, it is expected that parts manufactured on this machine using EOS Ti64 powder will still have a similar chemical composition to that of the standard specification for wrought annealed Ti-6Al-4V alloy for surgical implant applications as shown in Table 2.1 and also to the EOS GmbH manufacturer's material data sheet, in order to ascertain required standards.

The interstitial elements, such as oxygen, nitrogen and carbon are well known alpha phase stabilisers that act as solid solution strengtheners in titanium alloys (Leyens & Peters 2003: 1-24; Finlay & Snyder 1950: 277-286). The commercial pure titanium (grade 1 CP Ti) has the lowest concentration of interstitial elements and subsequently, has the lowest ultimate tensile strength, compared to the titanium alloys (see Table 2.1, ASTM B 265-13ae1 Grade 1 Standard). As the interstitial elements' concentration increases in the titanium alloys, the ultimate tensile strength increases. However, if the amount of these stabilisers is more or beyond what is required, ultimate tensile strength and ductility will be degraded. Matthew and Donachie (2000) indicate that should the Ti-6Al-4V alloy samples be subjected to any heat treatment at about 425°C or above, some reactions might take place due to interstitial elements, such as oxygen, nitrogen

and carbon. These will result in a surface layer of alpha case being formed and will eventually affect the chemical composition, leading to a change in mechanical properties as alpha case is brittle (Matthew & Donachie 2000: 56-58; Finlay & Snyder 1950: 277-286). It is very important for the heat treatment to be done in a controlled atmosphere, using either a vacuum furnace or heat treatment in an inert atmosphere, such as argon.

Table 2.1 Chemical composition and ultimate tensile strength of titanium and titanium alloys.

	Ti	**Al**	**V**	**FE**	**C**	**O**	**N**	**H**	**Ultimate Tensile Strength (MPa)**
Titanium Grade 1 (CPTi) *[ASTM B 265-13ae1 Grade 1 Standard]*	balance	-	-	0.2	0.1	0.18	0.03	0.015	240
Wrought annealed Ti-6Al-4V alloy *[ASTM F 1472-08$^{\varepsilon 1}$ Standard]*	balance	5.5-6.75	3.5-4.5	0.3	0.08	0.2	0.05	0.015	930
EOS As-laser sintered Ti64 parts *[EOS Gmbh-Material Data Sheet 2011: 3-4]*	balance	5.5-6.75	3.5-4.5	0.3	0.08	0.2	0.05	0.015	1200
EOS DMLS annealed Ti64 parts *[EOS Gmbh-Material Data Sheet 2011: 3-4]*	balance	5.5-6.75	3.5-4.5	0.3	0.08	0.2	0.05	0.015	930

2.2.2 Crystal Structure of Titanium Ti-6Al-4V Alloy

Pure titanium and other titanium alloys when crystallised at low temperatures form a Hexagonal Close-Packed (HCP) structure, known as alpha (α) phase, while at high temperatures form a Body Centred Cubic (BCC) structure, known as beta (β) phase (Leyens & Peters 2003: 4-9). However, these two phases α and β stabilise within a particular temperature range; thus, the transformation temperature is called transus temperature. The β-transus temperature for pure titanium is 882 ± 2ºC (Leyens & Peters 2003: 4-24; Carpenter technology 2011: 1; Gilbert et al. 1990: 913-923).

The existence of the α and β phases, together with their corresponding transus temperatures, play a major role in the basis of material performance and/or behaviour under different mechanical loadings. The α phase is an isotropic structure, meaning that the physical properties greatly depend on the orientation, the crystallographic texture and/or grains. The β phase has better plastic deformation compared to the α phase, resulting in an improvement in material ductility (Leyens & Peters 2003: 4-24; Matthew & Donachie 2000: 13-24).

Titanium alloys are generally classified into three main categories: alpha (α) alloys; beta (β) alloys; and alpha + beta (α + β) alloys. Ti-6Al-4V is an alpha + beta alloy with aluminium as the alpha stabiliser and vanadium as the beta stabiliser. The addition of

aluminium provides additional strength to the α phase, while vanadium improves the plasticity of the alloy. The slip deformation is more energetically favourable in BCC crystals than in HCP because it has a shorter path length. According to the Von Mises criterion, a minimum of five independent slip systems is needed in order to have homogeneous plastic deformation. In the case of HCP, there is a total of four independent slip systems which make the α (HCP) titanium difficult to plastically deform. The introduction of the β (BCC) phase in Ti-6Al-4V gives rise to independent slip systems and ultimately improves the ductility of the alloy (Leyens & Peters 2003: 4-24).

2.2.3 Microstructure of Ti64 Alloy

The microstructure of Ti64 Alloy is primarily described by the grain size and the arrangement of the two phases: α and β. The transformation from the β phase to the α phase upon cooling, results in a 'basket weave' structure which is seen as the lamellar structure which grows in different orientations. Figure 2.1 illustrates the microstructures of the Ti64 Alloy (Nalla et al. 2002: 899-901; Leyens & Peters 2003: 1-24).

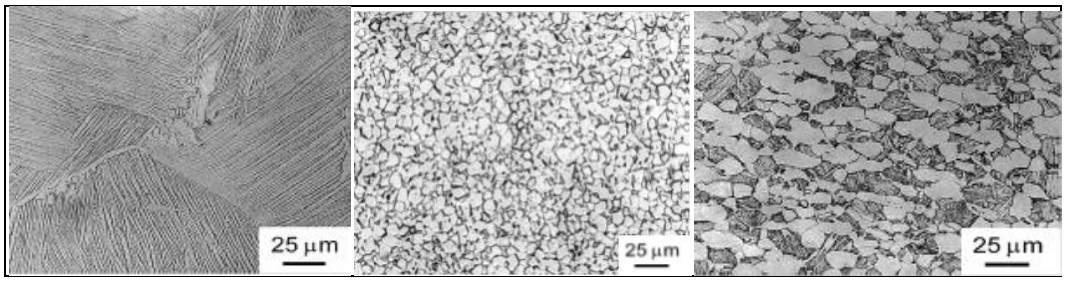

a) b) c)

Figure 2.1 OM micrographs of the Ti64 Alloy: a) A lamellar structure; b) An equiaxed structure; c) A bimodal structure (Nalla et al. 2002: 901; Leyens & Peters 2003: 7-32)

Equiaxed microstructure is formed during a re-crystallisation process. Figure 2.1b shows the equiaxed structure of cast Ti-6Al-4V. Upon subsequent solution heat treatment at temperatures in the α + β phase field, a re-crystallised equiaxed microstructure is generated; thus, solution heat treatment is done below β-transus temperature resulting in a bimodal structure that consists of both equiaxed and lamellar structures (Figure 2.1c) (Leyens & Peters 2003: 7-32). Various microstructures may be predicted but the microstructure depends on the alloying, processing and post-processing heat treatment. As it is generally accepted in the literature, the microstructure has a strong influence on the mechanical behaviour; thus, fine-scale microstructures increase the strength, while coarse microstructures are more resistance to creep and fatigue crack growth (Nalla et al. 2002: 899-901; Leyens & Peters 2003: 7-32; Matthew & Donachie 2000: 13-24; Filip et al. 2003: 85-88). On the other hand, equiaxed microstructures often have high ductility, as well as fatigue strength, while

lamellar structures have high fracture toughness. A combination of both equiaxed and lamellar structures, results in a well-balanced property profile (Leyens & Peters 2003: 7-32, Filip et al. 2003: 85-88).

2.2.4 Relationship Between Microstructure and Yield Strength

The grain size influences the hardness and strength of the material. Studies have shown that smaller grain sizes provide higher yield strength by inhibiting the dislocation motion (Armstrong 1987: 531-536; Hall 1951: 747-751; Petch 1953: 25-28). The yield stress increases because there are more boundaries to block the movement of dislocation during deformation (Armstrong 1987: 531-536). The Hall-Petch equation 2.1 illustrates the relationship between yield stress and grain size as described mathematically.

$$\sigma_y = \sigma_o + \frac{k}{\sqrt{d_g}}$$ ***.....Equation 2.1***

Where σ_y is the yield stress; σ_o is a materials constant for the starting stress for the dislocation movement (or the resistance of the lattice to dislocation motion); k is the strengthening coefficient (a constant, unique to each material); and d_g is the average grain diameter (Armstrong 1987: 531).

Equation 2.1 shows that the yield stress (σ_y) is inversely proportional to the grain diameter (d_g); thus, the bigger the grains become, the lower the yield stress of that particular material is induced (Armstrong 1987: 531-536; Hall 1951: 747-751; Petch 1953: 25-28). Clearly, there is a relationship between the microstructure and the yield stress. Depending on what is desired as per application, grain size can be altered by heat treatment.

2.2.5 Heat Treatment of Ti64 Alloy

Mechanical properties depend on the phases present in the material. Changing the physical properties, such as the grain size; the grain shape; the grain texture and/or arrangement of the phases; strongly influence the mechanical properties (Leyens & Peters 2003: 4-32).

Pure Titanium exhibits a β-transus temperature at 882 ± 2ºC; however, Gilbert et al. (1990) suggest that the heat treatment temperature should be around 1000°C β-transus temperature for Ti64 alloy. In the case of heat treating titanium alloy, the centre point which is of high interest is the β-transus, as it separates the single β phase field from the α/β phase fields. A variety of heat treatment methods, such as mill annealing, duplex annealing, beta annealing and solution treating, plus the aging treatments can be employed, depending on the desired mechanical properties. Different heating

temperatures and cooling rates lead to different microstructures which can either be fine or coarse. The cooling rates can either be furnace cool, air cool or water quench.

Beta annealing is done at temperatures above the beta transus of the Ti64 alloy. However, to avoid excessive grain growth, the annealing temperatures should not be excessively above the beta transus. The annealing times are dependent on the section thickness and should be long enough to complete the β transformation. The time at the temperature of transformation should be kept at a minimum to control grain growth (Matthew & Donachie 2000: 42-44). The annealing of Ti64 alloy serves primarily to increase ductility, fracture toughness and creep resistance at room temperature (Matthew & Donachie 2000: 42-44; Leyens & Peters 2003: 7-32). On the other hand, to some extent, the improvement of one or more properties is obtained at the expense of some other properties; for example, it is expected that when ductility increases, strength decreases. The Schematic phase diagram of Ti64 alloy with varying vanadium composition is normally used in selecting the heating temperature (Leyens & Peters 2003: 7-32; Matthew & Donachie 2000: 42-56). Figure 2.2 illustrates the Schematic phase diagram of Ti64 alloy at 4% per weight of vanadium.

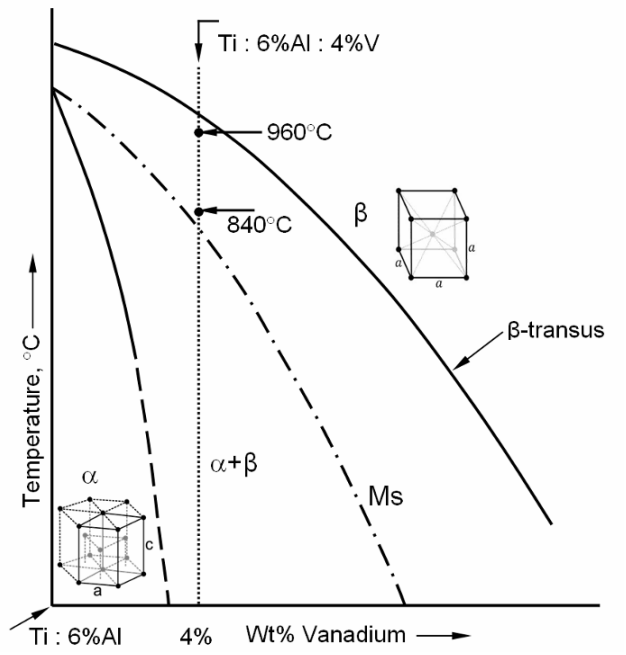

Figure 2.2 Schematic phase diagram of Ti64 alloy; for Ti64 alloy temperature of β-transus is 1050ºC (Matthew & Donachie 2000: 56); martensite start temperature Ms is 800°C (Matthew & Donachie 2000: 42-44)

2.2.6 Mechanical Properties of Ti64 Alloy

Mechanical properties are used as design factors when selecting material, the method of manufacturing, as well as the structure of the component. Mechanical properties are useful to designers and manufacturers as they indicate how the material behaves and/or performs under one or more mechanical loadings. They aid in the prediction of mechanical failure and deformation, and control/monitor the quality of the components produced.

Factors affecting mechanical behaviour:

- Porosity of the component;
- Material (chemical composition and microstructure);
- Method of manufacturing; and
- Mechanical loading (stretched, compressed, twisted, sheared, cyclic and/or combined loading) (Meyers & Chawla 1999: 71-76).

Mechanical loading is typically related to the real application of the component. In tensile loading, the following properties are significant: Young's modulus; yield strength; ultimate tensile strength; elongation and percentage reduction in area (Meyers & Chawla 1999: 71-76; Sander & Weintraub 2000; Philpot 2010: 1-54; Matthew & Donachie 2000: 43-45). The tensile properties such as elongation and area reduction indicate the ductility of the parts. Table 2.2 show the mechanical properties of wrought annealed Ti-6Al-4V alloy according to the ASTM F 1472-08$^{\varepsilon 1}$ standard and DMLS Ti64 samples, based on EOS GmbH manufacturer's material data sheet, respectively.

Table 2.2 Mechanical properties of Ti64 alloy

Properties	**Wrought annealed Ti-6Al-4V alloy** *[ASTM F 1472-08$^{\varepsilon 1}$ Standard]*	**EOS as-laser sintered Ti64 parts** *[EOS Gmbh-Material Data Sheet 2011: 3-4]*	**EOS DMLS annealed Ti64 parts** *[EOS Gmbh-Material Data Sheet 2011: 3-4]*
Hardness[HV]	300-400	320±12	-
Density (ρ) g/cm^3]	4.43	4.41	4.41
Tensile properties			
0.2% Proof Strength [MPa]	800-1100	1070±50	860
Ultimate Tensile Strength [MPa]	900-1200	1200±50	930
Percentage Elongation [%]	6-10	11±3	15±1
Area Reduction [%]	15-25	-	-

NOTE EOS DMLS TI64 PARTS:

1. *Tensile test was done according to ISO 6892-1:2009 (B) Annex D, proportional test pieces, diameter of the neck area 5 mm (0.2 inch), and original gauge length 25 mm (1 inch).*
2. *Specimens were treated at 800 °C (1470 °F) for 4 hours in argon inert atmosphere.*
3. *Vickers hardness measurement (HV) according to EN ISO 6507-1 on polished surface.*

2.2.7 The Hardness Measurement of Ti64 Alloy

Hardness is a fundamental mechanical property of any engineering material. The hardness test, in most cases, is regarded as a non-destructive test which can be used to quickly predict other mechanical properties, such as yield strength, ductility, and stiffness; thus, hardness is often a good indication of the tensile and wear properties of a material. The hardness of Ti64 alloy is shown in Table 2.2. The values of hardness are similar and range between 300 and 400 HV.

The hardness can be defined as the material resistance to indentation or permanent deformation as force is applied to the material. Vickers hardness is the standard method for measuring the hardness of metals, particularly those with extremely hard surfaces: the surface is subjected to a standard pressure for a standard length of time by means of a pyramid-shaped diamond. The diagonal of the resulting indention is measured under a microscope. The indenter employed in the Vickers test is a square-based pyramid whose opposite sides meet at the apex at an angle of 136º. The diamond is pressed into the surface of the material at loads ranging up to approximately 120 kilograms-force, and the size of the impression (usually no more than 0.5 mm) is measured with the aid of a calibrated microscope. The Vickers number (HV) is calculated using the following equation 2.2:

$$HV = 1.854\left(\frac{F}{D_2}\right) \quad \textit{Equation 2.2}$$

Where F is the applied load (measured in kilograms-force) and D_2 is the area of the indentation (measured in square millimetres) (Tabor 1951: 79; Rocha, Adabo, Henriques & Nóbilo 2006: 126-128; ASTM E 385-11e1 Standard).

2.3 Static Behaviour of Ti64 Alloy

2.3.1 Material's Elastic Limit

Fully elastic deformation is defined as reversible alteration of the form or dimensions of a solid body under stress or strain (Drotsky 1994: 29-34; Philpot 2010: 43-55). Under pure axial load, the shear in the bonding has to be great enough to break the bonds between the atoms or the atoms will return to their original form (Leyens & Peters 2003: 4-24). However, once the internal energy is enough to break the bonds, there will be permanent deformation (Leyens & Peters 2003: 4-24, Philpot 2010: 43-55). Fully elastic deformation is typically governed by Hooke's Law that states:

$$\sigma = E\varepsilon$$ ***……..Equation 2.3***

Where: σ = Stress

E = Modulus of Elasticity

ε = Strain

Hooke's law is a linear relationship that relates stress to strain by using the modulus of elasticity of the material (Philpot 2010: 43-55). Fully elastic analysis pertains only to stress and strain up to the yield point. Past yield point, the material should start to plastically deform. The stress-strain curve for most materials has an initial region in which the material stress is linearly related to the material strain. Figure 2.3 indicates the typical stress-strain curve of wrought annealed Ti-6Al-4V alloy based on ASTM F 1472-08$^{\varepsilon 1}$ standards. The proportional limit is determined by inspection of the stress-strain curve. The proportional limit marks the uppermost stress on this linear portion of the stress-strain curve (see point 3 in Figure 2.3). For stresses above the proportional limit, the stress-strain relationship is non-linear.

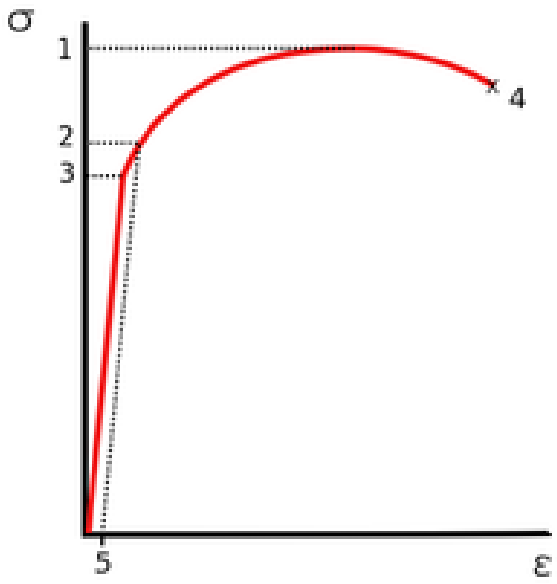

Figure 2.3 Typical stress-strain curve of wrought annealed Ti-6Al-4V alloy based ASTM F 1472-08$^{\varepsilon 1}$ standards

Where:

Point 1 is the Ultimate Tensile Stress (UTS);

Point 2 is the Yield stress at 0.2% offset strain;

Point 3 is the Proportional limit stress;

Point 4 is the Fracture stress; and

Point 5 is the Offset strain typically 0.2% (or strain of 0.002 mm/mm).

If the transition from a straight line to a curve on the stress-strain curve is gradual, it may be difficult to specify a precise value for the proportional limit (i.e. the material's elastic limit). Furthermore, it may be overly conservative to use the material's proportional limit as a practical elastic limit for design purposes. For these reasons, a yield stress (also called yield strength) can be established for use in design. The yield stress marks the point at which a significant increase in strain occurs without a significant increase in stress. The yield stress is often determined from stress-strain data by means of an offset method. This offset method defines the yield stress (or strength) according to the amount of permanent set that results in the material due to the applied stress. The 0.20% offset method was used in this project. A line was constructed having the same slope as the linear portion of the stress-strain curve, as illustrated by point 5 in Figure 2.3 (note that 0.20% strain is another way of writing a strain of 0.002 mm/mm). Point 2 on Figure 2.3 is where this line intersects the stress-strain data curve and is defined as the yield stress (Philpot 2010: 43-55). For this

project, the MDSolid program was used in order to determine and interpret the 0.2% offset yield point on the stress-strain curve precisely.

2.3.2 Failure Due to Yielding

A material's elastic limit (yield stress) determines the load bearing capability. The maximum distortion energy theory has established an equivalent stress quantity, known as Von Mises stress. The value of Von Mises stress as given by equations 2.4 and 2.5 is compared to the calculated true tensile yield stress from the tensile test results (Drotsky 1994: 336-338; Shigley & Mischke 2003: 331-337; Pilkey & Pilkey 2008: 28-34; Philpot 2010: 627-63).

$$\sigma_{vm} = \frac{1}{\sqrt{2}}\sqrt{(\sigma_x - \sigma_y)^2 + (\sigma_y - \sigma_z)^2 + (\sigma_z - \sigma_x)^2 + 6(\tau_{xy}^2 + \tau_{yz}^2 + \tau_{zx}^2)} \quad \textit{.....Equation 2.4}$$

And for plane stress

$$\sigma_{vm} = \sqrt{(\sigma_x^2 - \sigma_x\sigma_y + \sigma_y^2 + 3\tau_{xy}^2)} \quad \textit{.....Equation 2.5}$$

Where

σ_{vm} = Von Mises stress

σ_x = Stress in x-direction

σ_y = Stress in y-direction

σ_z = Stress in z-direction

τ_x = Strain in x-direction

τ_y = Strain in y-direction

τ_z = Strain in z-direction

During the tensile test, the stress was applied only in y-direction; therefore, the Von Mises stress equation 2.6 and 2.7 became:

$$\boldsymbol{\sigma_{vm(normal)} = \frac{1}{\sqrt{2}} \sqrt{2(\sigma_y)^2}} \quad \textbf{.....Equation 2.6}$$

And for plane stress

$$\boldsymbol{\sigma_{vm\,(normal)} = \sqrt{(\sigma_y)^2}} \quad \textbf{.....Equation 2.7}$$

The yielding of material is predicted to occur whenever Von Mises stress (σ_{vm}) $\geq$ yield stress (σ_{yield}) (Shigley & Mischke 2003: 331-337). The Von Mises stress is mostly used and tabulated in the form of colour-coded contour plots in most common finite analysis.

2.3.3 Finite Element Analysis (FEA) of Ti64 Alloy

One of the major aspects of finite element analysis is how to interpret simulation and how to verify whether the simulation results accurately portray the loading conditions. Inaccuracies within the FEA results can stem from various sources including modelling, input of material properties (fully elastic, elastic-plastic, thermal, fluid, etc.), mesh density, unrealistic stress concentration, loading conditions and environment, among other things (Cook et al. 2002: 8-18; Bao, 2003: 84-86).

Engineers understand FEA as an approximation tool and the analysis has to be validated by hand calculations, test results, or inspection to confirm the validity of the results. Hand calculations are sufficient for calculating theoretical solutions for a piece-part component under a single or simple loading condition (Cook et al. 2002: 8-18). As the design increases in complexity, as various loads are applied, and as the environmental complexity increases, engineers require more assurance when utilising FEA results. Multiple loading and environmental conditions make hand calculations

complex and untrustworthy (Cook et al. 2002: 8-18; Bao, 2003: 84-86; Joun 2007: 63-69).

In the ABAQUS^{TM} FEA program, in order to analyse specimens within the fully elastic range, only Young's modulus, Poisson's ratio and material density are required to perform a static analysis. The analysis is assumed to be accurate up to yield point; thus, stress and strain within plastic range will also be used in order to determine the accuracy of the yield point. It is expected that the stress-strain curves will start to obtain nonlinearity after the yield point; thus, the yield point will be determined. Elastic-plastic analysis uses Young's modulus, from the elastic material properties but the ABAQUS^{TM} FEA program requires yield stress and plastic strains of the material in the plastic range to be manually loaded into the material properties. If the plasticity data have not been entered into the ABAQUS^{TM} FEA program, the stress/strain relationship will continue to be linear (Joun 2007:63-69). This will not provide an accurate result of stress in the plastic range. Thus, the ultimate tensile stress illustrated by point 4 in Figure 2.3, provides the value maximum stress, as well as the plastic strain.

The ABAQUS^{TM} FEA program is an approximation tool and is as accurate as the operator allows it to be. The operator has to enter all of the material technical data that are found in various mechanical tests/experiments, material science books, commercial specifications, and various published works (Roylance 2001:1:14; Cook et al. 2002:

8-18). FEA results are influenced by the material and property section within the ABAQUS^{TM} framework.

This project used ABAQUS^{TM} FEA program to run an analysis closely resembling the static tensile behaviour of DMLS Ti64 samples. The material technical data used were found by investigations conducted, as explained in chapter 3 and 4, respectively. The FEA Von Mises stress of DMLS Ti64 samples was predicted and compared to the calculated Von Mises stress values. The MDSolid program was used in this project in order to interpret the yield point of FEA Von Mises stress-strain curve precisely. Thereafter, it was also used during the analyses of failure for DMLS Ti64 samples based on the maximum distortion energy theory, particularly looking at Von Mises stresses.

The MDSolid program is the software mostly used for any calculations involved in the Mechanics of Materials or Strength of Material courses (Philpot 2000:401-407). The software features a number of modules for topics in static courses, for example:

- The software aids in the calculations involved in material properties, such as the yield stress, ultimate stress, proportional limit, amongst others found in stress-strain curves;
- It does calculations involved in Mohr's circle analysis including stress and strain transformation and many more topics; and

- Furthermore assists in the analysis of material failure based on maximum distortion energy theory, maximum shear stress theory and many more (Philpot 2000:401-407).

2.4 Application of the Ti64 Alloy Parts in the Biomedical Environment

There are various materials, such as cobalt alloys, austenitic stainless steels and titanium alloys that have been used as replacements to bone in orthopaedic surgery (Berto et al. 2010: 3982–3986; Yuehuei et al. 1999: 42-43). To avoid a galvanic couple, it is beneficial to use identical metals. The original hip prosthesis's components were manufactured from stainless steel components. It was soon discovered that metal-on-metal artificial joints are not the best tribological design, due to a non-optimum fit between the articulating surfaces which results in excessive wear (Charnley 1970: 8-12; Long & Rack 1998: 1622-1630*).*

As an alternative to the metal-on-metal joints, Sir John Charnley developed the concept of low friction arthoplasty in the 1960s (Charnley 1970: 7-21). In his work he designed a small-diameter metallic femoral head articulating with a polymeric acetubular cup. The polymeric acetubular cup was originally made from polytetrafluoethylene (PTFE), which was later replaced with ultra-high-molecular-weight polyethylene (UHMWPE). Although this design was widely accepted, with UHMWPE being the dominant orthopaedic material for 30 years, the wear of UHMWPE when rubbing against metal femoral heads

was observed (Charnley 1970: 8-12; Long & Rack 1998: 1622-1630*).* It is not only the material that caused wear, but the structure of the implant also contributed to the process (Rosen et al. 2006: 11). There has been therefore, a shift away from UHMWPE and lattice-truss structures made of titanium or stainless steels have lately been taken into consideration due to their biological advantages. (Rosen et al. 2006: 11).

A truss is a structural frame relying on a triangular or rhombic arrangement of webs and chords to transfer loads to reaction points. This arrangement gives them a high strength-to-weight ratio and offers greater flexibility in the topology of a bone (Rosen et al. 2006: 1-3). They can be designed in almost any shape or size and are restricted only by manufacturing capabilities. There is consensus in the literature (Berto et al. 2010: 3982–3986; Rosen et al. 2006: 11-12) that lattice-truss structures, if used in bone prostheses, can provide the following, most suitable biological advantages:

- Lattice-truss structures can absorb impact as their stiffness matches that of the bone along the implant's outer region. Therefore, the use of a polyethylene liner in the acetabular components, as it absorbs impact, will be eliminated. The polyethylene liner is prone to wear causing particles to break off which can cause osteolysis, and the mechanical loosening of the joints at the implant bone interface.
- Lattice-truss structures can help with the fixation of the implant onto the healthy bone and its natural porosity will enhance the stability of the implant-bone interface.

- Lattice-truss structures can also facilitate bone in-growth.

The interior region of the ilium around the acetabular component is spongy bone with an average elasticity of 1GPa; thus, the implanted acetabular component is designed to comparably match the effective elasticity of 1GPa (see Figure 2.4 and 2.5).

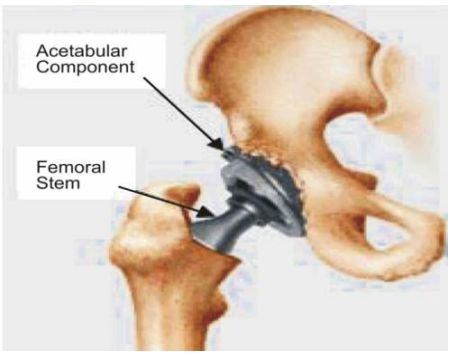

Figure 2.4 An acetabular component which is part of the hip joint (Rosen et al. 2006: 12).

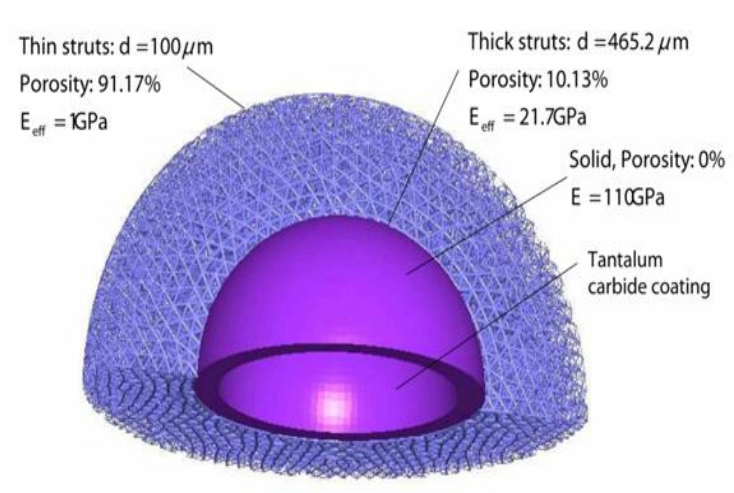

Figure 2.5 Lattice-truss structures in an acetabular component which is part of the hip joint (Rosen et al. 2006: 12)

In addition to the above mentioned biological advantages, the ductility of the material used for the lattice-truss structures, especially where the dimensions are in microns (μ) is of high importance. Some of the struts in Figure 2.5 are 100μm; if they are subjected to the load, there might be an instant break without warning. The bones and replacement components within the hip joint must support forces that originate from outside the body, such as those due to gravity. In addition, they must transit forces that result from muscular action, such as walking. These forces are complex in nature and fluctuate with time in magnitude, in direction, and in the rate of application (Yuehuei et al. 1999: 42-43). Thus, mechanical characteristics, such as modulus of elasticity, yield strength, ultimate tensile strength and ductility are important considerations relative to the material of choice for the formation for the prosthetic hip. An example can be given in the case of a femoral stem. The femoral stem should have minimum yield strength and ultimate tensile strength of approximately 500 MPa and 650 MPa, respectively, and a minimum ductility of about 8% elongation (Callister 2006: W111). Therefore, the material used must be ductile in order to show an indication of failure by yielding, before it breaks.

Titanium alloys have received the most attention in recent times due to the inherent properties of titanium that are very attractive to orthopaedic surgery. High chemical reactivity has delayed the development of titanium due to the difficulty associated with melting, casting and the hot working of this metal (Matthew & Donachie 2000: 47-58).

Ti64 alloy has an added advantage over other biomaterials, such as stainless steel and cobalt-chromium-molybdenum alloy because of a lower modulus of elasticity, although it is still higher than that of bone. The elastic modulus of titanium is about 5 times more than that of the cortical bone (Figure 2.6). The ultimate strength and elastic modulus of titanium is about 1250 MPa and 110 GPa, respectively, while that of the cortical bone by the tensile test is about 120 MPa and 21 GPa, respectively (Yuehuei et al. 1999: 42-44).

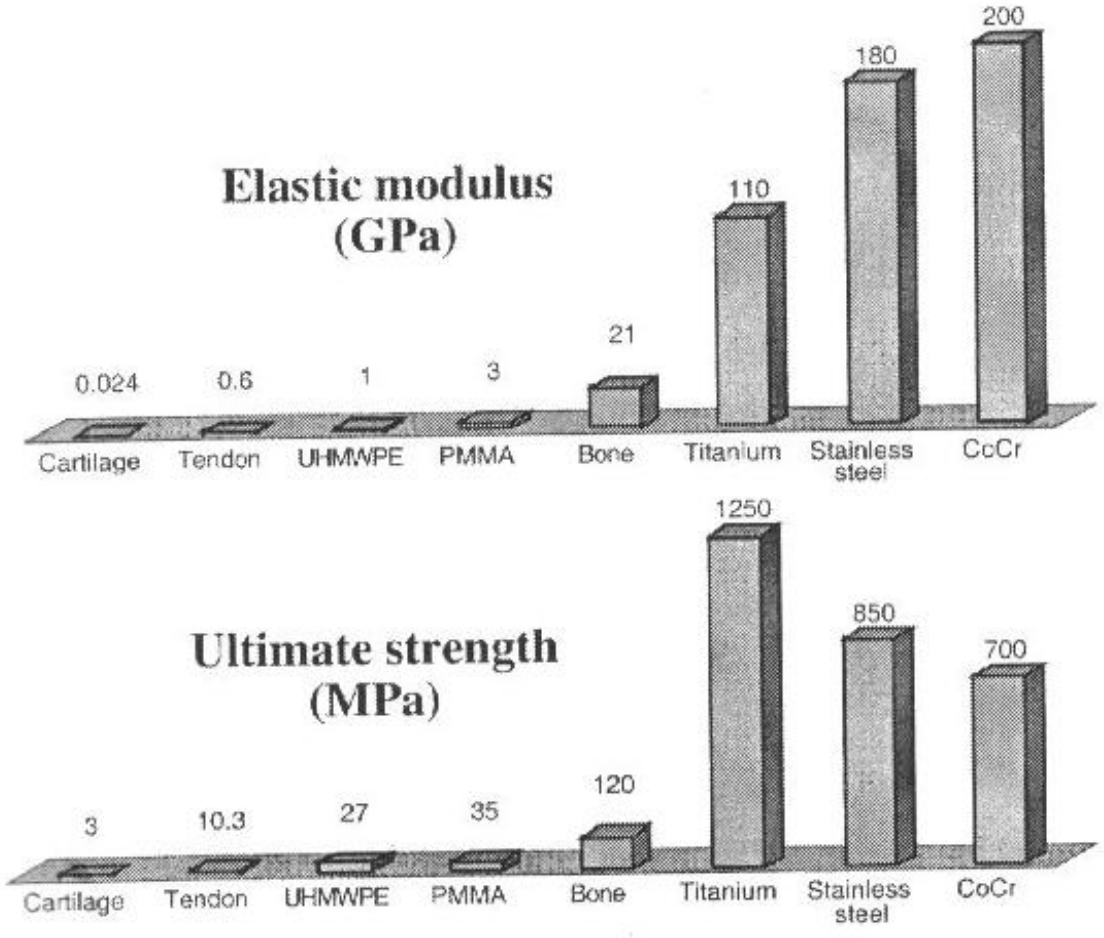

Figure 2.6 Some mechanical properties of tissues and biomaterials (Yuehuei et al. 1999: 43)

Ti64 alloy can also be heat treated to achieve the desired mechanical properties, such as ductility. The recommended service temperature of Ti64 alloy is up to 350ºC; thus, it is used mainly in aircraft turbine engine components, aerospace fasteners and in marine applications (Leyens & Peters 2003: 2). Ti64 alloy is also used in medical applications as it is a biocompatible material; thus, it is not rejected by the human body, especially when direct contact with tissue or bone is required (Leyens & Peters 2003: 2).

2.5 DMLS Manufacturing Process of Bone Prostheses

Most metal orthopaedic joint replacements and bone plate surgeries are fabricated by wrought or cast-bar stock by CNC, CAD-driven machining or powder metallurgy production techniques. Other processes which have been recently introduced include direct digital manufacturing, such as the Electron Beam Melting (EBM), Direct Metal Laser Sintering (DMLS), Laser Engineering Net-shaping (LENS) and Ultrasonic Consolidation (UC) (Murr et al. 2009: 20-32). In this study all the samples were manufactured using DMLS process hence; more emphasis is on DMLS process

The DMLS process is one of the latest additive technologies used in manufacturing implants. This technology is capable of producing intricate customised biomaterial implant parts. DMLS works by laser sintering very fine layers of metal powder, layer by layer, from the bottom up into a three-dimensional component. Each layer is scanned

by a laser beam of high intensity so as to provide thermal energy that is required for the melting of the adjacent surfaces of particles of powder (Hänninen et al. 2002: 33-36).

The laser sintering process strengthens powder mass and increases the density of the particles. Therefore, parts manufactured by the DMLS process do not require post-sintering and/or the infiltrating process (Hänninen et al. 2002: 17-19). A support structure is required to hold the parts in position during building and this is anchored onto a substrate. Supports are used in order to withstand thermal and recoating forces. The supports and parts are built with the same layer thickness, ranging between 20-60 microns, depending on the material used. The finished part will go through the support removal process, shot peening, and lastly through polishing. Heat treatment will be employed if required. Figure 2.7 shows a schematic diagram of the DMLS process (EOS Gmbh-Material Data Sheet 2011: 1-5; Lind et al. 2003: 119-126; Ning et al. 2004: 183-195).

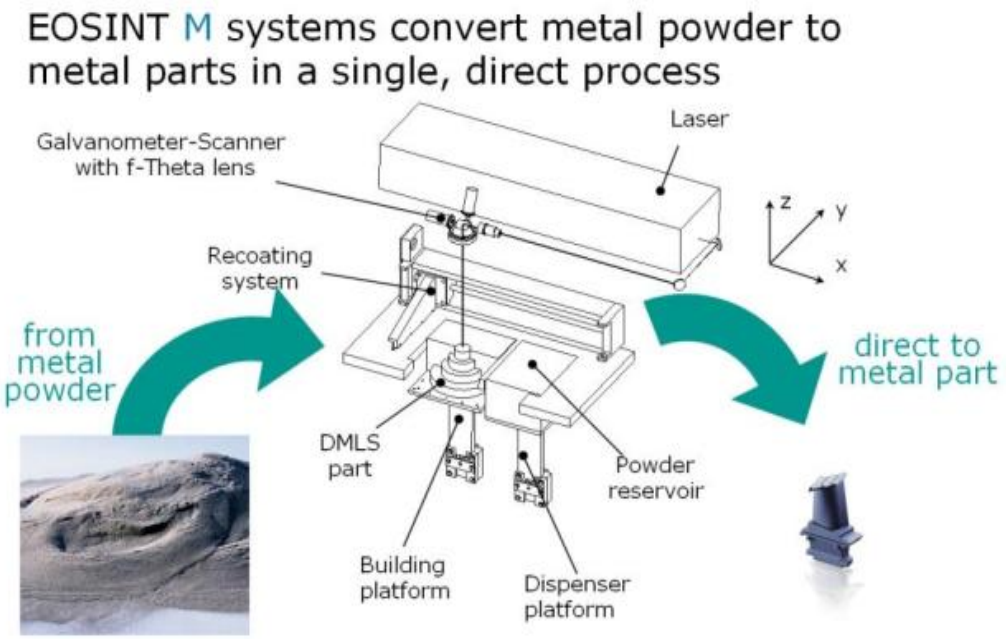

Figure 2.7 Schematic diagram showing the DMLS process on EOSINT M 270 machine [Courtesy of EOS GmbH]

Some of the variables are machine dependent and can be controlled as they control the sintered density of the final part. The main controlling aspect is the amount of laser energy. The overall material structure and properties of the DMLS parts are greatly dependent on the build strategies (laser exposure patterns) and the parameters used, such as the laser power, scan rate, scan line spacing and bed temperature (Ning 2004: 183-199; Ning et al. 2005: 15-25). Increasing the laser power and decreasing the scanning speed, building with thinner layer thickness and overlapping the scan lines all increase the part density, but a too high energy input results in delaminations due to residual thermal stresses (Sustaryc et al. 2009: 837- 841).

Chapter 3. EXPERIMENTAL PROCEDURES AND FEA APPROACH

3.1 Introduction

EOS Ti64 powder was characterised in order to learn its morphology, particle size and chemical composition prior to using it in experimental work. Therefore, the focus was in the acquisition of the mechanical properties of samples manufactured from EOS Ti64 powder using DMLS process, which would later assist in the tailoring of the desired ductility.

DMLS Ti64 samples were manufactured at CRPM in Bloemfontein with EOS Ti64 powder on the EOSINT M 270 machine, using the DMLS process. Heat treatment, metallographic analysis, and tensile testing were performed at the CSIR's Material Science and Manufacturing Division in Pretoria. Ultrasonic and density tests were done at the Element Six Research Laboratory in Springs, Gauteng.

The FEA model was calibrated using the trial-and-error method in order to determine the optimum material property set for DMLS Ti64 samples. To achieve this calibration, a comparison between the experimental tensile test and the FEA tensile test results was made. Thereafter, a simulated tensile test was conducted using the ABAQUS^{TM} FEA

program. The FEA results were then used to examine the DMLS Ti64 samples under static tensile load up to a yield point.

3.2 Characterisation of EOS Ti64 Powder

Powder particle size distribution analyses were done using a Microtack Bluewave Particle Analyser (Figure 3.1). The powder's morphological features were studied using a Leica Optical Microscope and a LEO 1525 Field-Emission Scanning Electron Microscope (FE-SEM), coupled with a Robinson Backscatter Electron Detector (RBED). Energy Dispersive X-Ray (EDX) analyses were performed using a Scanning Electron Microscope (SEM). To study the phases present and their evolution, a Phillips PW 1830 X-Ray Diffraction (XRD) analyser fitted with Cu Kα irradiation was used.

Figure 3.1 The Microtrack Bluewave Analyser

3.3 Preparation of DMLS Ti64 Samples and Their Characterisation

3.3.1 Manufacturing of DMLS Ti64 Samples

The design of the tensile specimen was drawn using the CAD software Solid Edge^{TM} program according to ASTM E8 / E8M standards. The initial gauge length and diameter were 17mm and 4.25mm respectively (Figure 3.2a). The dimensions were reduced due to the fact that titanium is very expensive, but the aspect ratio of length to diameter which is 4:1 was maintained as specified in the ASTM E8 standards (ASTM E8 / E8M - 11 Standard). Tensile test specimens were manufactured on the EOSINT M 270 machine (Figure 3.2d) using EOS Ti64 powder (Figure 3.2c). The EOSINT M 270 machine was set at standard building parameters according to EOS GmbH the manufacturer of the EOSINT M 270 machine as shown in Table 3.1.

Table 3.1 EOSINT M 270 machine's set process parameters

Build layer thickness: 30 µm Powder re-coater speed: 500 mm/s Base plate temperature: 35 degrees Celsius				
	Stripes (Hatching)	**Up-Skin**	**Down-Skin**	**Contour**
Laser Power	170 W	120 W	120 W	150 W
Speed	1250 mm/s	1000 mm/s	1000 mm/s	1250 mm/s

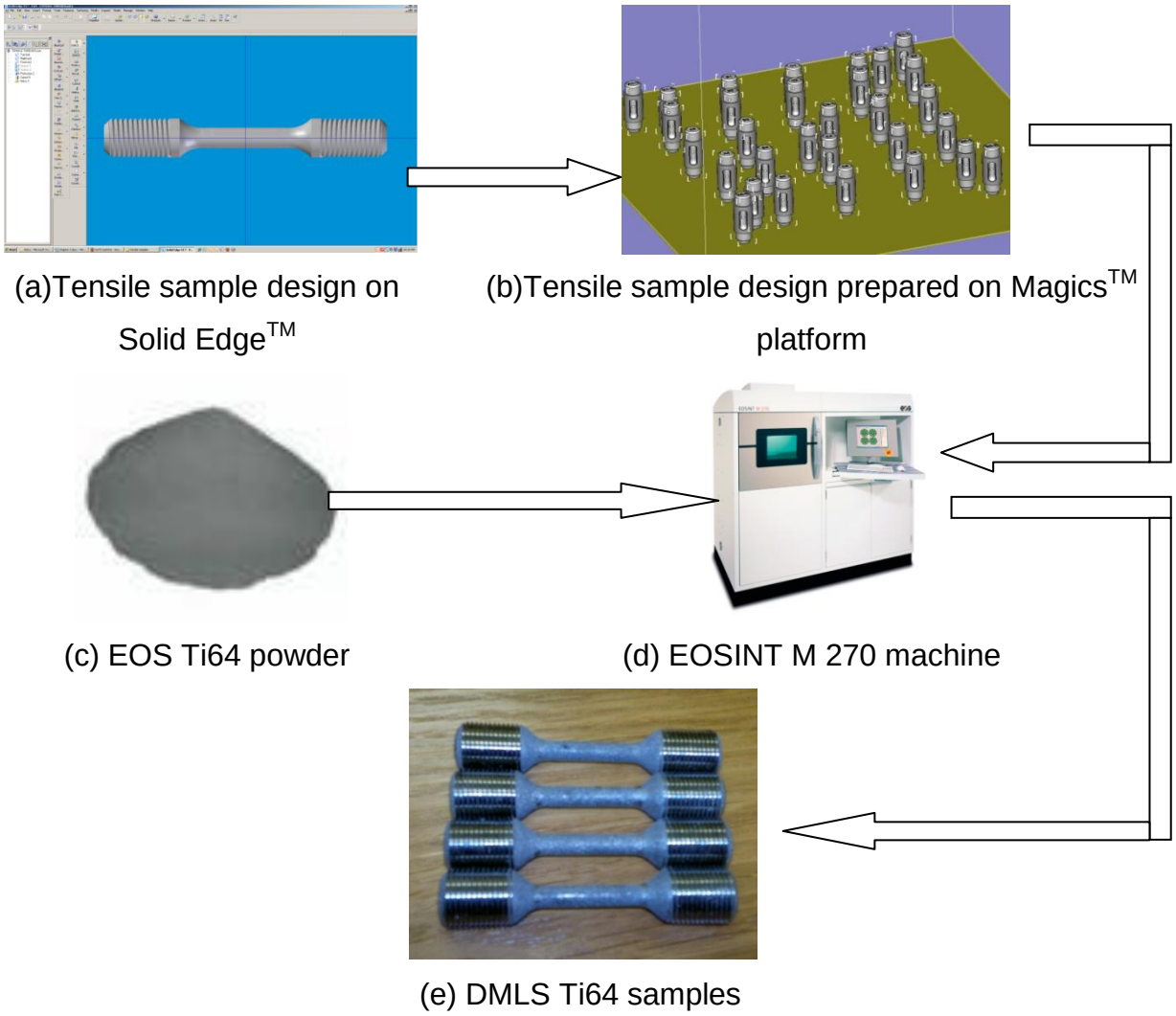

Figure 3.2 A pictorial summary of DMLS process

Computer-aided design data Figure 3.2b were prepared on the Magics™ program, where the designs were vertically positioned on the building platform. The supporting structures were generated at this stage as they were required to support the parts built, due to thermal stress. Both the designs and supporting structures were sliced into 30 µm layers so that the computer of the EOSINT M 270 machine could process part data, layer by layer. The following were done on the EOSINT M 270 machine before the

building process started: the EOSINT M 270 machine was filled with EOS Ti64 powder; the machine was set to the standard building parameters as shown in Table 3.1; the base plate (platform) was then heated to 35°C; the process computer transmitted parts information of 30 µm layer on the EOSINT M 270 machine and started generating layer by layer up until the parts were built. Parts were manufactured in an argon atmosphere in order to reduce the oxygen content in a chamber to 0.07%. The parts were allowed to cool in the chamber until they reached room temperature and then were removed from the machine. The removal of support structures was done using a CNC wire cutting machine.

3.3.2 Characterisation of DMLS Ti64 Samples

3.3.2.1 *Determination of the Density of DMLS Ti64 Samples*

The densities of twelve (12) DMLS Ti64 samples were measured using the Archimedes' principle. The Archimedes' principle states that when a body is immersed in a fluid, there is buoyant force acting upward on the body equal to the weight of the displaced fluid. Thus, the density of materials is given by

$$\rho_{material} = \frac{M_{dry}}{V_{material}} \quad \textit{Equation 3.1}$$

Where; 'M_{dry}' is a measured mass of material, '$V_{material}$' is the volume of material, and '$\rho_{material}$' is the density of the material.

The samples were ground using a surface grinding machine and then polished to ensure parallel sides. The same samples were used to obtain elastic constants as well. Density was measured based on the Archimedes' principle and the liquid used was water at room temperature. Both the dry and wet masses were measured using a mass density scale. The recorded and calculated values are presented in chapter 4.

3.3.2.2 *Determination of the Elastic Constants of DMLS Ti64 Samples*

Elastic constants of twelve (12) DMLS Ti64 samples were measured according to the ASTM E494-48 using an ultrasonic pulse echo technique on the Krautkramer USIP12 machine. The varying thicknesses of the samples were also recorded. The transducers which were connected to an oscilloscope, were pressed onto each sample (one sample is tested at a time). The oscilloscope recorded the wavelength as the sound passed through the sample; thus, the time taken was measured. Transverse and longitudinal velocities were then calculated using the thickness of the sample and the time measured from the oscilloscope (ASTM E 494-48 Standard). Figure 3.3 shows the formulas according to the ASTM E494-48 which were used to calculate the elastic constants.

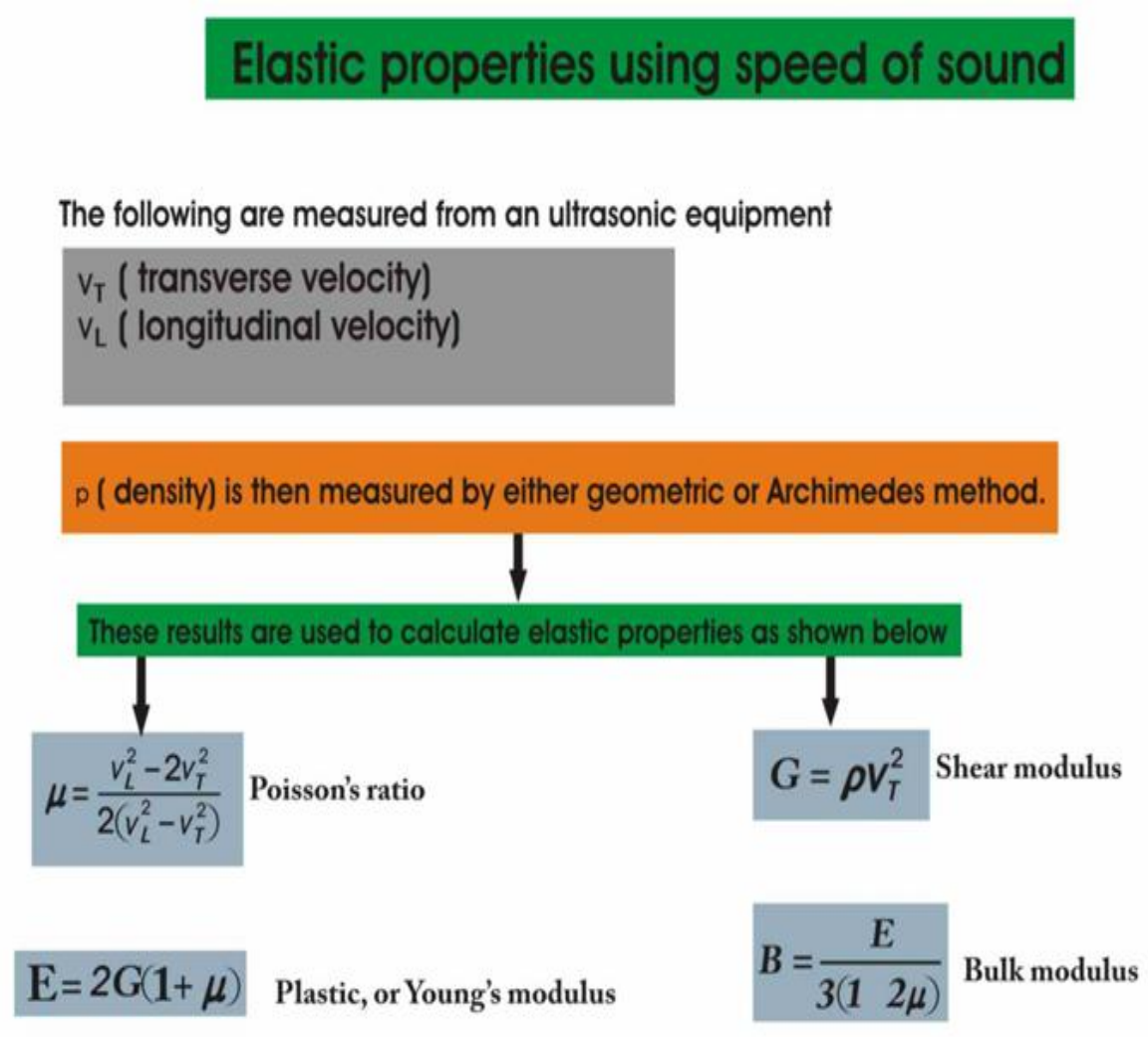

Figure 3.3 Elastic properties' formulas according to ASTM E494-48 standard

3.3.2.3 *Metallographic Analyses Procedures*

The Optical Microscope (OM) and the Scanning Electron Microscope (SEM) were used to reveal phases of the microstructure and also to observe the fabrication imperfections, such as voids and/or inclusions. Both as-laser sintered and heat treated samples were prepared for metallographic analyses using the standard methods, as explained in the

following steps below (ASTM F 136-96 wrought annealed standards; Leyens & Peters 2003: 11-12; Žitňanský & Čaplovič 2004: 781-787; Voort 2004; Matthew & Donachie 2000: 13-24).

1. Cross-sections of the DMLS Ti64 samples were cut using the Brilant 221 machine (Figure 3.4a) with the diamond cutting wheel at a cutting speed of 3200 rpm with a feed rate of 1.5 mm per min.
2. The cut DMLS Ti64 samples were mounted on the Cpal 450 machine. The mounted samples were then heated at temperatures between 100ºC and 200ºC, after which the machine turned off automatically.
3. Grinding and rough polishing were done using 380 to 1200 grit SiC on a Saphir 550 polishing machine (Figure 3.4b). Fine polishing was performed on a micro-cloth using 1 micron alumina, followed by final polishing with colloidal Silica. An ultrasonic cleaner was used before each polishing step and for the final cleaning of the samples.

(a) (b)

Figure 3.4 (a) Brilant 221 cutting machine; (b) Saphir 550 polishing machine

4. The samples were etched for 15-30 seconds using Keller's reagent (1 volume part Hydrofluoric acid; 1.5 volume part hydrochloric acid; 2.5 volume part nitric acid; and 95 volume parts water).

5. The revealed microstructures were then examined under the Leica DMI 5000 M Optical Microscope (Figure 3.5a); JSM-6510 SEM machine (Figure 3.5b); and Leica MZ 16A Stereo Microscope (Figure 3.5c). All the micrographs are shown in Appendix B, C, D, E and F.

(a) (b) (c)

Figure 3.5 (a) Leica DMI 5000 M optical microscope; (b) JSM-6510 SEM machine; (c) Leica MZ 16A stereo microscope

3.3.2.4 *Hardness Measurement of DMLS Ti64 Samples*

Macro hardness measurement of DMLS Ti64 samples used in metallographic analyses was measured using a Digital Low Load Tester. Hardness tests were done according to ASTM E 385-11e1 Standard, based on Hardness Vickers 'HV' (ASTM E 385-11e1 Standard).

3.3.2.5 *Determination of the Tensile Properties of DMLS Ti64 Samples*

Tension tests were performed according to the ASTM E8 / E8M standards, in order to evaluate the tensile properties of the sample, such as strength and ductility. DMLS Ti64 tensile samples were as follows:

- Set A consisted of four as-sintered samples (B1, B2, C1, and C2).
- Set B consisted of four samples (B4, B5, C4, and C5) which were heat treated in a vacuum furnace from 25°C to 1000°C; held/soaked at 1000°C for 1 hour thereafter; and cooled from 1000°C to 25°C in a furnace for 4 hours.
- Set C also consisted of four samples (D4, D5, E1 and E5) which were heat treated in the same way as set B, but cooled for 34 hours.

Samples were each mounted on an Instron 50 kN (model 1342) tension testing machine. Samples were pulled at a constant rate of 5 mm/min until fracturing occurred. The tensile test measured the load (force) against the elongation (displacement) (ASTM E8 / E8M - 11 Standard). The force and change in length during the experiment were recorded and used to calculate engineering stress and strain. The formulas used to calculate engineering stress (σ) in MPa and engineering strain (ε) in mm/mm are shown in equations 3.2 and 3.3.

$$\boldsymbol{\sigma = \frac{F}{Ao}} \quad \textbf{\textit{Equation 3.2}}$$

$$\boldsymbol{\varepsilon = \frac{\Delta L}{Lo}} \quad \textbf{\textit{Equation 3.3}}$$

Where,

ΔL is the displacement;

L_o is the initial length of the sample;

F is the applied force; and

A_o is the initial area of the sample.

The relationship between engineering stress and strain is only valid before necking in an elastic region; therefore, to get the correct relationship in the plastic region, true stress and strain were calculated from engineering stress and strain. This relationship between engineering values and true values is given in equations 3.4 and 3.5.

$$\sigma_{true} = \sigma(1 + \varepsilon) \quad \textit{Equation 3.4}$$

$$\varepsilon_{true} = In\,(1 + \varepsilon) \quad \textit{Equation 3.5}$$

Where'σ' and 'ε' are the engineering stress and strain respectively, the 'σ_{true}' and 'ε_{true}' are the true stress and strain, respectively. For determining the plastic strain ($\varepsilon_{plastic}$), equation 3.6 was used and 'E' is Young's Modulus (Meyers & Chawla 1999: 71-76; Sander & Weintraub 2000; Philpot 2010: 1-54).

$$\varepsilon_{plastic} = \varepsilon_{true} - \frac{\sigma true}{E} \quad \textit{Equation 3.6}$$

3.3.2.6 *Heat Treatment Procedure for DMLS Ti64 Samples*

The results from the characterisation of the EOS Ti64 powder revealed that the material used was alpha-beta type and it was Ti-6Al-4V. Therefore, heating temperatures were selected based on a schematic phase diagram of Ti64 alloy (Figure 2.2, page 16). First, heat treatment regimens were investigated in order to determine the heat treating temperature and suitable cooling rate for the increase of ductility of the DMLS Ti64 samples.

Different heating temperatures and cooling rates lead to different microstructures which can either be fine or coarse. A horizontal carbolite tube furnace (Figure 3.6) was used. Titanium has a strong tendency to react with oxygen, carbon and nitrogen (Leyens & Peters 2003: 4-32). Therefore, the heat treating atmosphere in a horizontal carbolite tube furnace was filled with argon gas. The samples were soaked at the selected temperature for an hour, and then cooled using cooling rates as shown in Table 3.2. The microstructures were revealed, together with hardness measure for all samples as shown in Table 3.2. These results were used to determine the heat treatment regimen that will be studied further in the second heat treatment.

Figure 3.6 The horizontal carbolite tube furnace

Table 3.2 First heat treatment regimes done using horizontal carbolite tube furnace

Sample Label	**Temperature**	**Soaking Time**	**Cooling rate**
A	700^{o}C	1 hour	Water Quench (WQ)
B	700^{o}C	1 hour	Air quench (AQ)
C	700^{o}C	1 hour	Furnace Cool (FC)
D	1000^{o}C	1 hour	Water Quench (WQ)
E	1000^{o}C	1 hour	Air quench (AQ)
F	1000^{o}C	1 hour	Furnace Cool (FC)
G	1100^{o}C	1 hour	Water Quench (WQ)
H	1100^{o}C	1 hour	Air quench (AQ)
I	1100^{o}C	1 hour	Furnace Cool (FC)

For the first heat treatment regimens both water quenched and air cooled samples had a layer that indicated contamination by interstitial elements, such as nitrogen, carbon and oxygen. Samples were gold-like in colour. This indicated that even though

samples were heat treated in an argon atmosphere there was some contamination that did happen perhaps, during water quenching and air cooling as samples were taken out of the furnace while were still on high temperature. The furnace cooled samples did not show any contamination.

Overall, with the different heat treatment temperatures, high hardness values were obtained in samples that had undergone water quenching followed by air cooled ones. Therefore, both air cooling and water quenching were disregarded as the correct cooling rates for the present case. Higher heat treatment temperatures, even though there was a decrease in hardness at lowest cooling rate (furnace cool), were also disregarded because it is believed that the elevated hardness values were due to the difference in orientation of the alpha and beta laths in one grain. Lower hardness values were obtained from the samples heat treated at 1000ºC which were furnace cooled. This due to the coarse microstructure, compared to all other heat treatment temperatures. It was then concluded that the best heat treatment procedure was beta annealing at 1000ºC, which is only slightly higher than the beta-transus for the Ti64 alloy. Heat treatment was carried in vacuum furnace (Figure 3.7) to control the atmosphere, which proved to be working, as there were no colour changes on the samples after heat treatment in the vacuum furnace. The cooling rate considered was furnace cool, which was regarded as the lowest cooling rate.

The second regimens of heat treatments were conducted, as indicated in Table 3.3. The temperature selected was 1000ºC which is just below the beta-transus temperature of 1050^{o}C. Temperature selection was done using a schematic phase diagram of Ti64 alloy (Figure 2.2, page 16). A furnace cooling was also used as the cooling rate, based on the results obtained from the first heat treatment experiments. A vacuum furnace (Figure 3.7) was also used. Samples were cleaned with methanol using ultrasonic bath in order to eradicate all impurities, such as oil. Heat treatment was then followed by a tensile test. The same procedures as mentioned in Section 3.3.2.5, page 45-46, were deployed when performing the tensile test. After the tensile test, specimens were cut and prepared as mentioned in Section 3.3.2.3, page 42-44 for metallographic analysis.

Table 3.3 Second heat treatment regimens done using a vacuum furnace

Sample Label	**Temperature**	**Soaking Time**	**Cooling rate**
B1 B2 C1 C2	1000^{o}C	1 hour	Furnace Cool (FC) for 4 hours
B4 B5 C4 C5	1000^{o}C	1 hour	Furnace Cool (FC) for 34 hours

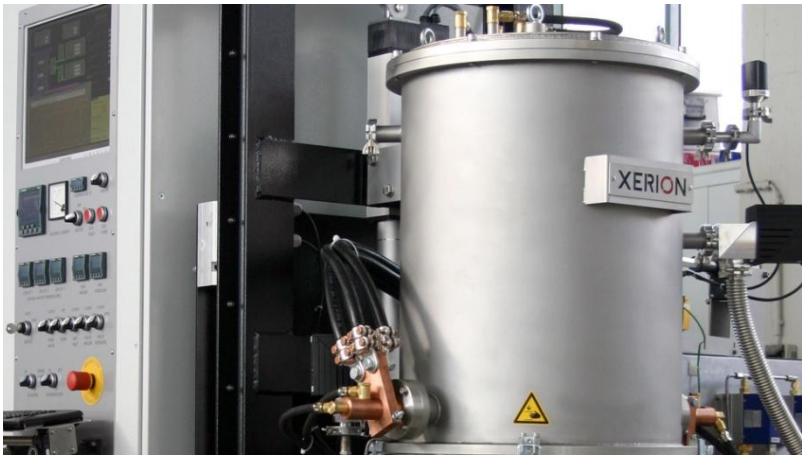

Figure 3.7 Xerion vacuum furnace

3.4 ABAQUS™ Finite Element Analysis Approach

3.4.1 DMLS Ti64 Samples Property Calibration

The following steps were performed on the ABAQUS™ FEA program in order to model the DMLS Ti64 samples:

1. The geometry of the part was created in the ABAQUS™ FEA program (Figure 3.8 and 3.9).

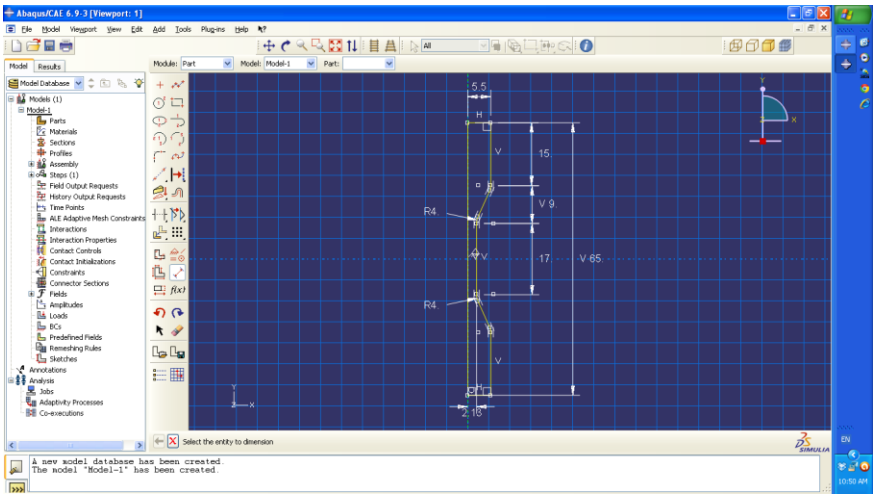

Figure 3.8 Sketch of test specimen

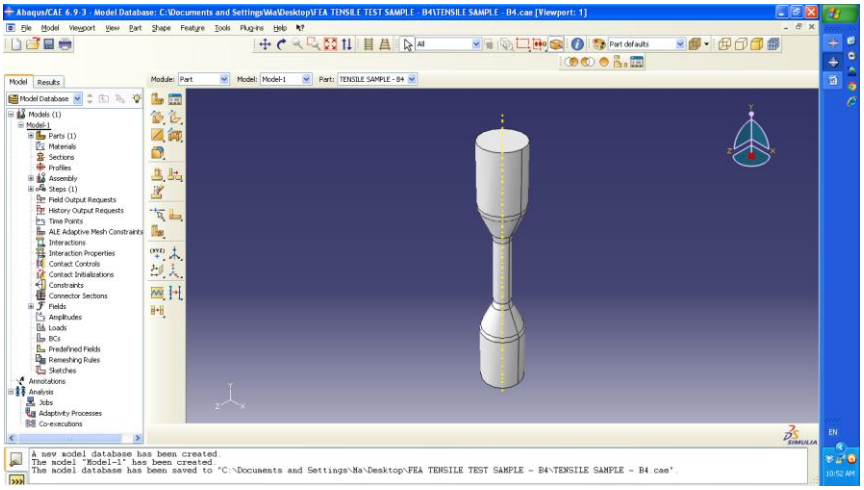

Figure 3.9 Created part revolved around centre line

2. The elastic input data, such as Young's modulus, Poisson's ratio and density are from ultrasonic and density test results, as illustrated in Table 4.3 chapter 4, page 74. See Figure 3.10 and 3.11 for elastic input data in the ABAQUS™ FEA program.

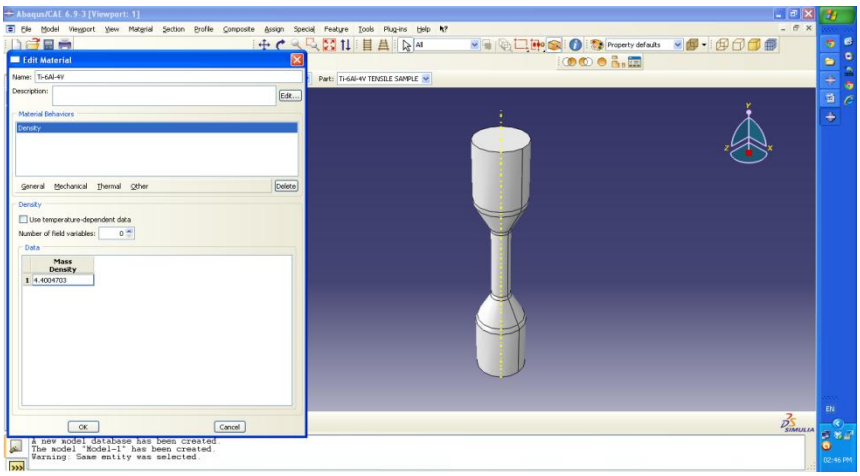

Figure 3.10 General material properties inserted into ABAQUS™

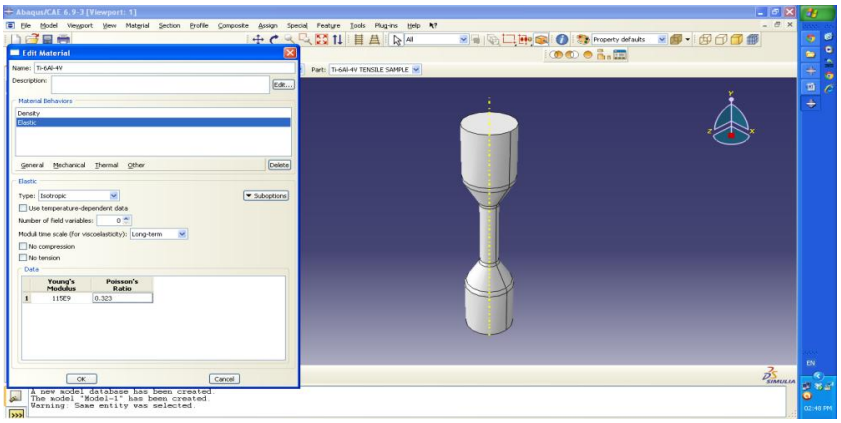

Figure 3.11 Elastic material properties inserted into ABAQUS™

3. The true yield stress, the true ultimate tensile stress and plastic strain were calculated using equations 3.4, 3.5 and 3.6 page 46, as previously mentioned and were used as input plasticity data in the plasticity model (Figure 3.12).

4. From the shape of the stress-strain graphs as illustrated in Appendix H (H1, H2 & H3), it can be seen that hardening increased with increased plastic strain. Therefore, an isotropic hardening model was adopted for the FEA modelling.

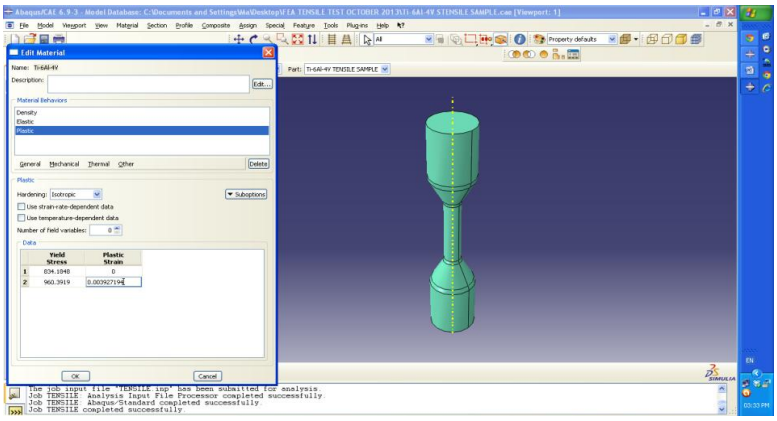

Figure 3.12 Plastic material properties inserted into ABAQUS™

5. The sections were created, on ‘Plane Stress Properties’, and ‘Solid’ was selected as the category, while for the type ‘Homogeneous’ was chosen. Then the material was assigned to the specimen (Figures 3.13, 3.14 and 3.15).

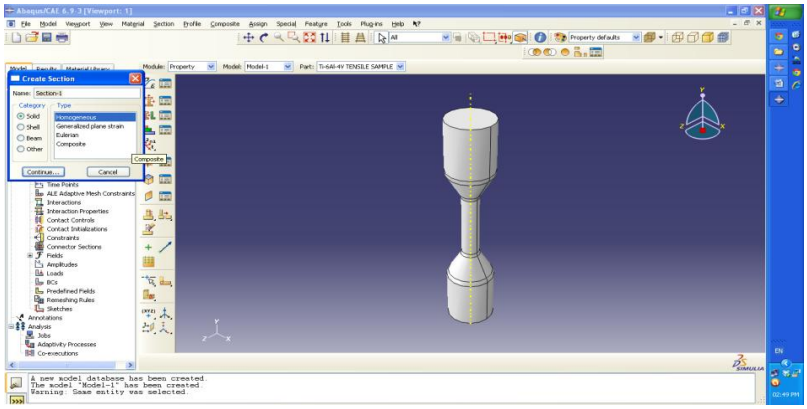

Figure 3.13 Material section created

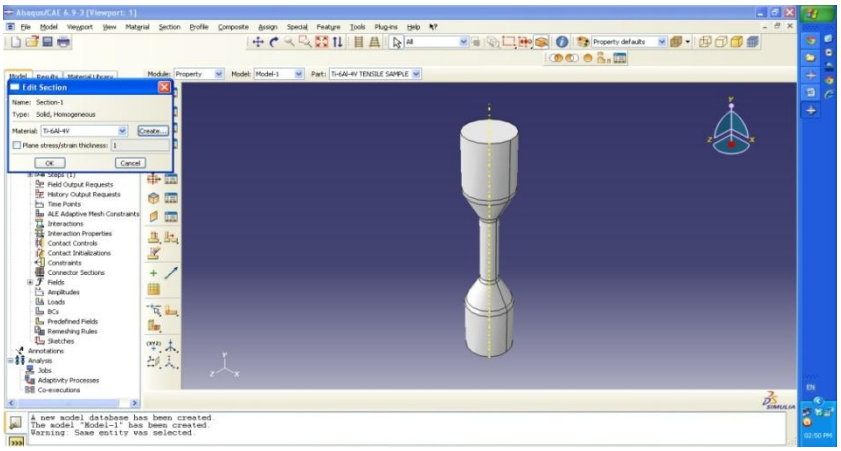

Figure 3.14 Material section created

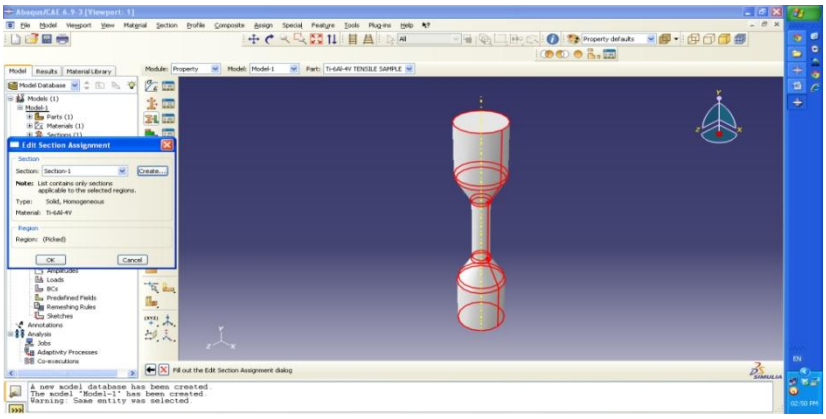

Figure 3.15 Material properties assigned to the test specimen

6. The boundary conditions created for FEA to simulate the tensile test were based on the tensile test apparatus. The reference point created at one end was indicated as a fixed point (Figure 3.16) of the specimen and was fixed from displacing or rotating in the x, y, and z direction. The other reference point indicated as load point (Figure 3.17) of the specimen was fixed from displacing or rotating in the x and z direction but allowed movement to be only in y direction.

This simulates the specimen being threaded into the test apparatus where it would not be able to deflect, rotate, or translate.

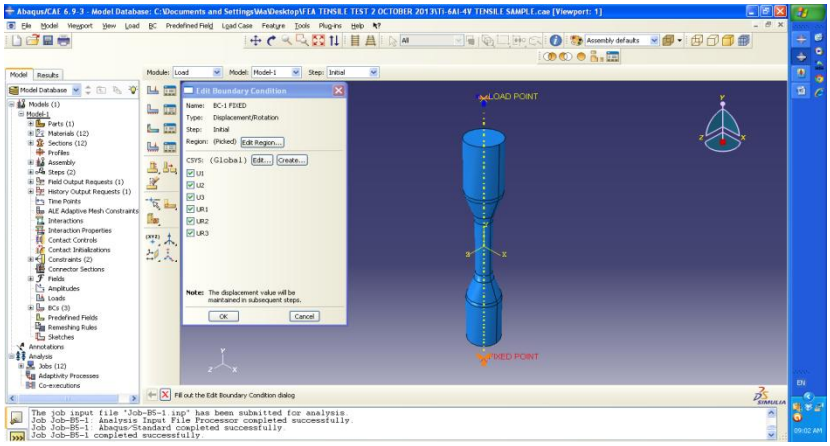

Figure 3.16 Fixed boundary conditions

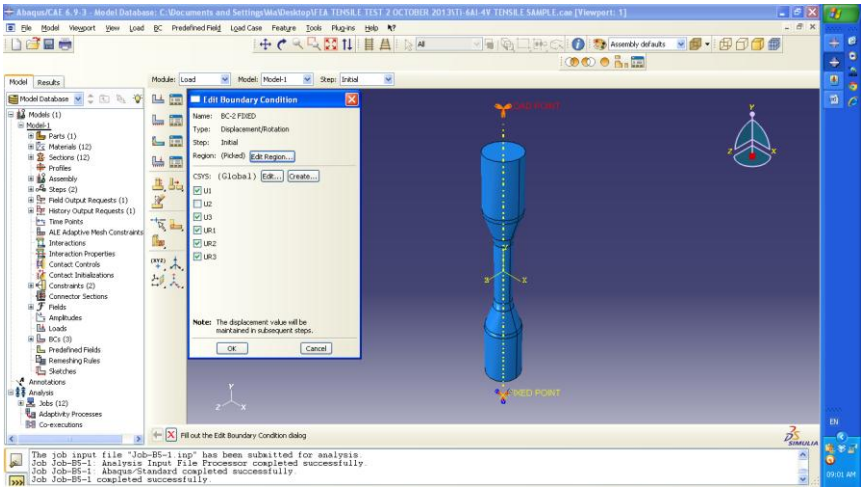

Figure 3.17 Fixed boundary conditions

7. Then, on a load point, as indicated in Figure 3.18, the sample was pulled in y-direction until the maximum stress was reached.

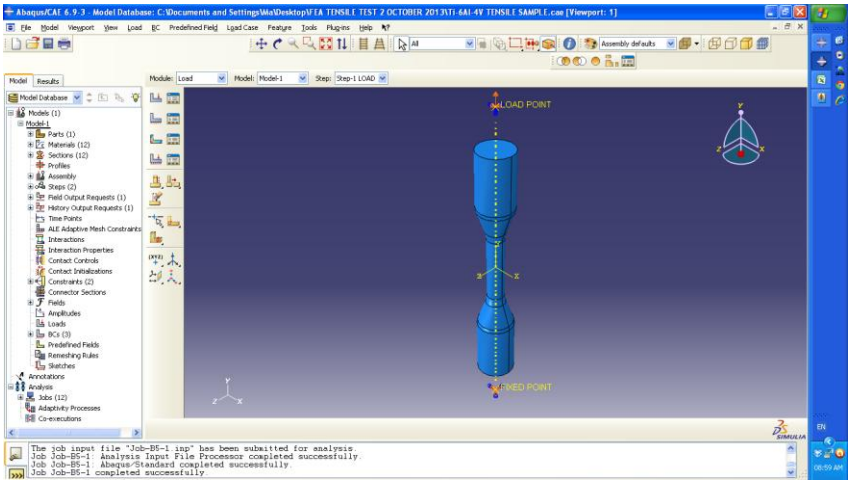

Figure 3.18 Tensile load applied

8. Mesh was created. On the mesh control menu, Tetrahedron (tet) mesh was selected as the element shape (Figure 3.19).

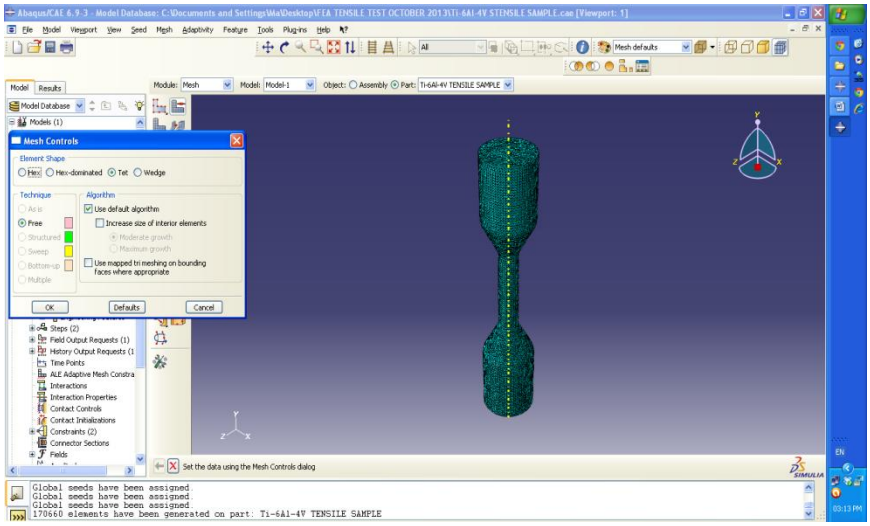

Figure 3.19 Mesh element shape created

9. The coarse and fine meshes were also developed in order to check mesh convergence of the note. A mesh density study was performed by changing the

seed size of each element, running the analysis and viewing the results to see if the forces changed with the change in seed size. This was done until there was no significant change in force. The final element size for meshing the test specimen was 0.5 mm as illustrated in Figure 3.20.

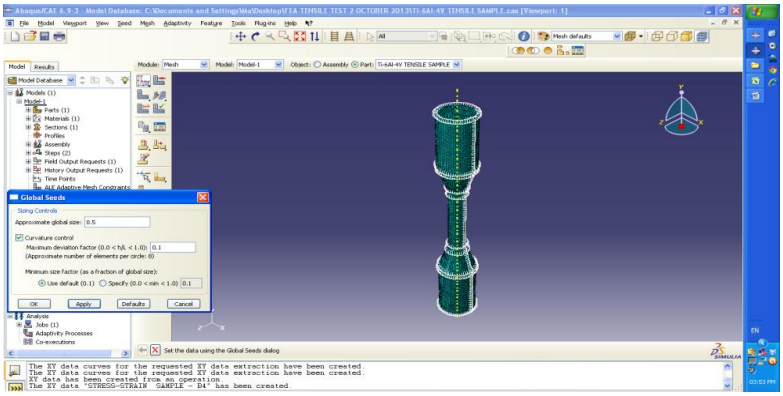

Figure 3.20 Seed size created

10. The job was created and submitted for analysis (Figure 3.21).

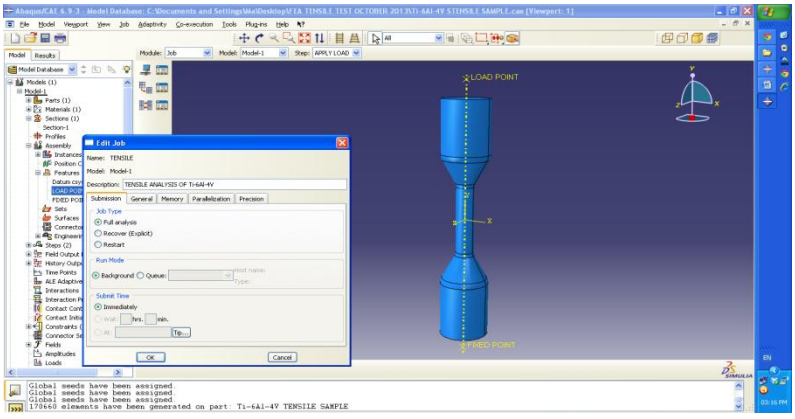

Figure 3.21 Job created and submitted for analysis

11. The experimental load-extension curve was compared to the simulated load-extension curve for the calibration of the DMLS Ti64 samples. In order to obtain a correct and accurate simulated load-extension curve, the trial-and-error method was used, based on previous research (Bao 2003: 84-86). This method compares the load-extension curves of the experiment to those of simulation, then calculates the relative error of the force. This error is then adjusted in the material data during simulation. The trial-and-error method is repeated until the relative error becomes small (Bao 2003: 84-86). The simulated load and extension data were extracted from the ABAQUS^{TM} FEA program in Excel format in order to be drawn in the same axis with the experimental ones for comparison purposes. Figures 3.22 and 3.23 compare the experimental and simulated force-extension curves before and after calibration. It was found that the simulated results are about 0.05% lower than the experimental ones; this might be due to the small reaction forces found during simulation in both the x and z directions. Once the model was calibrated, it was applied to twelve (12) DMLS Ti64 samples in order to analyse the yield failure based on Von Mises stress.

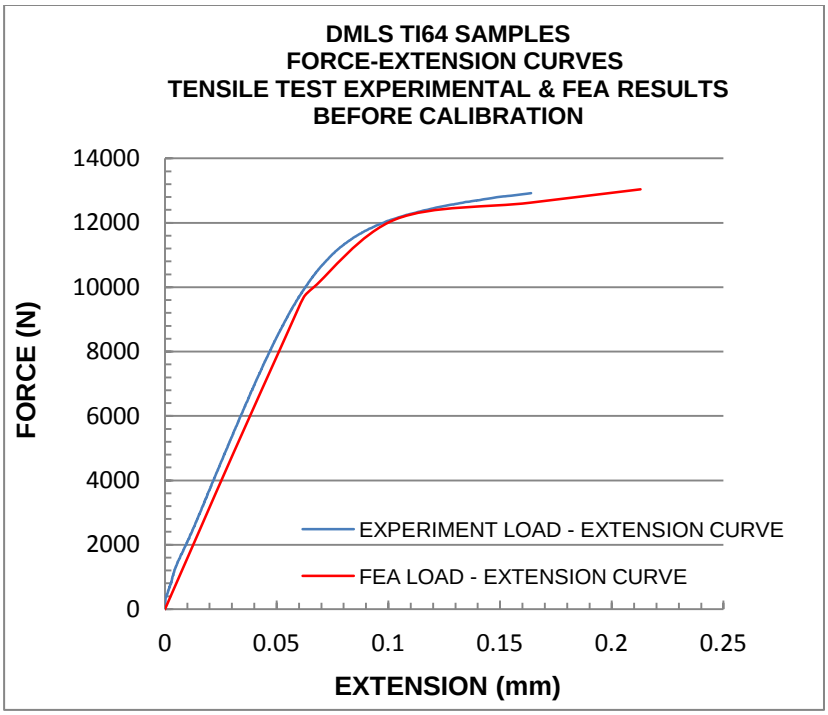

Figure 3.22 Force-extension curves from experimental and simulation results before calibration

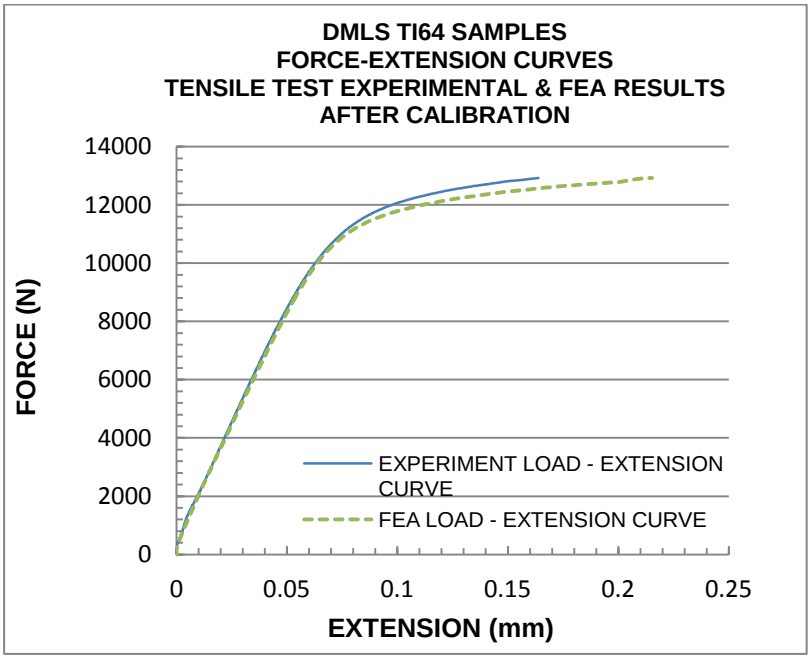

Figure 3.23 Force-extension curves from experimental and simulation results after calibration

3.4.2 Simulation of Tensile Test on both As-laser Sintered and Heat Treated DMLS Ti64 Samples

The FEA model was calibrated using the trial-and-error method. Thereafter, a simulation of tensile test was conducted. The ABAQUS^{TM} FEA was performed based on the tensile test results of the three sets. Set A consisted of four as-laser sintered samples (B1, B2, C1, & C2). Set B consisted of four samples (B4, B5, C4, & C5) which were heat treated in a vacuum furnace at 1000°C, soaked for 1 hour and cooled in a furnace for 4 hours. Set C also consisted of four samples (D4, D5, E1 & E5) which were heat treated in the same way as set B, but cooled for 34 hours.

The material technical data used for the three sets mentioned above are indicated in Table 3.4. The elastic data of the entire sample were the same. The elastic input data used were Young's Modulus of 115 GPa, Poisson's Ratio of 0.323 (adapted from the elastic constant results; chapter 4 Table 4.3, page 72 and in Appendix A) and density of 4.4 g/cm^3 (considered from density test results; Table 4.3 chapter 4, page 72 and in Appendix A). The plasticity data, such as true yield stress, true ultimate tensile stress and plastic strain used for each sample differed and was based on the tensile test and calculations done using equations 3.4, 3.5 and 3.6 on page 46.

Table 3.4 Input material data used in the ABAQUS™ FEA program

GENERAL PROPERTY	ELASTIC DATA	
Density [g/cm3]	Young's Modulus [GPa]	Poisson's Ratio
4.4	115	0.323
PLASTIC DATA		
Sample Label	True Yield Stress [MPa]	True UTS Stress [MPa]	Plastic Strain [mm/mm]
NO HEAT TREATMENT			
B1	991	1210	0.000162
B2	1007	1150	0.000147
C1	1030	1211	0.000163
C2	1025	1239	0.000170
HT1000, SOAK 1HR, FC 4HRS			
B4	835	960	0.003927
B5	840	964	0.003885
C4	823	956	0.004004
C5	833	950	0.004563
HT1000, SOAK 1HR, FC 34HRS			
D4	813	922	0.004591
D5	810	916	0.004378
E1	814	929	0.004503
E5	805	913	0.004655

Once the analysis was done, the Von Mises stress results were viewed as tabulated in the form of colour-coded contour plots; then followed the stress-strain graphs. The stress and strain data from the ABAQUS^{TM} FEA program were also extracted in Excel format and copied to MDSolid program for results interpretation. The results are explained in chapter 4.

Chapter 4. RESULTS

4.1 Introduction

Knowledge of the microstructure and mechanical behaviour of DMLS Ti64 samples is essential if the material is to be used in the design of engineering components. Additionally, the mechanical properties of DMLS Ti64 samples are limited due to the fact that this technology is relatively new. In this chapter, the results of characterising EOS Ti64 powder and DMLS Ti64 samples will be presented. The results will include: powder particle analyses; density measurements; elastic constants; tensile properties; as well as results of failure due to yielding.

4.2 Characterisation of EOS Ti64 Powder

The morphology of the EOS Ti64 powder particles was found to be spherical in shape (Figure 4.1). This is typical of powders produced by the gas-atomisation process (Simchi 2006: 148-158). The powder was produced and optimised by the EOS GmBH company for the DMLS process. The spherical morphology is preferred in DMLS production process (Simchi 2006: 148-158; Simachi & Pohl 2003: 119-128; Leyens & Peters 2003: 7-32).

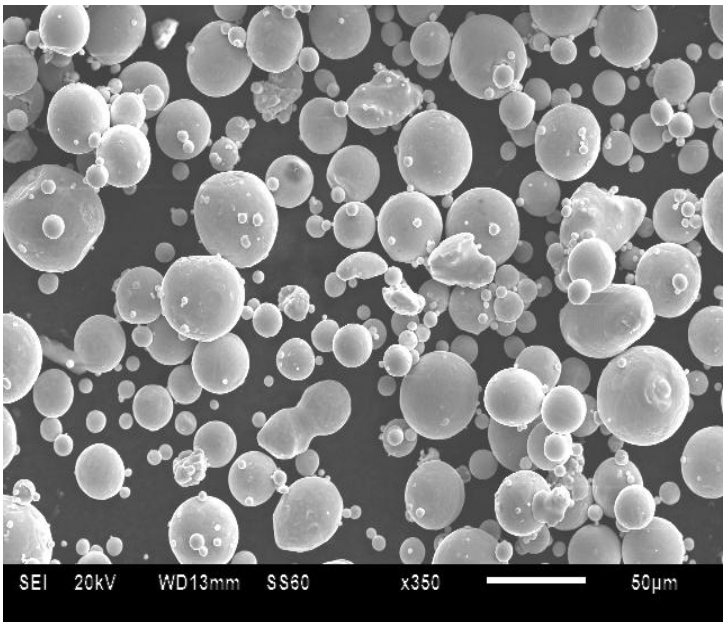

Figure 4.1 SEM-EDX micrograph of EOS Ti64 powder indicating the particles' shape

Figure 4.2 shows the particle size distribution measured by the Malvern particle analyser. The particle size distribution ranged from 10µm to approximately 100 µm.

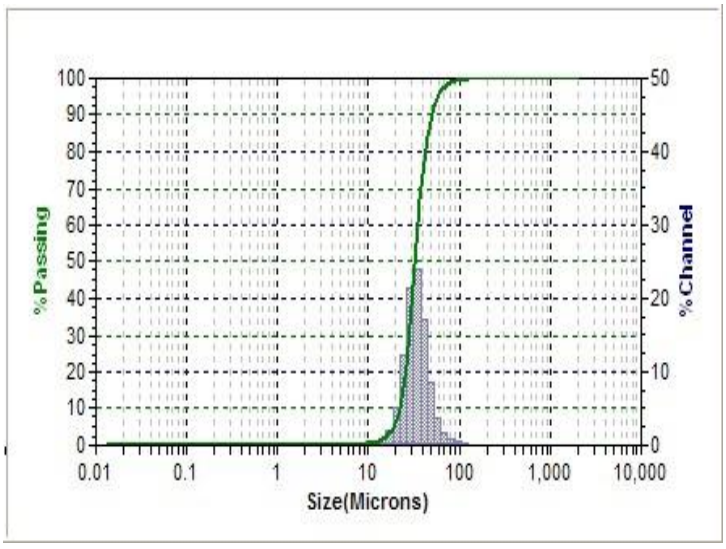

Figure 4.2 The particle size distribution of the EOS Ti64 powder

The percentage distribution size as presented in Table 4.2, indicates 10 percent of powder particles to be 22.2 µm, 32.6 µm, and 48.7 µm for 50 percent and 90 percent, respectively. Owing to the narrow particle size and a spherical shape, better densification is expected. There should be a good powder flow-ability and undisrupted powder transport during the DMLS process.

Table 4.1 Percentiles particle size of EOS Ti64 powder

Percentiles (%)	**Particle Size (um)**
10	**22.2**
20	**25.7**
30	**28.1**
40	**30.4**
50	**32.6**
60	**35.1**
70	**37.9**
80	**41.8**
90	**48.7**
95	**56.8**

The SEM-EDX analysis as shown in Table 4.1 represents the chemical composition of EOS Ti64 powder. The results were compared to those of wrought annealed Ti-6Al-4V alloy and to the EOS GmbH manufacturer. Both aluminium and vanadium values were within the range and there is no contamination on the material, as all the interstitial elements are within the required concentration.

Table 4.2 The chemical composition of EOS Ti64 powder compared to those of wrought annealed Ti-6Al-4V alloy and EOS GmbH material data sheet

Element	**EOS Ti64 powder** *[Experimental results]*	**Wrought annealed Ti-6Al-4V alloy parts** *[Based on ASTM F1472-08$^{\varepsilon 1}$ Standard]*	**EOS as-laser sintered Ti64 samples** *[Based on EOS GmbH Material Data Sheet 2011: 3]*
Ti	Balance	Balance	Balance
Al	5.52-5.75	5.5 -6.75	5.5 -6.75
V	3.71-4.19	3.5 -4.5	3.5 -4.5
Other elements such as Nitrogen (N), Carbon (C), Oxygen (O), Hydrogen (H) and Iron (Fe)	>0.4	>0.4	>0.4

The X-Ray diffraction pattern of EOS Ti64 powder is shown in Figure 4.3. Reflections of alpha phase and alpha+beta phases were detected in the diffraction pattern. The

intensity of alpha+beta phase was much higher than that of alpha phase. No traces of beta phase were visible. The major phase as identified was the alpha+beta phase.

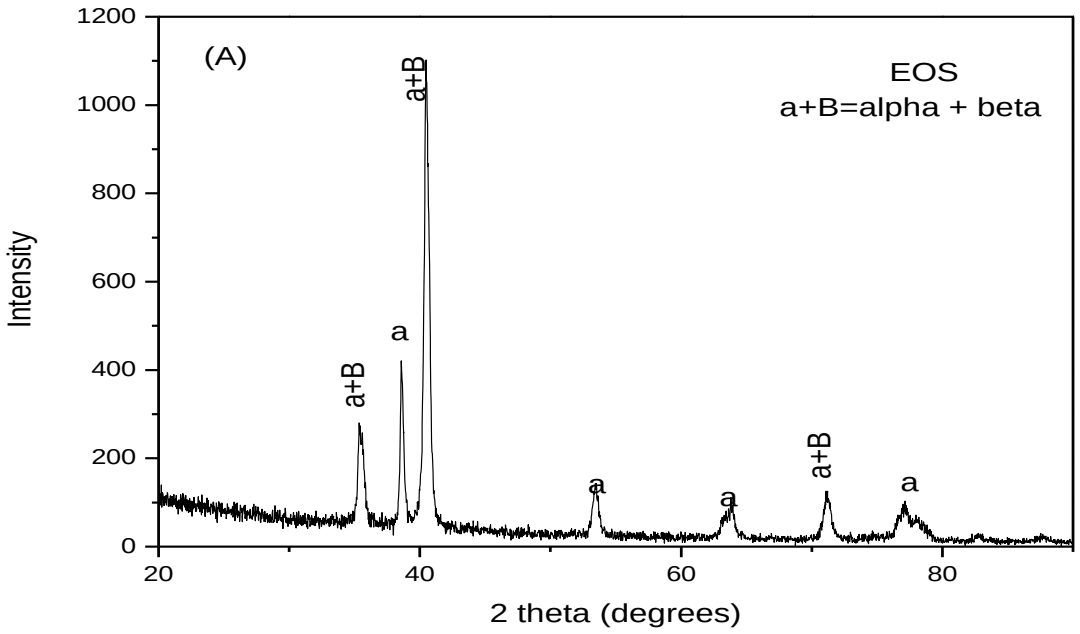

Figure 4.3 X-ray diffraction pattern indicating phases present in EOS Ti64 powder

4.3 Characterisation Results of As-laser Sintered Ti64 Samples

4.3.1 Metallographic Analyses Results

Microstructures studied using OM and SEM revealed the presence of fabrication imperfections, such as voids and/or inclusions, even though they were not quantified as

it was not part of this study. However, these findings can be investigated further in future studies, as voids affect mechanical properties. Figure 4.4 shows islands of martensitic plates. Fine plates of martensite with an average size in the nano-range (known as alpha prime) are clearly seen in the SEM photo micrograph in Figure 4.5. These fine micro-structural features are considered to be due to the high cooling rates experienced during laser sintering. During the DMLS process, layers of powder are heated up to melting temperatures by the laser and then quickly cooled. As more powder layers are added and immediately laser sintered, the resulting part/component has a quenched microstructure. Therefore, the DMLS process results in a martensitic, non-equilibrium structure.

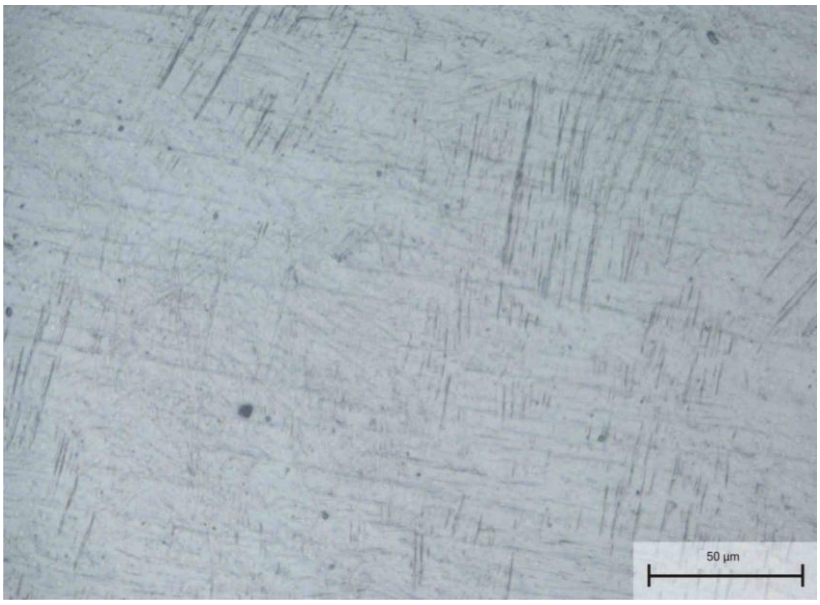

Figure 4.4 OM micrograph at 50 µm showing microstructure of as-laser sintered Ti64 samples

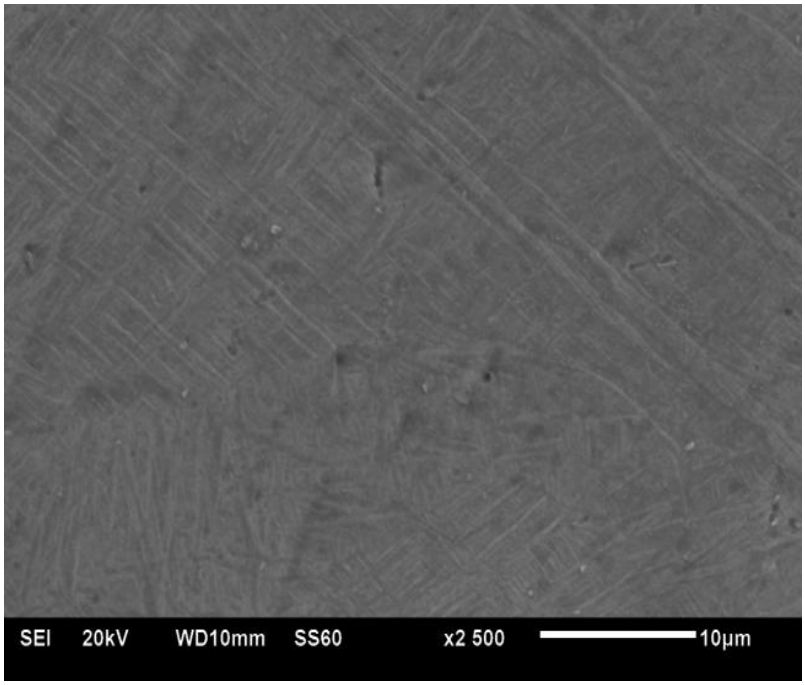

Figure 4.5 SEM micrograph at 10 µm showing microstructure of as-laser sintered Ti64 samples

4.3.2 Macro Hardness Measurement of As-laser Sintered Ti64 Samples

Macro hardness of the same sample used for metallographic analyses was measured according to Hardness Vickers "HV" as per ASTM E 385-11e1 Standard. The martensitic non-equilibrium structure of as-laser sintered Ti64 samples has an average macro hardness of 344 HV and standard deviation of 1.43. Figure 4.6 shows some results, while detailed results are illustrated in Appendix G.

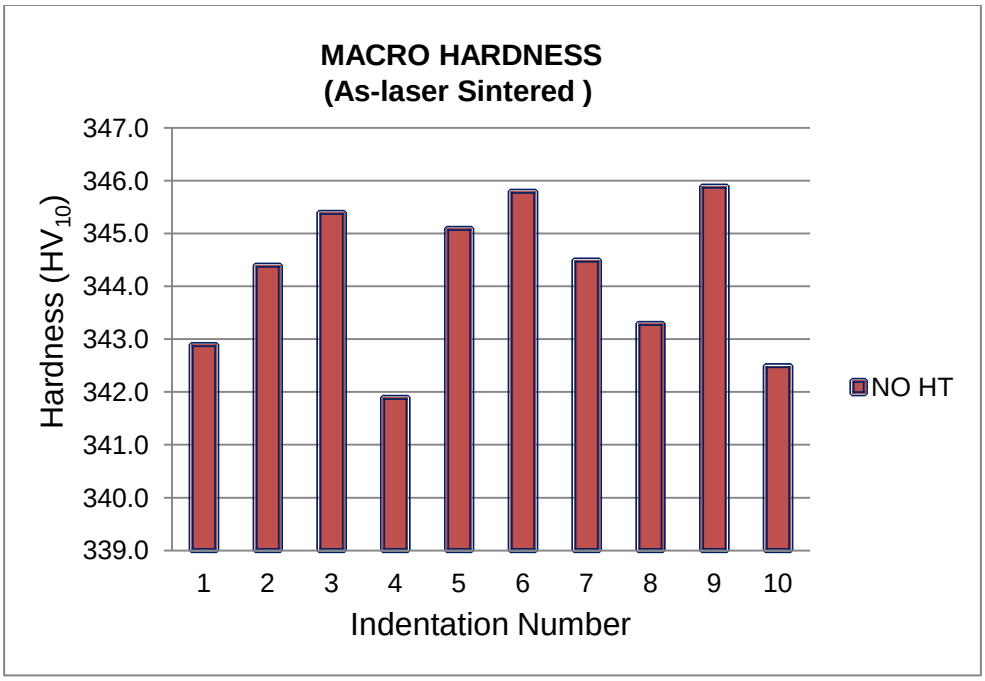

Figure 4.6 Macro hardness of as-laser sintered Ti64 samples

4.3.3 Density Measurement of As-laser Sintered Ti64 Samples

The density was determined based on the Archimedes' principle. The average density of these samples was found to be 4.4 g/cm^3 with a standard deviation of 0.02. The recorded values are shown in Appendix A.

4.3.4 Elastic Constants Measurements of As-laser Sintered Ti64 Samples

Elastic constants of samples were measured according to the ASTM E494-48 using an ultrasonic pulse echo technique on the Krautkramer USIP12 machine. The average and standard deviation of elastic constants of the twelve (12) as-laser sintered Ti64 samples

obtained are shown in Table 4.3. The recorded and calculated values are shown in Appendix A.

Table 4.3 The mean and standard deviation of elastic constants of as-laser sintered Ti64 samples

	Density [g/cm^3]	Poisson's Ratio	Shear Modulus G [GPa]	Young's Modulus E [GPa]	Bulk Modulus K [GPa]
Mean	4.4	0.323	44	115	108
Standard Deviation	0.02	0.01	0.25	0.64	0.32

4.3.5 Tensile Properties of As-laser Sintered Ti64 Samples

Tensile properties of four (4) as-laser sintered Ti64 samples are shown in Table 4.4. The average values of yield stress (at 0.2% offset) of 1005 MPa and the ultimate tensile stress of 1190 MPa were found. A percentage elongation and a percentage area reduction of 2.6 and 3.51% respectively, were also found.

Table 4.4 Tensile properties of as-laser sintered Ti64 samples

	Tensile Stress at Yield (0.2 % Offset) [MPa]	Ultimate Tensile Stress [MPa]	Elongation [%]	Area Reduction [%]
Mean	1005	1190	2.6	3.51
Standard Deviation	17.44	36.64	0.55	1.72

4.4 Characterisation Results of the DMLS Ti64 Samples: First Heat Treatment Regimens Done Using Horizontal Carbolite Tube Furnace

First, experiments were performed in order to relate microstructure and hardness, so as to choose an appropriate heat treatment method when inducing ductility. It is through heat treatment that two well known microstructures that exist in the alpha-beta type can be produced. In these microstructures, the size of the alpha grain, play a major role in controlling the maximum dislocation slip length. The effect of temperature on microstructures and hardness is illustrated in Figures 4.7 to 4.29.

4.4.1 Heat Treatment DMLS Ti64 Samples Done at 700ºC and Cooled at Different Cooling Rates

Heat treatment was done at 700ºC which is a temperature much lower than the beta-tansus where diffusion rates are lower. Figures 4.7, 4.8 and 4.9 showed very fine plates of martensitic. Figures 4.8 and 4.9 show a gold-like colour which indicates the contamination of interstitial elements. More of the photo micrographs for both samples cut in transverse and those cut in longitudinal are shown in Appendix C. The hardness obtained in all samples heat treated at 700ºC are illustrated in Figure 4.10 and Table 4.5, while detailed results are shown in Appendix G. The mechanical properties of Ti64 alloy are strongly influenced by the grain size as indicated by the well-known Hall-Petch Relation. The lower heat treatment temperature (700ºC) did not show much difference on the microstructure of the as-laser sintered samples. The microstructure is

still very fine and according to the Hall-Petch Relation, high hardness values are expected and therefore confirmed by high values of hardness found. The increasing rate of cooling after heat treatment at 700ºC does not show any significant change in the microstructural features as well.

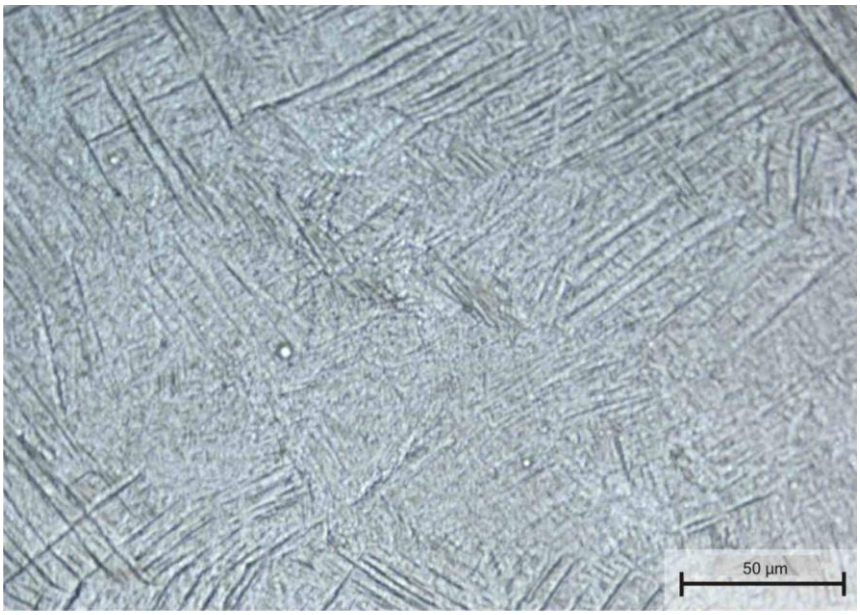

Figure 4.7 OM micrograph of at 50 µm showing microstructures of DMLS Ti64 samples heat treated at 700ºC, soaked for 1 hour then furnace cooled

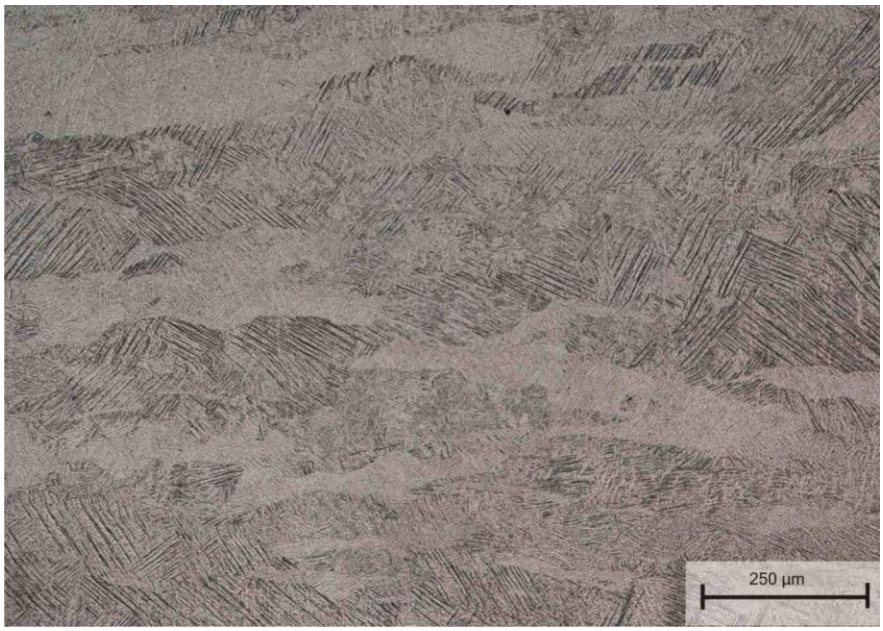

Figure 4.8 OM micrograph of at 250 µm showing microstructures of DMLS Ti64 samples heat treated at 700ºC, soaked for 1 hour then air cooled

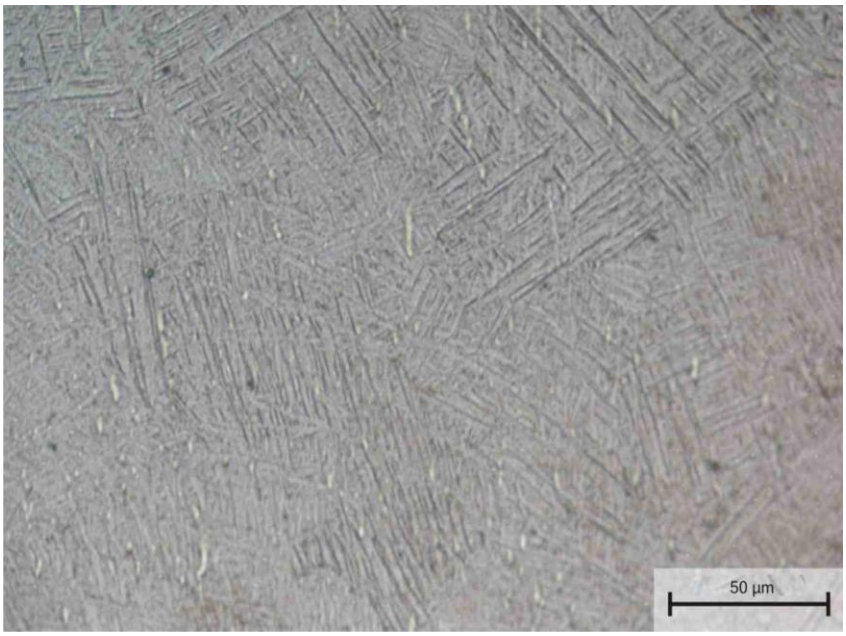

Figure 4.9 OM micrograph of at 50 µm showing microstructures of DMLS Ti64 samples heat treated at 700ºC, soaked for 1 hour then water quenched

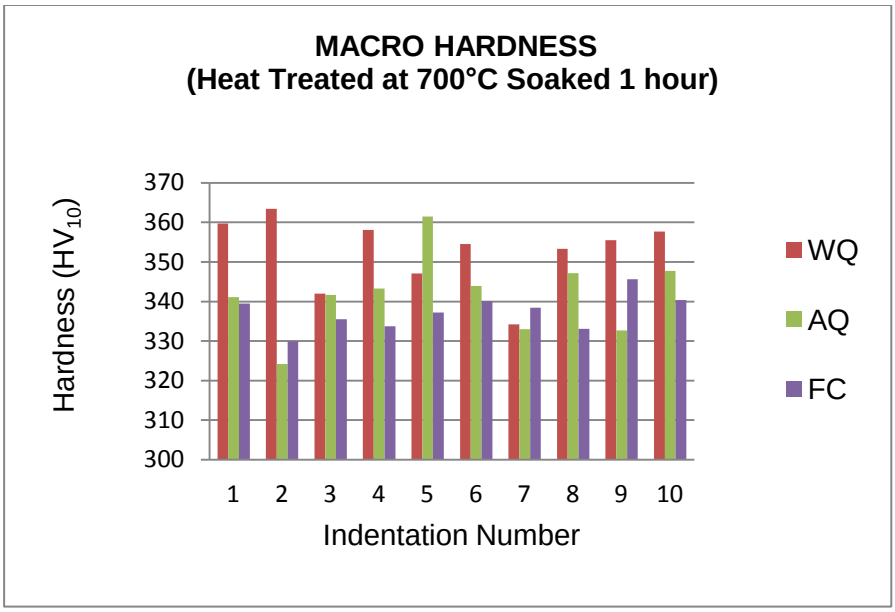

Figure 4.10 Macro hardness of DMLS Ti64 samples heat treated at 700ºC and cooled at different cooling rates

Table 4.5 Average macro hardness of DMLS Ti64 samples heat treated at 700ºC and cooled at different cooling rates

	HT at 700ºC/1hr/ FC	HT at 700ºC/1hr/ AQ	HT at 700ºC/1hr/ WQ
Average	337	342	353
Standard Deviation	4.51	10.21	8.92

4.4.2 Heat Treatment of DMLS Ti64 Samples Done at 1000ºC and Cooled at Different Cooling Rates

A second heat treatment was done at 1000^{o}C which is a temperature just lower than a tranus temperature of 1050^{o}C. OM photo micrographs (Figure 4.11, 4.12 & 4.13) show

that the very fine martensitic microstructure changed to a coarser alpha colony with a beta phase on the grain boundaries. The slowest cooling rate (furnace cool) resulted in a fully lamellar microstructure comprising colonies of parallel alpha laths separated by beta laths which are in different lath orientation. The grain sizes are larger and the grain boundaries consist of a globular alpha phase. These were observed clearly in the SEM photo micrographs (Figure 4.14 at 10 µm). The photo micrographs for both samples cut in transverse and those cut in longitudinal are shown in Appendix D. It was also observed that the hardness decreased with the increase in the cooling rate from 344 to 301 HV, considering furnace cooling as the lowest cooling rate. Figure 4.15 and Table 4.6 show the hardness obtained in heat treatment done at 1000ºC. A gold-like colour was seen on the surface of the specimens cooled with air and water quench.

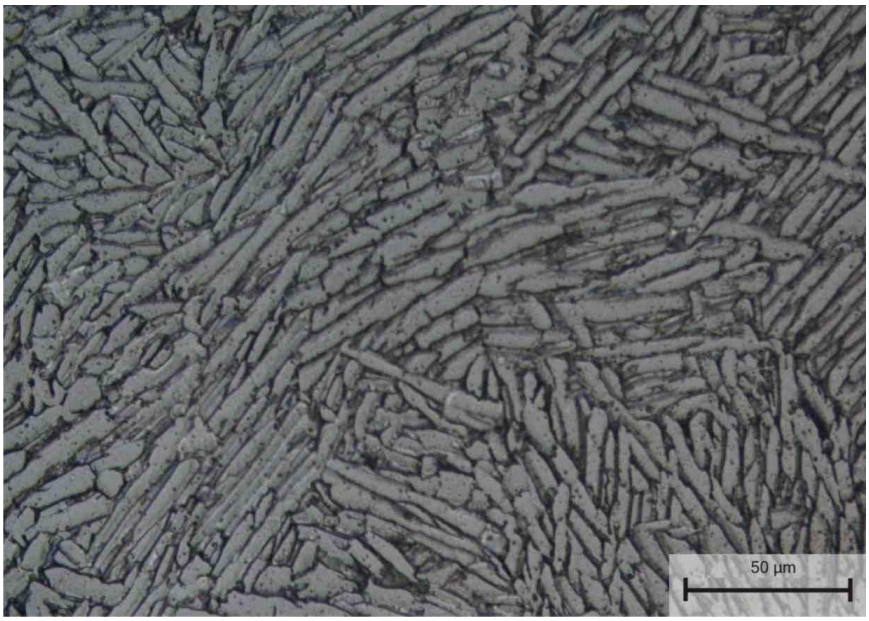

Figure 4.11 OM micrograph at 50 µm showing microstructures of DMLS Ti64 samples heat treated at 1000ºC, soaked for 1 hour then furnace cooled

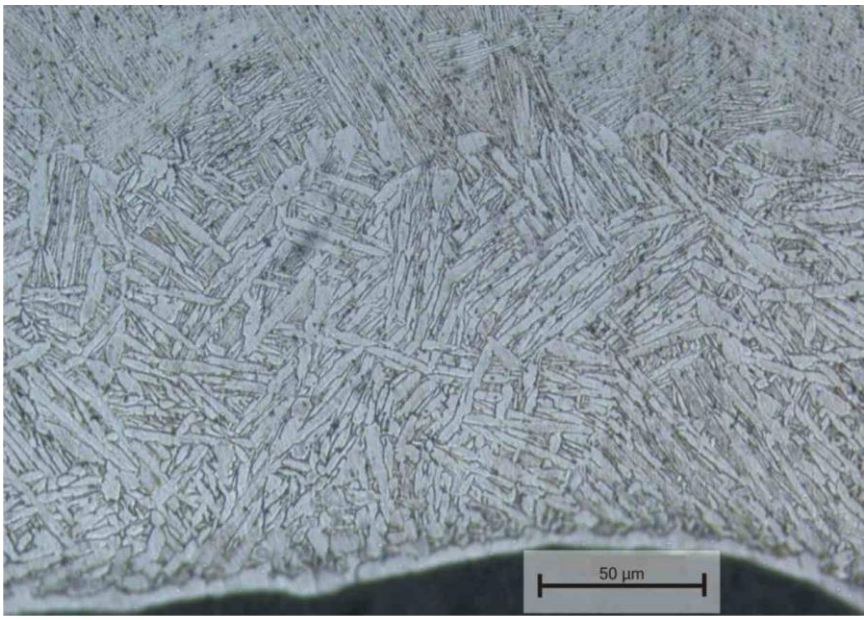

Figure 4.12 OM micrograph of at 50 µm showing microstructures of DMLS Ti64 samples heat treated at 1000ºC, soaked for 1 hour then air cooled

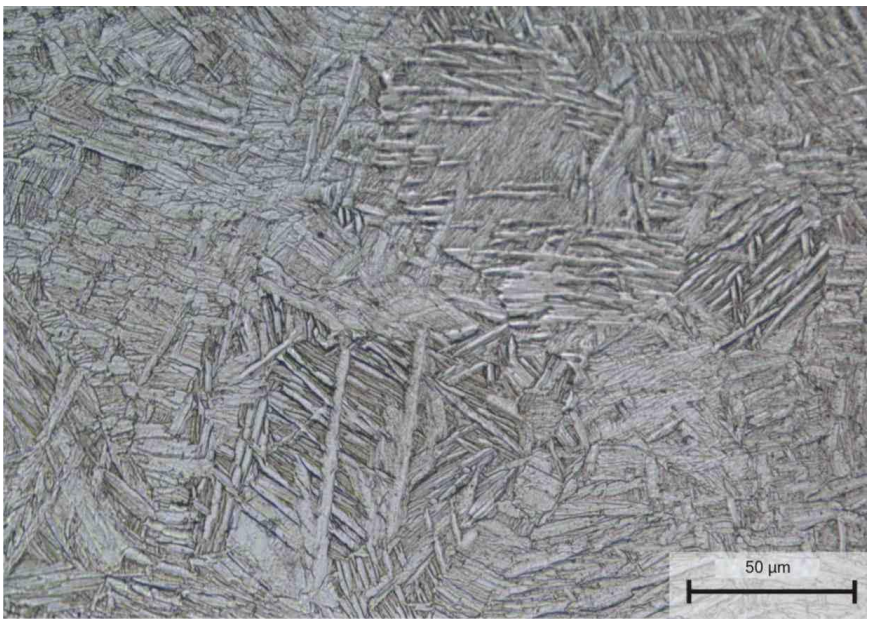

Figure 4.13 OM micrograph at 50 µm showing microstructures of DMLS Ti64 samples heat treated at 1000ºC, soaked for 1 hour then water quenched

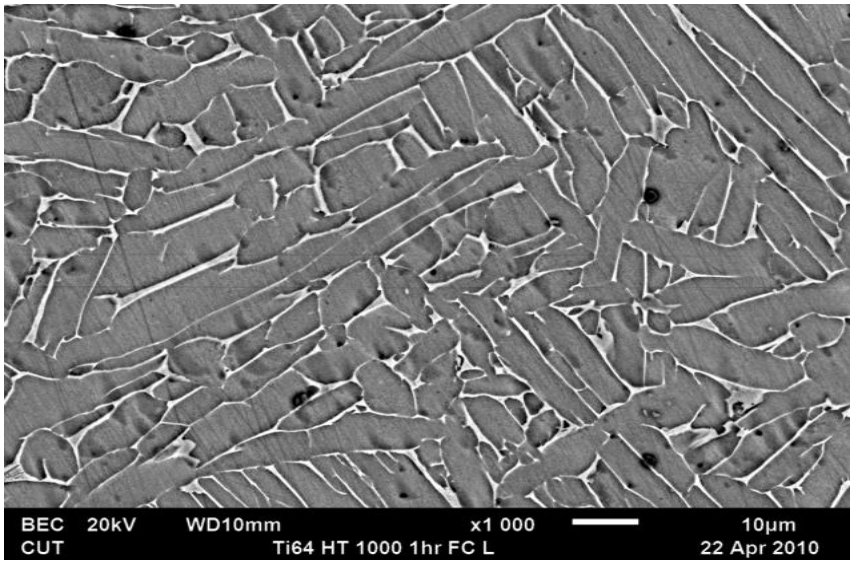

Figure 4.14 SEM micrograph at 10 µm showing microstructures of DMLS Ti64 samples heat treated at 1000ºC, soaked for 1 hour then furnace cooled

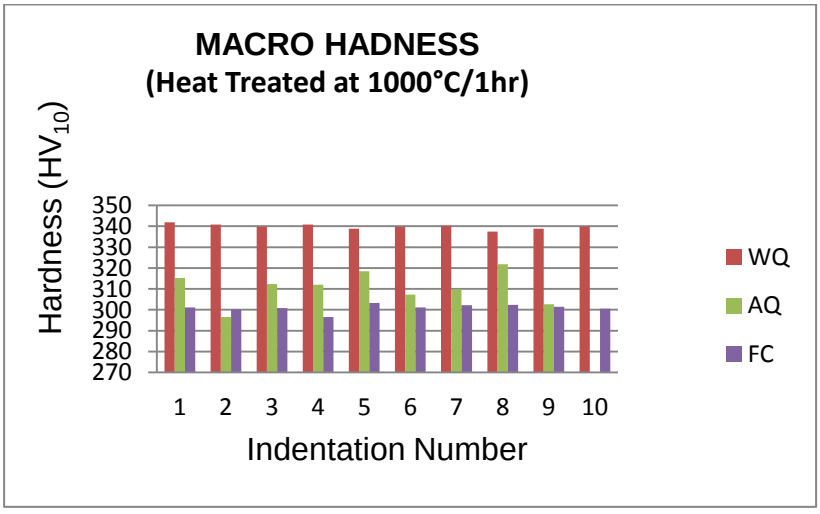

Figure 4.15 Macro hardness of DMLS Ti64 samples heat treated at 1000ºC and cooled at different cooling rates

Table 4.6 Average macro hardness of DMLS Ti64 samples heat treated at 1000ºC and cooled at different cooling rates

	HT at 1000ºC/1hr/ FC	HT at 1000ºC/1hr/ AQ	HT at 1000ºC/1hr/ WQ
Average	301	312	340
Standard Deviation	1.81	8.32	1.31

4.4.3 Heat Treatment of DMLS Ti64 Samples Done at 1100ºC and Cooled at Different Cooling Rates

A third heat treatment was done at 1100^{o}C which is a temperature above the beta transus. The very fine martensitic microstructure changed to a coarser alpha grain with more beta phase on the grain boundaries compared to the microstructures at 1000^{o}C. However, as heat treating temperatures are increased, aluminium tends to isolate to the alpha phase while the vanadium segregates to the beta phase. With slower cooling, the volume fraction of alpha increased; thus, there is no surprise at the elevated hardness values when samples were furnace cooled [Matthew & Donachie 2000: 50-57)]. See OM photo micrographs, Figures 4.16, 4.17 and 4.18, and more clearly on the SEM photo micrographs Figure 4.19. More of the photo micrographs for both samples cut in transverse and those cut in longitudinal are shown in Appendix E.

The hardness measurement also decreased from 344 to 312 HV with furnace cooling. The hardness obtained in all heat treatment done at 1100^{o}C is illustrated in Figure 4.20 and Table 4.7. These values are higher than those of the specimens which were heat

treated at 1000^{o}C. Figure 4.19 shows the different orientations of both alpha and beta laths in one grain; thus also contributing to a greater hardness measurement of the specimens. Additionally, the microstructure at 1100^{o}C showed more of beta on the grain boundary; thus, the more beta grain, the harder the specimen is as beta is the hard phase compared to alpha. A gold-like colour was also seen on the surface of the specimens cooled with air cooled and water quenched.

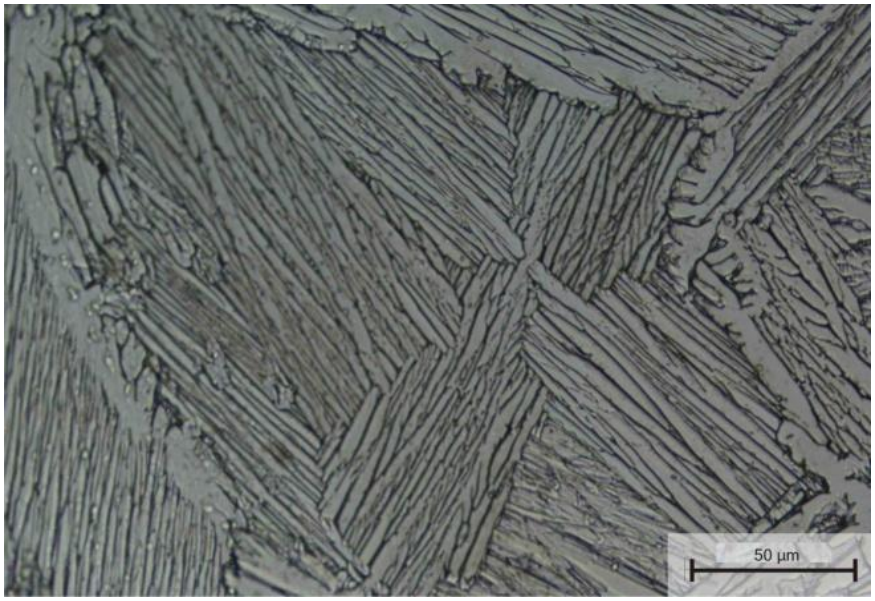

Figure 4.16 OM micrograph at 50 µm showing microstructures of DMLS Ti64 samples heat treated at 1100ºC, soaked for 1 hour then furnace cooled

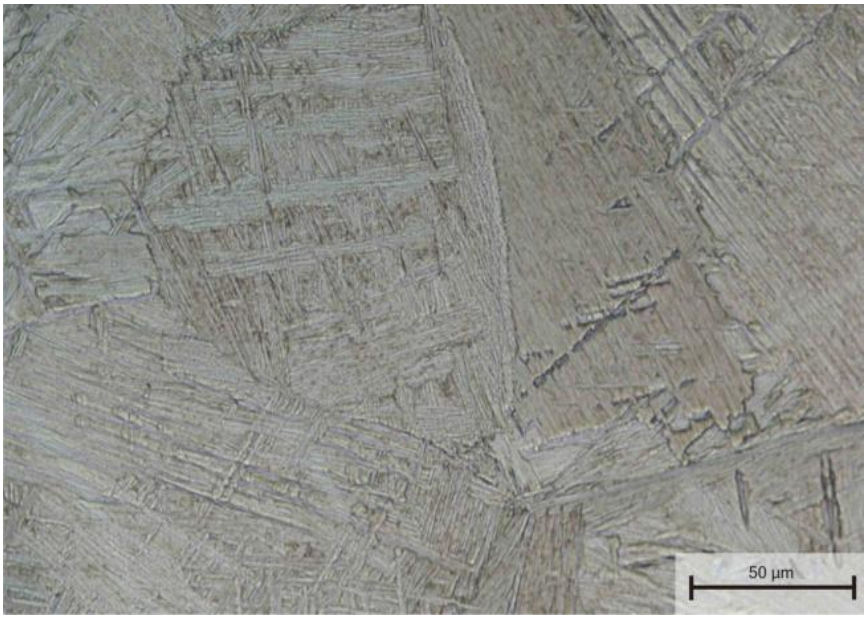

Figure 4.17 OM micrograph at 50 µm showing microstructures of DMLS Ti64 samples heat treated at 1100ºC, soaked for 1 hour then air cooled

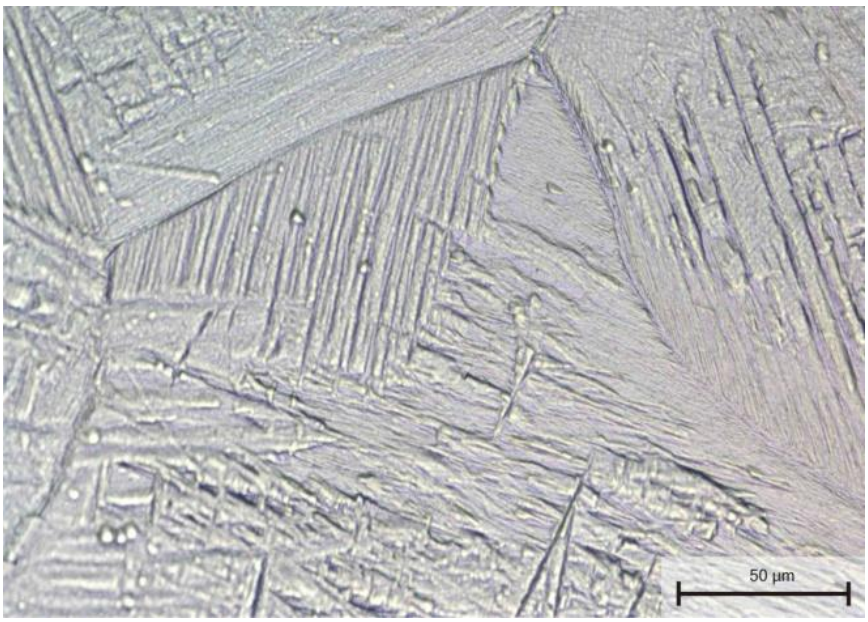

Figure 4.18 OM micrograph at 50 µm showing microstructures of DMLS Ti64 samples heat treated at 1100ºC, soaked for 1 hour then water quenched

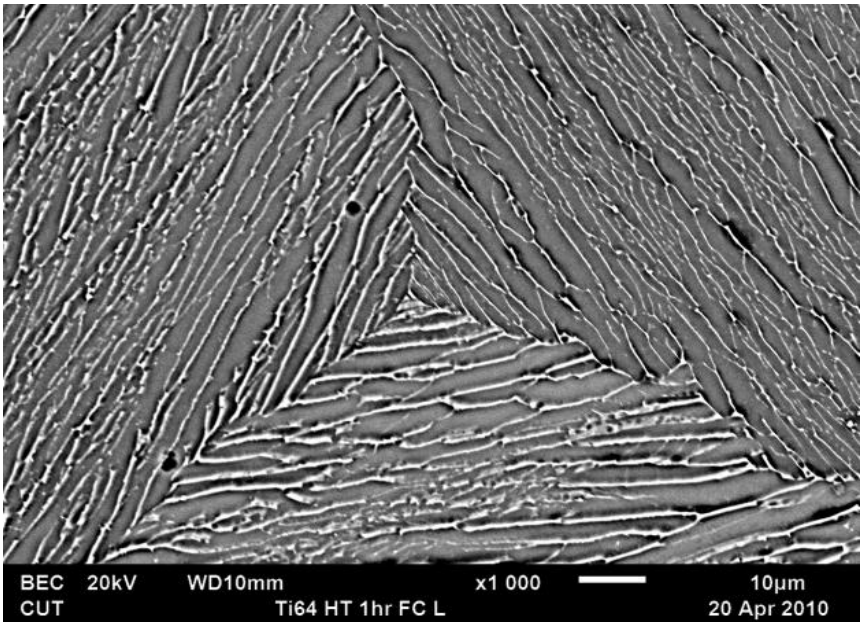

Figure 4.19 SEM micrograph at 10 µm showing microstructures of DMLS Ti64 samples heat treated at 1100ºC, soaked for 1 hour then furnace cooled

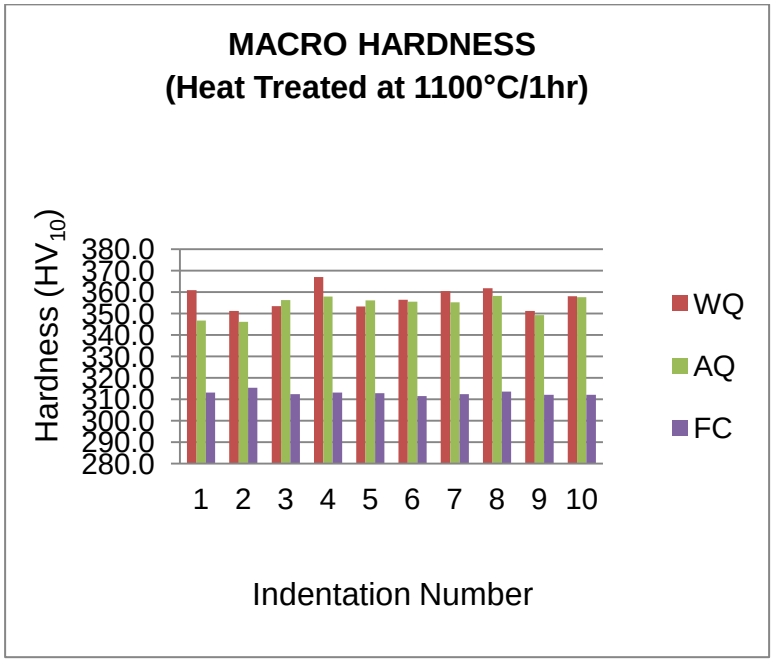

Figure 4.20 Macro hardness of DMLS Ti64 samples heat treated at 1100ºC and cooled at different cooling rates

Table 4.7 Average macro hardness of the DMLS Ti64 samples heat treated at 1100ºC and cooled at different cooling rates

	HT at 1100ºC/1hr/ FC	HT at 1100ºC/1hr/ AQ	HT at 1100ºC/1hr/ WQ
Average	313	353	357
Standard Deviation	1.12	4.71	5.22

Overall, with the different heat treatment temperatures, high hardness values were obtained in samples that had undergone water quenching, followed by air cooled samples, while the lowest hardness was found in samples that were furnace cooled. Therefore the fastest cooling rate was achieved by water quench followed by air cooling and furnace cooling. This can be clearly seen in Figure 4.10 and Table 4.5; Figure 415 and Table 4.6 as well as in Figure 20 and Table 4.7. As a result, both air cooling and water quenching were disregarded as the correct cooling rates for the present case. Higher heat treatment temperatures, even though there was a decrease in hardness at the lowest cooling rates, were also disregarded because it is believed that the elevated hardness values were due to the difference in orientation of the alpha and beta laths in one grain. Lower hardness values were obtained from the samples heat treated at 1000ºC which were furnace cooled. This is due to the coarse microstructure, compared to all other heat treatment temperatures, especially when cooled slowly. It was thus concluded that the best heat treatment procedure would be beta annealing at 1000ºC, which is only slightly higher than the beta-transus for Ti6Al4V alloy. Both water quenched and air cooled samples had a layer that indicated contamination by gases, such as nitrogen, carbon and oxygen. Oxygen, carbon or

nitrogen reacts with a titanium surface, resulting in an alpha case, which is brittle. Thus, the contaminated surface layer must be removed using a machining, as this directly affects the ductility (Matthew & Donachie 2001: 56-57). It should be noted that when dealing with complex dimensions (for example, manufacturing lattice-truss structures in an acetabular component which is part of the hip joint, see Figure 2.5, page 31) dimensional tolerances are too tight. Because any contaminated layers cannot be removed, there cannot afford to be any contamination from the atmosphere. Ti64 alloy alloy must be heat treated in a controlled atmosphere where contamination can be eliminated as it is very reactive with other elements, more with oxygen, carbon and nitrogen at a high temperature (Matthew & Donachie 2000: 48-57). Therefore, heat treatment was carried in vacuum furnace (Figure 3.8) to control the furnace atmosphere, which proved to be working as there was no colour change on the samples after heat treatment in the vacuum furnace.

4.5 Characterisation Results of the DMLS Ti64 Samples: Second Heat Treatment Regimens Done Using Vacuum Furnace

Heating at 1000^{o}C and cooling slowly allowed the alpha grain to grow bigger and the material became softer. Therefore, from the previous three experiments it was concluded that for inducing ductility on the DMLS Ti64 samples, beta annealing at 1000^{o}C and cooling with the furnace should be deployed. Another observation made by the visual examination from the Carbolite tube furnace was the discolouring of the

samples, indicating that there was a reaction with gases, such as nitrogen, carbon and oxygen. Therefore, samples should be cleaned in order to eradicate all impurities, such as oil and a vacuum furnace should be used.

4.5.1 Heat Treatment of DMLS Ti64 Samples Done at 1000ºC, Soaked for 1 Hour and Furnace Cooled for 4 Hours

The fourth heat treatment was done at 1000^{o}C; soaked for 1 hour and then furnace cooled for 4 hours, based on the results of the first three experiments. The OM photo micrographs (Figure 4.21) showed that the very fine martensitic microstructure changed to a coarser alpha colony with the beta phase on the grain boundaries. These were observed clearly in the SEM photo micrographs (Figure 4.22 at 10 µm). More of the photo micrographs are shown in Appendix F.

Macro hardness measurements obtained can be seen in Figure 4.23. An average hardness of 304 HV with a standard deviation of 2.31 was obtained for the specimens that were heat treated at 1000ºC, held for 1 hour, and furnace cooled for 4 hours. These values relate to the coarsening observed. Appendix G illustrates detailed results which clearly show the comparison of hardness at different conditions.

Tensile properties of four (4) DMLS Ti64 samples, heat treated at 1000^{o}C, soaked for 1 hour and then furnace cooled for 4 hours are shown in Table 4.8. Yield stress (at 0.2% offset) of 827 MPa and the ultimate tensile stress of 946 MPa were found. An

improvement in a percentage elongation and a percentage area reduction of 12.67% and 25.94%, respectively were also found. The tensile test results and graphs are shown in Appendix H.

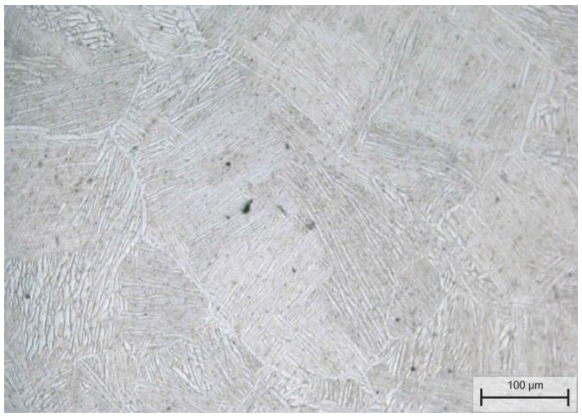

Figure 4.21 OM micrograph at 100 µm showing microstructures of DMLS Ti64 samples heat treated at 1000ºC, soaked for 1 hour then furnace cooled for 4 hours

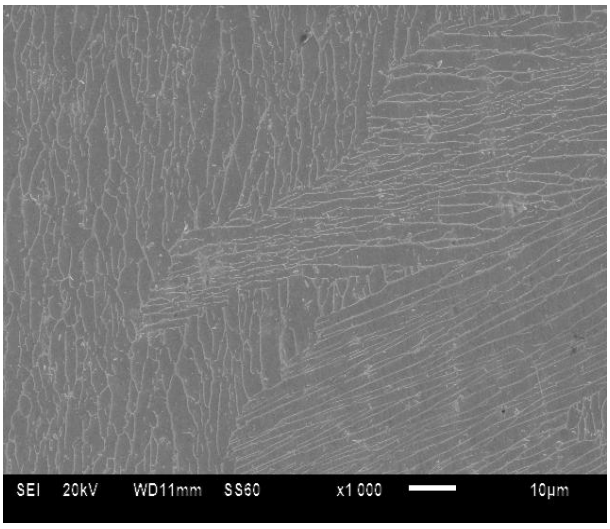

Figure 4.22 SEM micrograph at 10 µm showing microstructures of DMLS Ti64 samples heat treated at 1000ºC, soaked for 1 hour then furnace cooled for 4 hours

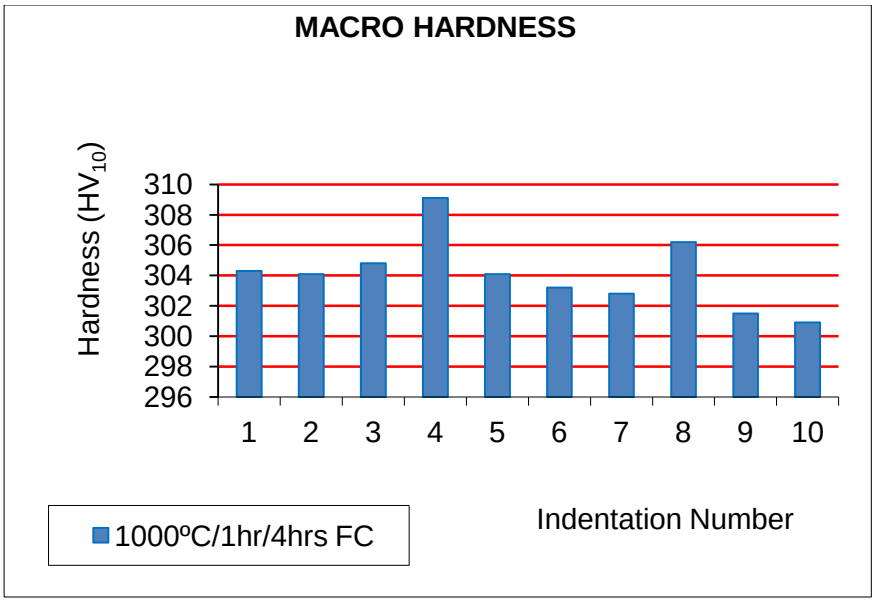

Figure 4.23 Macro hardness of DMLS Ti64 samples heat treated at 1000ºC, soaked for 1 hour then furnace cooled for 4 hours

Table 4.8 Tensile properties of DMLS Ti64 samples heat treated at 1000ºC, soaked for 1 hour then furnace cooled for 4 hours

	Tensile Stress at Yield (0.2 % Offset) [MPa]	Ultimate Tensile Stress [MPa]	Elongation [%]	Area Reduction [%]
Mean	827	946	12.67	25.94
Standard Deviation	7.02	6.30	2.17	10.02

4.5.2 Heat Treatment of DMLS Ti64 Samples Done at 1000ºC, Soaked for 1 Hour and Furnace Cooled for 34 Hours

The fifth heat treatment was done at 1000^{o}C; soaked for 1 hour and then furnace cooled for 34 hours based on the results of the first three experiments. The OM photo micrograph (Figure 4.24) shows that the very fine martensitic microstructure changed to a coarser alpha colony with the beta phase on the grain boundaries. These were observed clearly in the SEM photo micrographs (Figure 4.25 at 20 µm). More of the photo micrographs are shown in Appendix F. Macro hardness measurements obtained can be seen in Figure 4.26. An average hardness of the specimens which were furnace cooled for 34 hours was 296 HV with a standard deviation of 1.01.

Tensile properties of four (4) DMLS Ti64 samples heat treated at 1000^{o}C, soaked for 1 hour and then furnace cooled for 34 hours are shown in Table 4.9. Further improvement on ductility was evidently seen on tensile properties; a percentage elongation and a percentage area reduction of 18.11% and 33.39%, respectively were found. Yield stress (at 0.2% offset) of 805 MPa and the ultimate tensile stress of 909 MPa were also found. The tensile test results and graphs are shown in Appendix H.

Figure 4.24 OM micrograph at 100 µm showing microstructures of DMLS Ti64 samples heat treated at 1000ºC, soaked for 1 hour then furnace cooled for 34 hours

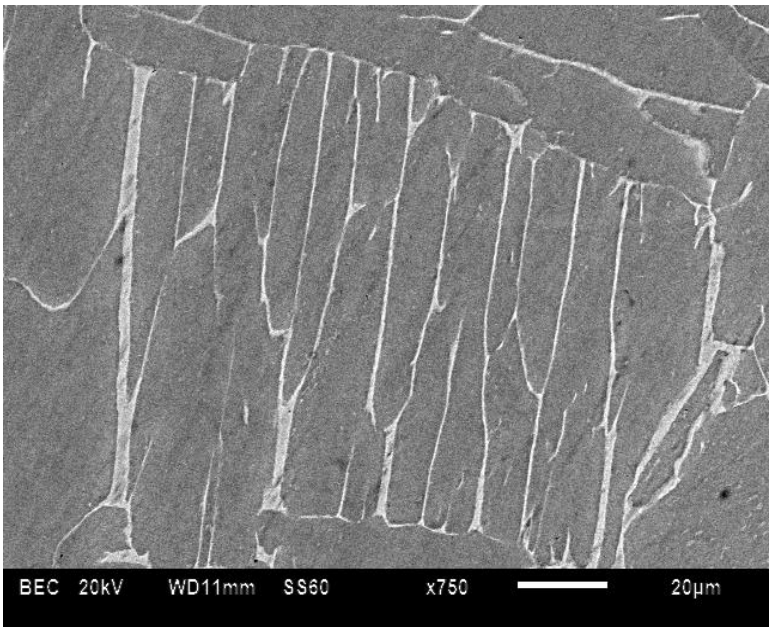

Figure 4.25 SEM micrograph at 20 µm showing microstructures of DMLS Ti64 samples heat treated at 1000ºC, soaked for 1 hour then furnace cooled for 34 hours

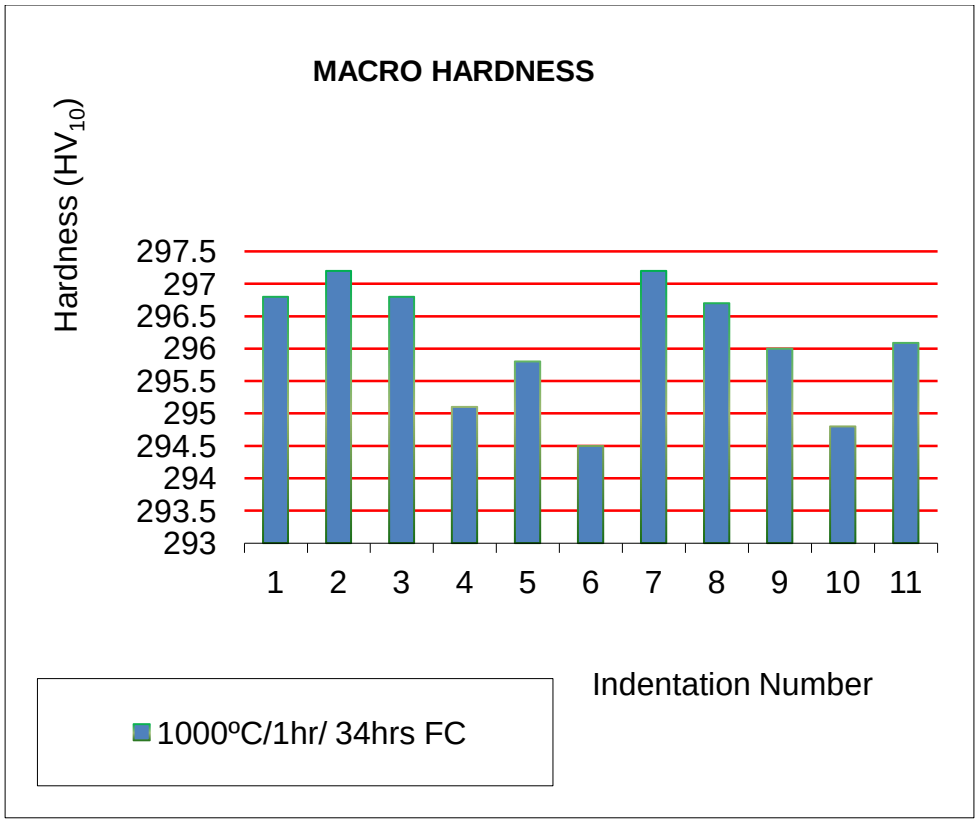

Figure 4.26 Macro hardness of DMLS Ti64 samples heat treated at 1000ºC, soaked for 1 hour then furnace cooled for 34 hours

Table 4.9 Tensile properties of DMLS Ti64 samples heat treated at 1000ºC, soaked for 1 hour then furnace cooled for 34 hours

	Tensile Stress at Yield (0.2 % Offset) [MPa]	Ultimate Tensile Stress [MPa]	Elongation [%]	Area Reduction [%]
Mean	805	909	18.11	33.39
Standard Deviation	3.76	7.22	1.75	0.90

Overall, the alloy was furnace cooled, for 4 hours; we obtained a different microstructural morphology. The overall microstructure had large grains. The alpha +

beta laths are finely distributed in different orientations. The alpha lath size was, on average, at about 2µm, while the beta lath size was even smaller and difficult to measure. Owing to an increase in the grain size, the hardness after the heat treatment was lowered, compared to the as-sintered samples. Increasing cooling time increases the grain size to approximately 300µm. The average alpha lath size measured about 8-10 µm for samples cooled for 4 hours, while samples cooled for 34 hours the laths were found to be fine and around 17-20µm. The beta laths were fine and could not be measured.

4.6 Overall Chemical Analysis of DMLS Ti64 Samples

SEM-EDX analyses were done in order to investigate a change in the chemical composition of the Ti64 alloy, due to the DMLS process and/or heat treatment. The chemical analysis was bulk done on an area as indicated by red or blue lines in Figures 4.27 to 4.32. The results obtained on all samples investigated (as-laser sintered and heat treated) confirmed the percentage of aluminium and vanadium that are within the percentage range set by the ASTM F1472-08$^{\varepsilon 1}$ standards. The weight percentage for Aluminium ranges between approximately 5.50 to 6.75%, while vanadium ranges between approximately 3.5 and 4.5%. The following are the results of SEM-EDX analyses:

1. The SEM-EDX results of the as-sintered samples are presented in Figure 4.27; 5.53% of aluminium and 3.86% of vanadium elements were found.

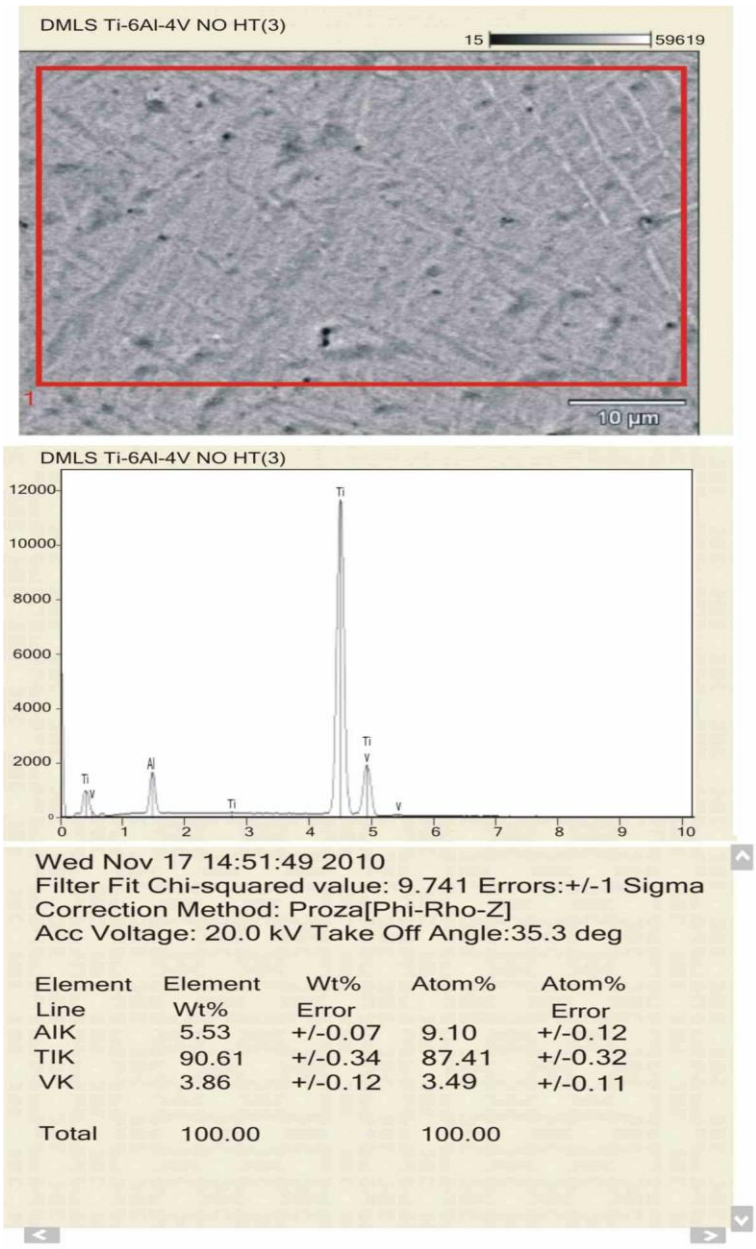

Figure 4.27 SEM-EDX results and micrograph at 10 µm of as-laser sintered Ti64 samples

2. The sample that was heat treated in the horizontal carbolite tube furnace at 700ºC, held for one hour then cooled by water quenching is presented in

Figure 4.28. The 5.86% of aluminium, 3.88% of vanadium and 1.51% Carbon elements were found.

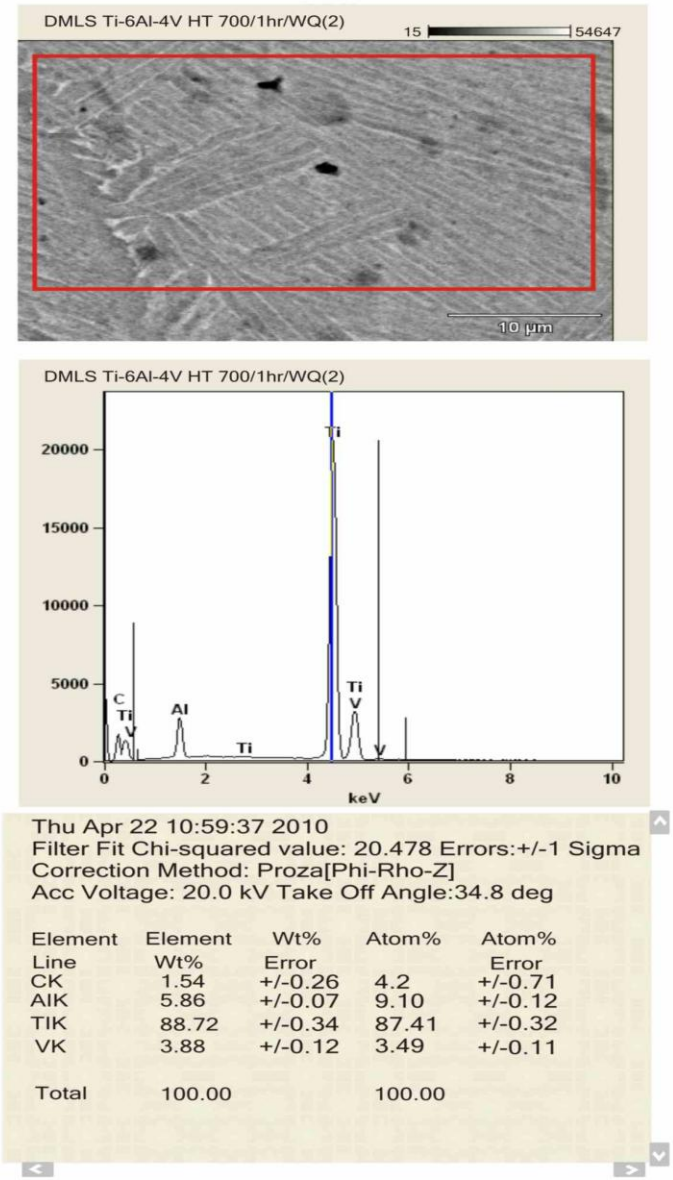

Figure 4.28 SEM-EDX results and micrograph at 10 µm showing microstructures of DMLS Ti64 samples heat treated at 700ºC, soaked for 1 hour then water quenched

3. The sample heat treated in the horizontal carbolite tube furnace at 1000ºC, held for one hour then furnace cooled is presented in Figure 4.29. The 5.73% of aluminium, 3.57% of vanadium and 1.22% carbon elements were found.

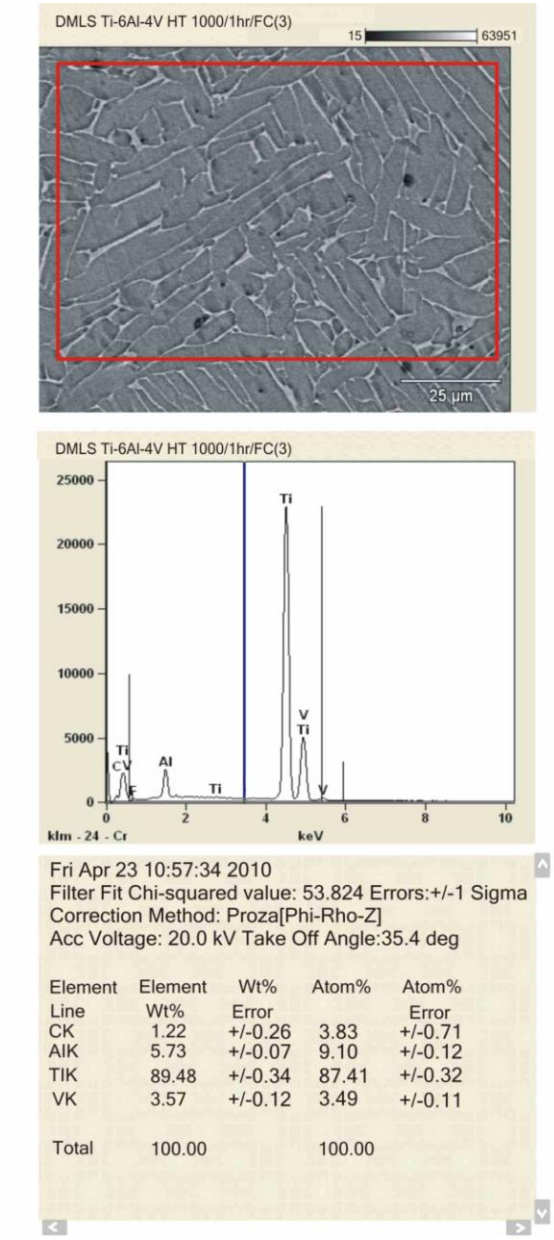

Figure 4.29 SEM-EDX results and micrograph at 25 µm showing microstructures of DMLS Ti64 samples heat treated at 1000ºC, soaked for 1 hour then furnace cooled

4. The sample heat treated in the horizontal carbolite tube furnace at 1100ºC, held for one hour then furnace cooled for four hours is presented in Figure 4.30. The 5.57% of aluminium, 3.59% of vanadium and 1.60% carbon elements were found.

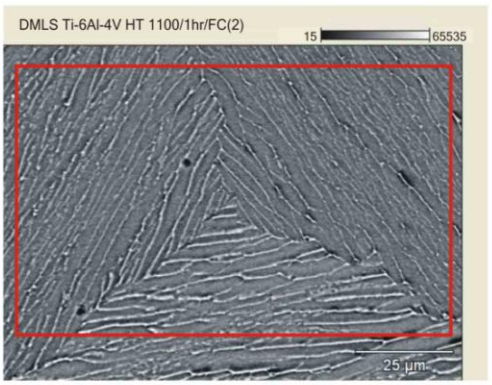

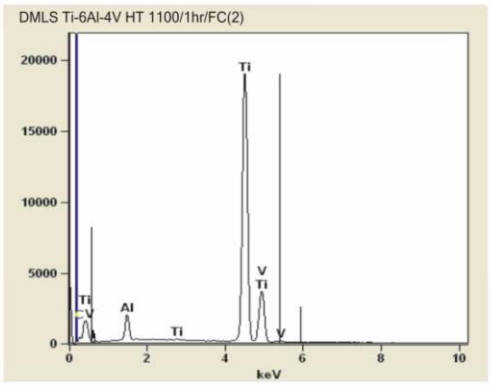

Tue Apr 20 12:57:34 2010
Filter Fit Chi-squared value: 37.476 Errors:+/-1 Sigma
Correction Method: Proza[Phi-Rho-Z]
Acc Voltage: 20.0 kV Take Off Angle:34.4 deg

Element Line	Element Wt%	Wt% Error	Atom%	Atom% Error
CK	1.60	+/-0.24	5.83	+/-0.71
AlK	5.57	+/-0.05	7.10	+/-0.12
TiK	89.24	+/-0.24	87.88	+/-0.25
VK	3.59	+/-0.14	3.59	+/-0.12
Total	100.00		100.00	

Figure 4.30 SEM-EDX results and micrograph at 25 µm showing microstructures of DMLS Ti64 samples heat treated at 1100ºC, soaked for 1 hour then furnace cooled

5. The sample heat treated in the vacuum furnace at 1000ºC, held for 1 hour then furnace cooled for 4 hours is presented in Figure 4.31 with 5.54% of aluminium and 4.44% of vanadium elements. The carbon element is not present.

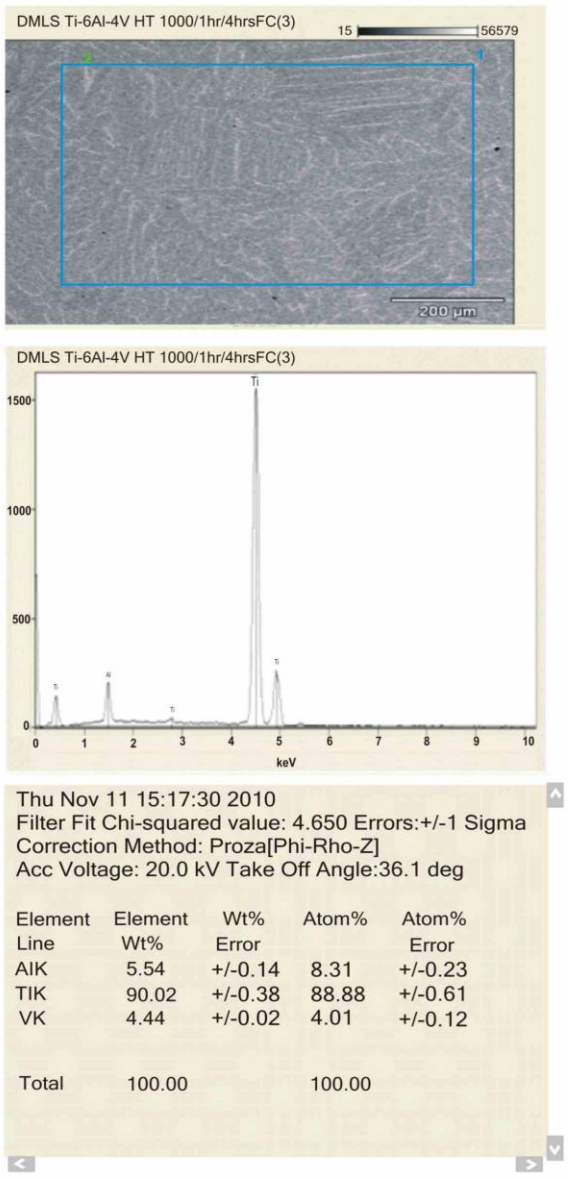

Figure 4.31 SEM-EDX results and micrograph at 200 µm showing microstructures of DMLS Ti64 samples heat treated at 1000ºC, soaked for 1 hour then furnace cooled for 4 hours

6. The sample heat treated in the vacuum furnace at 1000ºC, held for one hour then furnace cooled for thirty-four hours is presented in Figure 4.32 with 6.41% of aluminium and 3.72% of vanadium elements, with no carbon element presents.

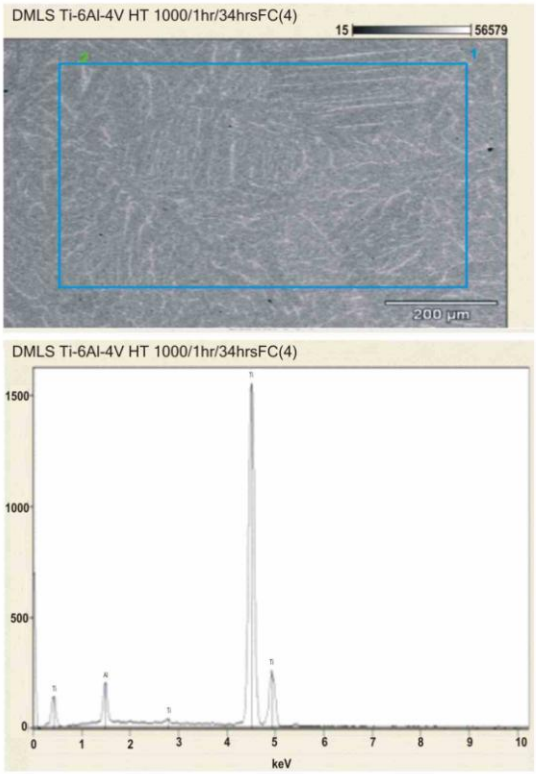

Figure 4.32 SEM-EDX results and micrograph at 200 µm showing microstructures of DMLS Ti64 samples heat treated at 1000ºC, soaked for 1 hour then furnace cooled for 34 hours

There were no significant changes found, especially in titanium, aluminium and vanadium. However, samples which were heat treaded in the horizontal carbolite tube furnace cooled by water quenching and air cooling indicated a presence of about 1.6% of carbon which is one of the interstitial elements. This shows that there was contamination, which was also observed as the gold-like colour on optical photo micrographs. The contamination might have happened during the time samples were taken out of the furnace, in order to be cooled by water and air. The samples were still at high temperatures.

4.7 ABAQUS^{TM} Finite Element Analysis Results

4.7.1 ABAQUS^{TM} FEA Program Results

This section illustrates how the simulation results were interpreted and compared to the calculated ones. The sample – B4 (HT 1000ºC, soak 1 hr, FC 4 hrs) results were considered in order to show how the FEA results were interpreted. The force, deformation, stress and strain results are tabulated in Table 4.10, while Figure 4.33 shows the Von Mises stresses. Figure 4.34 illustrates the stress-strain curve from the ABAQUS^{TM} FEA program. All twelve (12) samples were simulated but it was decided to only show one (1) sample (sample - B4) of the twelve simulation results. The other eleven (11) samples correlated well with sample B4.

Table 4.10 Sample – B4 (HT 1000ºC, soak 1 hr, FC 4 hrs) data extracted from the ABAQUS™ FEA program

Force	**Deformation**	**Stress**	**Strain**
[N]	[mm]	[MPa]	[mm/mm]
0	0	0	0
1828	0.01895	128	0.00111
3654	0.03789	256	0.00222
6391	0.06628	448	0.00389
10491	0.10881	736	0.00640
13297	0.19825	933	0.01166
13693	0.21029	961	0.01237

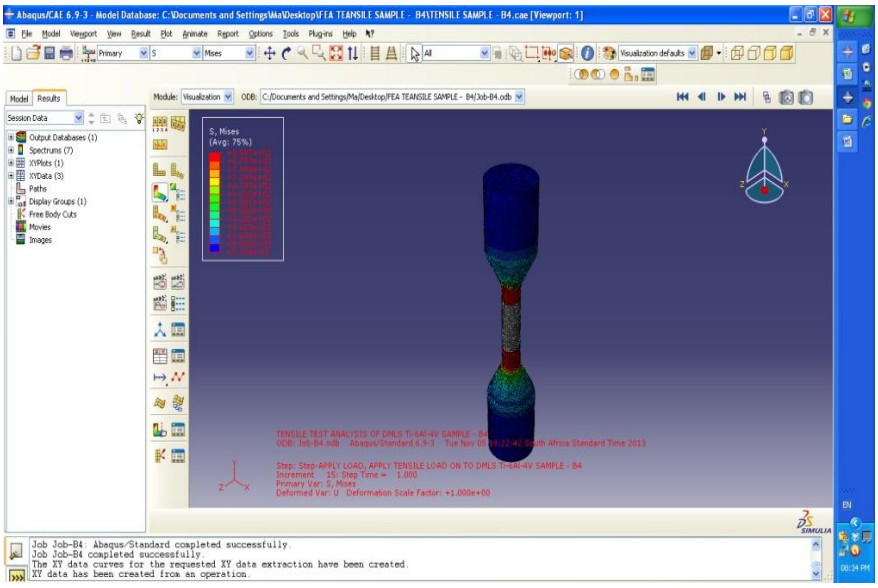

Figure 4.33 The Von Mises stress results from the ABAQUS™ FEA program for the sample – B4 (HT 1000ºC, soak 1 hr, FC 4 hrs)

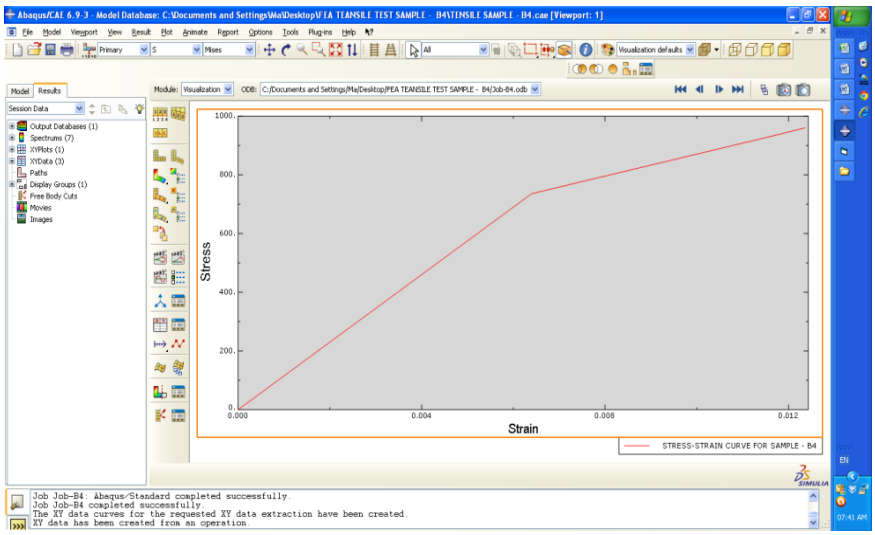

Figure 4.34 Stress-strain curve from the ABAQUS™ FEA program for the sample B4 (HT 1000ºC, soak 1 hr, FC 4 hrs)

4.7.2 Reaction Force from the ABAQUS™ FEA Program

The Table 4.11 indicates the reaction forces in all three directions. There are small reaction forces (highlighted and underlined in red) in the x-axis and z-axis which show that small stress is induced due to the nodal bonds between each element. The link transmits load in all three directions and applies a small load in areas where force may not be acting in that direction. This is a source of error between the calculations and the ABAQUS™ program.

Table 4.11 Field output reported at nodes for part indicating small reaction forces induced in x and z direction: tensile sample B4 (HT 1000ºC, soak 1 hr, FC 4 hrs)

Node	**RF.RF1 [N]** **x-axis**	**RF.RF2 [N]** **y-axis**	**RF.RF3 [N]** **z-axis**
1	34.875E-09	-13.4078E+03	-21.5948E-09
2	-1.83962E-09	13.4078E+03	-1.1473E-09
Minimum At Node	-1.83962E-09 2	-13.4078E+03 1	-21.5948E-09 1
Maximum At Node	34.875E-09 1	13.4078E+03 2	-1.1473E-091 2
Total	33.0354E-09	0	-22.7421E-09

.

4.7.3 Interpretation of Yield Stress Results from MDSolid Program

The force and displacement values from the ABAQUS^{TM} FEA program indicated in Table 4.10 were used in the MDSolid program in order to interpret the stress-strain curve precisely. Figure 4.35 shows the stress-strain curve which is similar to the one from the ABAQUS^{TM} FEA program (Figure.4.34). The yield stress defined by the 0.20% offset method was 847 MPa (see blue line on Figure 4.35) where it intersects the stress-strain curve.

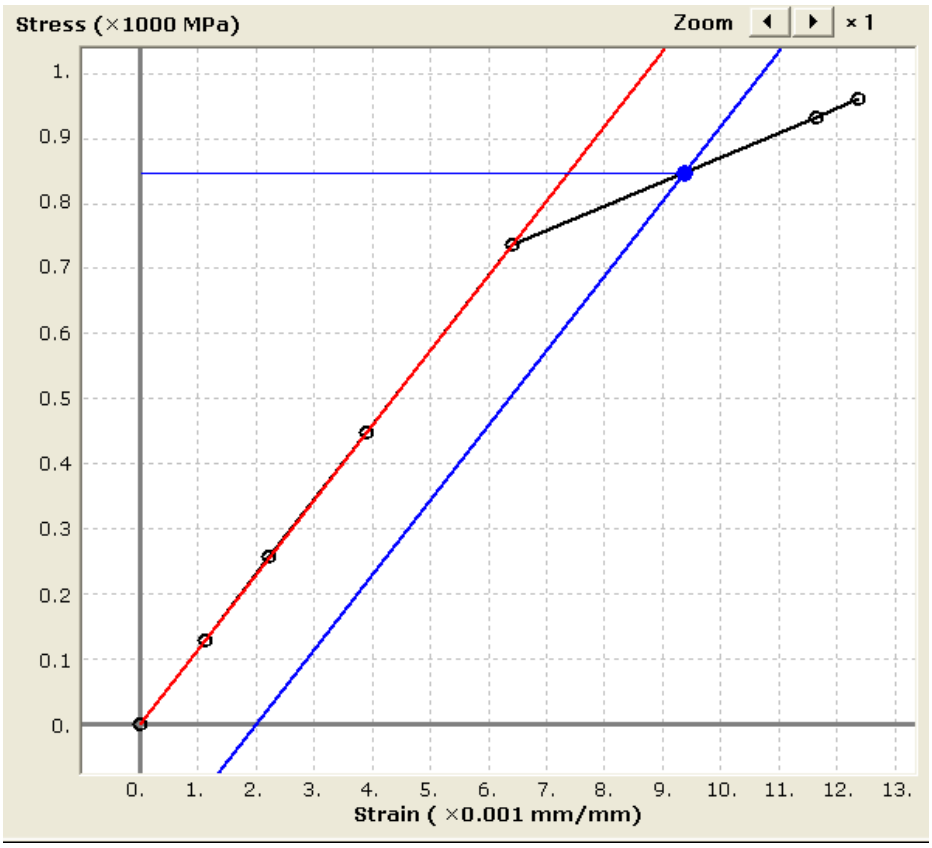

Figure 4.35 Stress-strain curve from MDSolid program for the sample B4 (HT 1000ºC, soak 1 hr, FC 4 hrs)

4.7.4 The Von Mises Stress Results

Calculated 0.20% offset true yield stress of the sample – B4 (HT 1000ºC, soak 1 hr, FC 4 hrs) was found to be 835 MPa. From the interpreted results above, the FEA 0.20% offset yield stress was found to be 847 MPa which is a higher value than the calculated one by 1.62%. This difference is due to the stress concentration as the samples broke near the shoulder fillet during the tensile test (Figure 4.36). It was decided not to machine or polish the tensile samples, as some medical implants can be used without being polished. The surface roughness of the sample might have also contributed to the

stress concentration; however, this is one of recommendations that can be studied further.

The sample in Figure 4.36 broke just near the notch or fillet, but still within the gage length. This is an indication that the stress concentration was induced due to the fact that the tensile load applied to the sample had caused the yielding to be in, or close to the notch. The yielding can cause the strain-strengthening of the material and increase yield stress at the notch location. Therefore, the stress concentration factor must be included, but only applied to the ductile materials with static loads. (Shigley & Mischke 2003: 331-337). The stress concentration factor was considered when simulating.

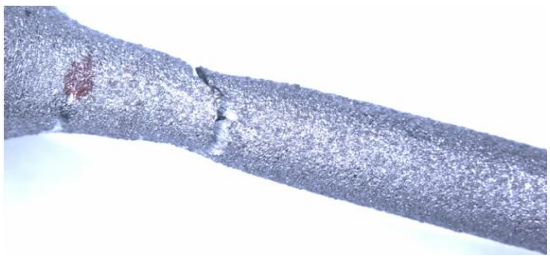

Figure 4.36 The sample – B4 (HT 1000ºC, soak 1 hr, FC 4 hrs) showing the position where it broke during tensile test experiment

The stress is a function of force over the area; thus, as the area is decreased the stress will increase (Shigley & Mischke 2003: 331-337). Therefore, for this case of tensile loading, the formula of Equation 4.1 corresponds closely for a variety of cases with the finite element analyses of Gooyer and Overbeeke (1991) and (Pilkey and Pilkey (2008: 142-143). Thus, the stress concentration factor (K_t) for a shaft with shoulder fillet in axial tension was considered and calculated from equation 4.1.

$$K_t = 0.493 + 0.48\left(\frac{D}{d}\right)^{-2.43} + \left(\frac{r}{d}\right)^{-0.48} + \sqrt{\frac{3.43 - 3.41\left(\frac{D}{d}\right)^2 + 0.0232\left(\frac{D}{d}\right)^4}{1 - 8.85\left(\frac{D}{d}\right)^2 - 0.078\left(\frac{D}{d}\right)^4}} \quad \textit{Equation 4.1}$$

where

D – Large diameter of circular bar (mm)

d – Small diameter of circular bar (mm)

r – Fillet radius of circular bar (mm)

In tension $K_t = \frac{\sigma_{vm(maximun)}}{\sigma_{vm(normal)}}$ thus, the maximum Von Mises stress was therefore calculated from equation 4.2.

$$\sigma_{vm(maximum)} = K_t \sigma_{vm(normal)} \quad \textit{Equation 4.2}$$

The measured values for the Sample - B4 were: large diameter of circular bar (D) was 11mm; small diameter of circular bar (d) was 4.259 mm, while fillet radius of circular bar (r) was 6mm. Using the equation 4.1, the stress concentration factor (K_t) became 1.017. Thereafter, the equation 4.2 was applied and the maximum Von Mises stress was found to be 848 MPa. Comparing this maximum Von Mises stress (848 MPa) with the FEA interpreted results (847 MPa), the difference was reduced to 0.07%. The Von Mises stress results of all samples are shown in Table 4.12.

The theory of failure based on the maximum distortion energy theory was interpreted using the MDSolid program. The 0.2% offset yield stress of 1110 MPa as maximum yield stress for wrought Ti64 alloy (Table 2.2) was compared to the Von Mises 0.2% yield stresses found in both the calculated and FEA results. The samples which were not heat treated failed as they fell outside the Von Mises criterion. Figure 4.37 illustrates as-sintered sample B1. On the other hand, all samples that were heat treated fell within the Von Mises criterion. Figure 4.38 indicated sample B4 (HT 1000ºC, soak 1 hr, FC 4 hrs), while Figure 4.39 shows sample D4 (HT 1000ºC, soak 1 hr, FC 34 hrs).

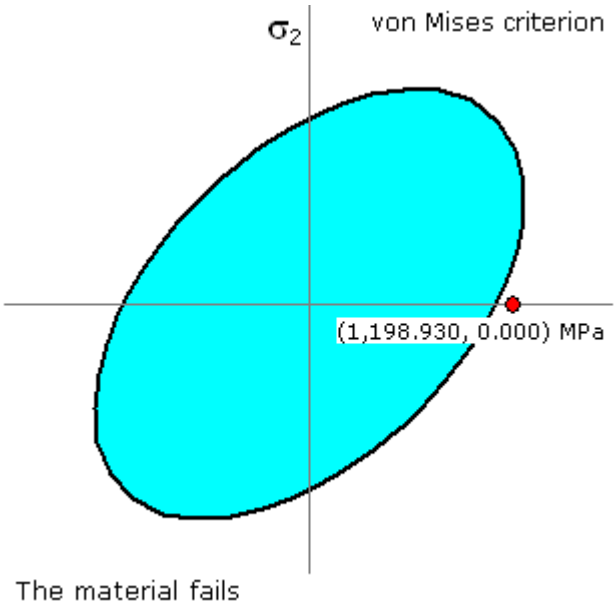

Figure 4.37 Von Mises stress from the MDSolid program for the as-laser sintered sample B1

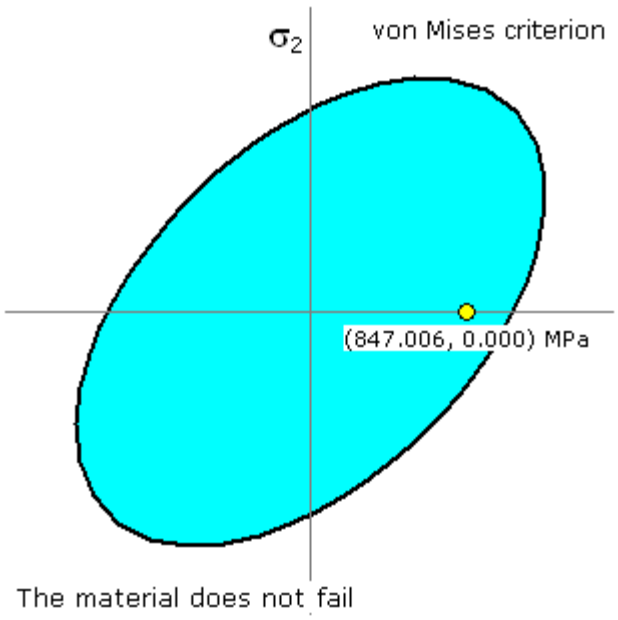

Figure 4.38 Von Mises stress from the MDSolid program for the sample B4 (HT 1000ºC, soak 1 hr, FC 4 hrs)

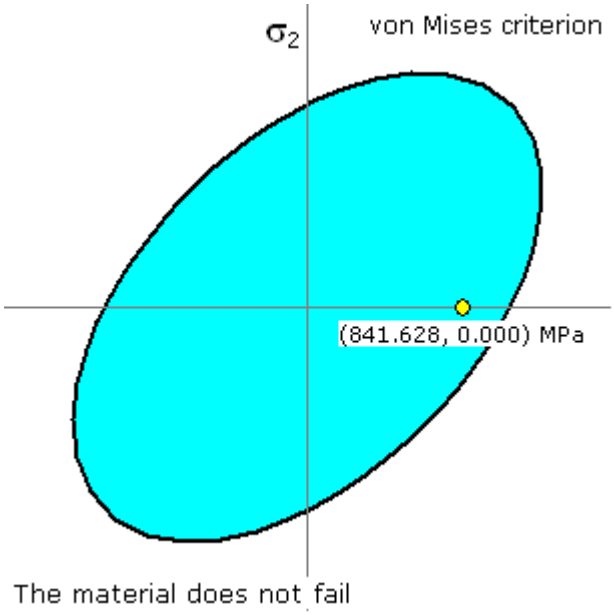

Figure 4.39 Von Mises stress from MDSolid program for the sample D4 (HT 1000ºC, soak 1 hr, FC 34 hrs)

Table 4.12 The calculated Von Mises stress with and without stress concentration factor together with FEA results. Percentage error with and without stress concentration factor is also indicated.

Sample Label	Small Diameter of Circular Bar [mm]	Large Diameter of Circular Bar [mm]	Fillet Radius of Circular Bar [mm]	Stress Concentration Factor K_t	Calculated Von Mises Stress Without K_t [MPa]	Calculated Von Mises Stress (With K_t) [MPa]	FEA Von Mises Stress [MPa]	%Error (Without K_t)	%Error (with K_t)
NO HEAT TREATMENT									
B1	4.25	9	5	1.209	991	1198	1199	20.94	0.05
B2	4.22	10	5	1.131	1007	1139	1141	13.32	0.15
C1	4.229	9	6	1.170	1030	1205	1204	16.85	0.12
C2	4.22	9	6	1.164	1025	1193	1194	16.44	0.06
HT1000, SOAK 1HR, FC 4HRS									
B4	4.259	11	6	1.017	834	848	847	1.62	0.07
B5	4.259	11	6	1.017	840	853	852	1.65	0.05
C4	4.259	11	5	1.025	823	843	842	2.58	0.06
C5	4.27	10	6	1.057	833	879	878	5.64	0.06
HT1000, SOAK 1HR, FC 34HRS									
D4	4.259	11	5	1.037	813	841	842	3.75	0.03
D5	4.27	10	6	1.086	810	878	877	8.58	0.03
E1	4.27	11	5	1.036	814	842	841	3.55	0.06
E5	4.28	11	5	1.046	805	841	840	4.54	0.05
							AVERAGE	8.29	0.07

Chapter 5. DISCUSSION OF RESULTS

5.1 Introduction

This chapter presents a discussion of the results of the morphological and chemical composition analysis of EOS Ti64 powder. It also provides an analysis of the metallographic, density, mechanical properties and FEA results of the DMLS Ti64 samples.

5.2 Discussion of Results

The EOS Ti64 powder used had a spherical morphology, which is typical of gas-atomised powders as shown in Figure 4.1, page 65. Simchi (2006) argues that there is a close relationship between the densification, the processing parameters and the powder characteristics. He also found that the density of laser sintered iron was influenced by powered particle size. However, Simchi (2006) concluded that the density is related to powder characteristics, such as the chemical composition, particle shape, size and distribution. Although Simchi worked with DMLS iron, it is reasonable to assume that DMLS behaves in a similar way.

The DMLS Ti64 samples manufactured in a vertical orientation on the EOSINT M 270 machine by the DMLS process resulted in dense parts of density 4,4 g/cm^3 which is comparable to that of the standard specification for wrought annealed Ti-6Al-4V alloy for

surgical implant applications (4,43 g/cm^3). However, the density is critical for titanium based alloys because porosity has very detrimental effects on fatigue and fracture properties. Sedlak et al. (2010) argues that the mechanical properties are also affected by the porosity when full densification is not achieved. Nevertheless, the DMLS process has become very advantageous regarding porosity issues, since it can be controlled and changed over the whole cross section of the sintered product. In this project the density achieved was approximately 99% close to that of the annealed wrought Ti-6Al-4V alloy.

However, DMLS Ti64 samples indicated voids. Figure 5.1 is one of the photo micrographs that show the voids. The voids are about 2µm or less and are more or less round in shape. Murr et al. (2009) also suggests that the range of built parameters should be tested for this alloy in order to determine the full range of mechanical properties that can be tailored through the DMLS technique. Perhaps changing built parameters may decrease the voids in terms of quantity, shape and size.

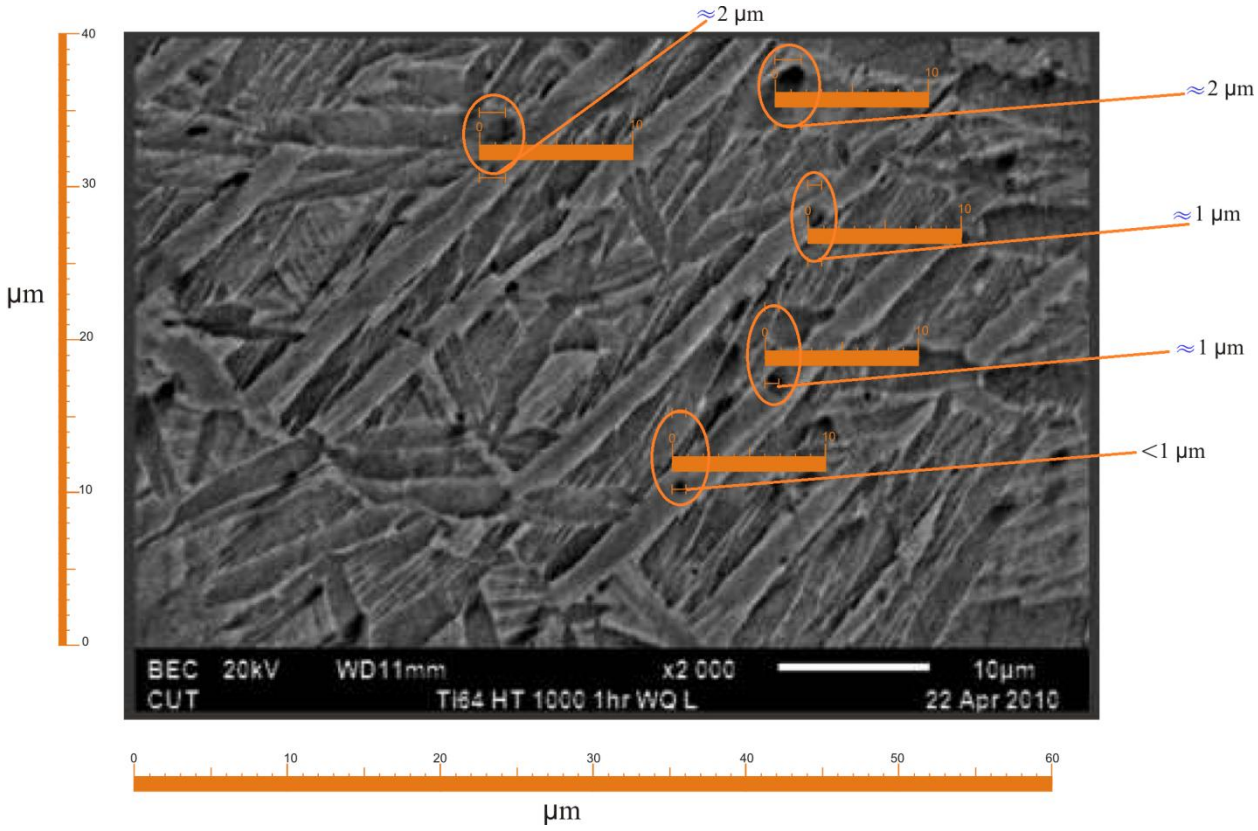

Figure 5.1 Photo micrographs of DMLS Ti64 sample indicating voids

The SEM-EDX results confirm the DMLS Ti64 samples composition. Titanium, aluminium and vanadium were in their expected quantities, as illustrated in Figures 4.27 to 4.32, page 93-98. The weight percentages of aluminium and vanadium were within the range of the ASTM F1472-08$^{\varepsilon 1}$ standard.

Conversely, the SEM-EDX also indicated carbon which is one of the interstitial elements with a weight percentage of about 1.6% in both water quenched and air cooled samples that were heat treated using a Carbolite tube furnace in an argon atmosphere. Based on the ASTM F1472-08$^{\varepsilon 1}$ standards, the maximum weight percentage of carbon must be 0.08%. This justified the discolouring seen in the optical photo micrographs of the

samples cooled with air and water quenched (discolouring is seen more clearly in Figure 4.8, page 75; Figure 4.13, page 78; and Figure 4.17, page 82). Finlay and Snyder (1950) indicate in their study that this interstitial element found is one of the alpha stabilisers which are well-known solid solution strengtheners that react with a titanium surface to form an alpha case layer. They further indicate that the interstitial elements' concentration must not be excessive but should be controlled, based on what is required. Should it be more concentrated, the mechanical properties, such as ultimate tensile strength and hardness will increase, while ductility decreases, as alpha case layer is brittle. The high hardness found on the samples justifies this research. Matthew and Donachie (2000) are also in agreement and further indicate that this alpha case layer must be removed before the component is put into service. They also opine that the heat treatment atmosphere must be controlled and the samples be cleaned in order to avoid contamination.

Samples which were heat treated in a vacuum furnace, as well as the as-sintered ones did not indicate the presence of any of the interstitial elements or any discolouration. It is therefore acknowledged that some contamination happened during heat treatment while using the Carbolite tube furnace. Therefore, use of the vacuum furnace is recommended whenever DMLS Ti64 samples need heat treatment.

Leyens and Peters (2003) and Matthew and Donachie (2000) point out in their literature that mechanical properties depend on the phases present which, in turn, depend on the elemental constituencies present in the material. Changing the physical properties, such as grain size, grain shape, grain texture and/or the arrangement of the phases, strongly

influences the mechanical properties. Ti64 alloy can be heat treated to achieve the desired mechanical properties. It is through heat treatment that two well-known microstructures that exist in (α + β) type can be produced and altered.

An average elongation of 2.6% and an area reduction of 3.51% were found in as-laser sintered samples. Owing to the fact that both percent elongation and area reduction are low, it was confirmed that the DMLS process produces brittle parts which can cause the parts to fail without warning. Conversely, biomedical implants need to indicate failure and therefore, high ductility parts are required. It is then logical to suggest that a post DMLS heat treatment be conducted to improve ductility.

Slow cooling of the DMLS EOS titanium Ti-6Al-4V alloy samples from 1000°C and 1100°C resulted in more alpha than beta phases of lower hardness than as-sintered material. The highest hardness was obtained by water quenching and thus, the hardness increases with higher β-phase in the alloy. Quenching from 1000°C allowed a small fraction of the alpha phase, probably due to a decrease in the sample temperature prior to the cooling process. The samples quenched from 1100°C illustrated a martensitic structure, as well as higher hardness than the annealed samples. Therefore, hardness decreased with the increase in cooling rate (the comparison is clearly seen in Figure 4.10, page 76; Figure 4.15, page 79; Figure 4.20, page 83). The decrease in hardness is more obvious in samples heat treated at 1000ºC, soaked for 1 hour and furnace cooled at different times (Figure 5.2).

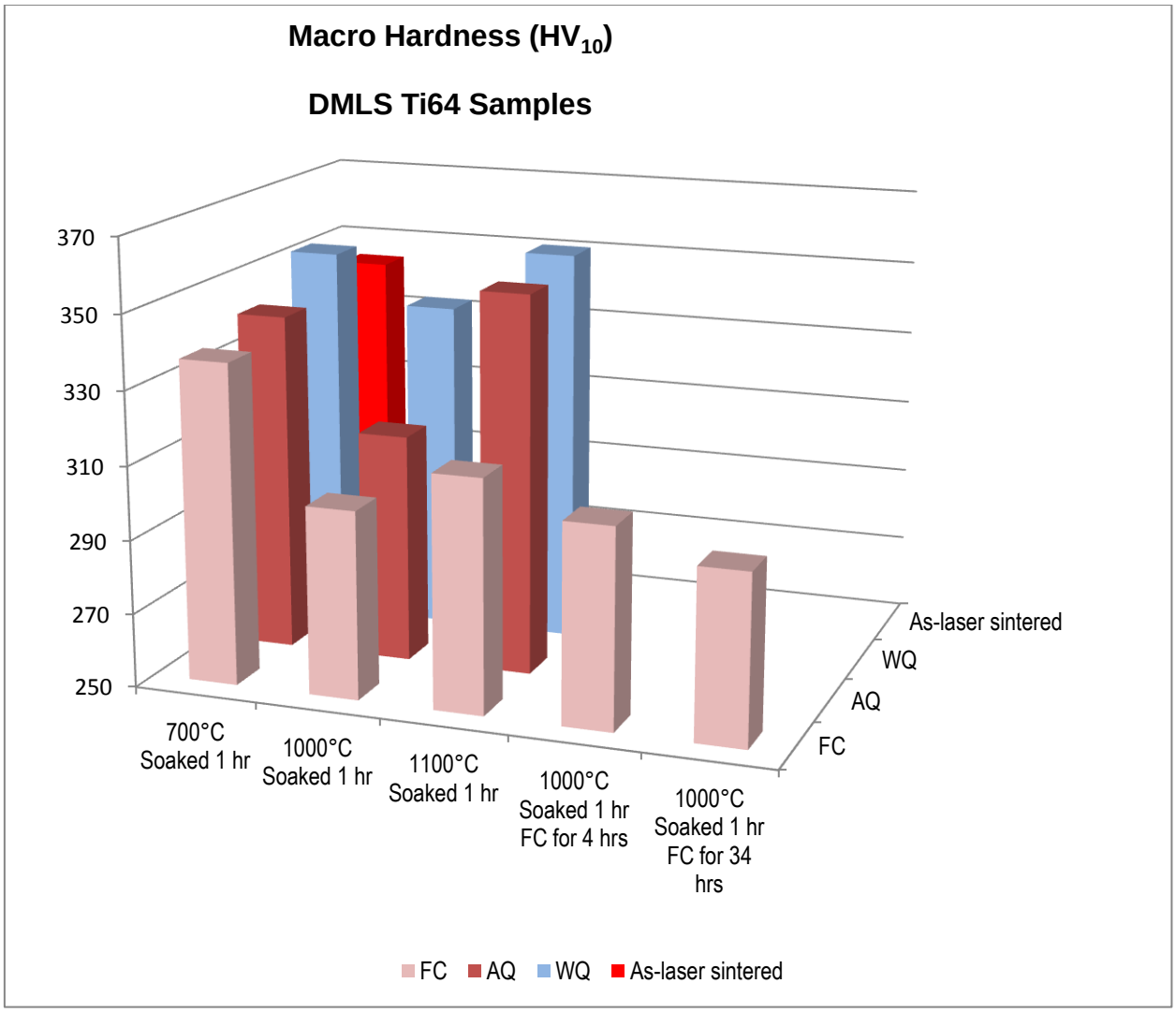

Figure 5.2 Comparison of macro hardness for DMLS Ti64 samples (experimental data)

Detailed tensile properties are shown in Appendix H. The effect of the heat treatment can be seen on the tensile properties of the specimens. Heat treatment at 1000°C soaked for 1 hour then furnace cooled for 4 hours improved the ductility from 2.61% to 12% elongation and even to a higher value of 18%, when the cooling time was increased to 34 hours. The area reduction increased from 3.51% to 25.95% for samples that were heat treated at 1000°C soaked for 1 hour then furnace cooled for 4 hours and

increased further to 33.39% at 34 hours cooling (see Figure 5.3). Conversely, both yield and ultimate strength decreased from 1005 to 827 and further to 805 MPa and from 1190 to 946 and 909 MPa, respectively (Figure 5.4). The tensile stress-strain curves of the DMLS Ti64 samples display the typical behaviour of Ti64 alloy, characterised by isotropic hardening. Tensile test results of all samples heat treated are within the acceptable values according to the ASTM F1472-08$^{\varepsilon 1}$ standards.

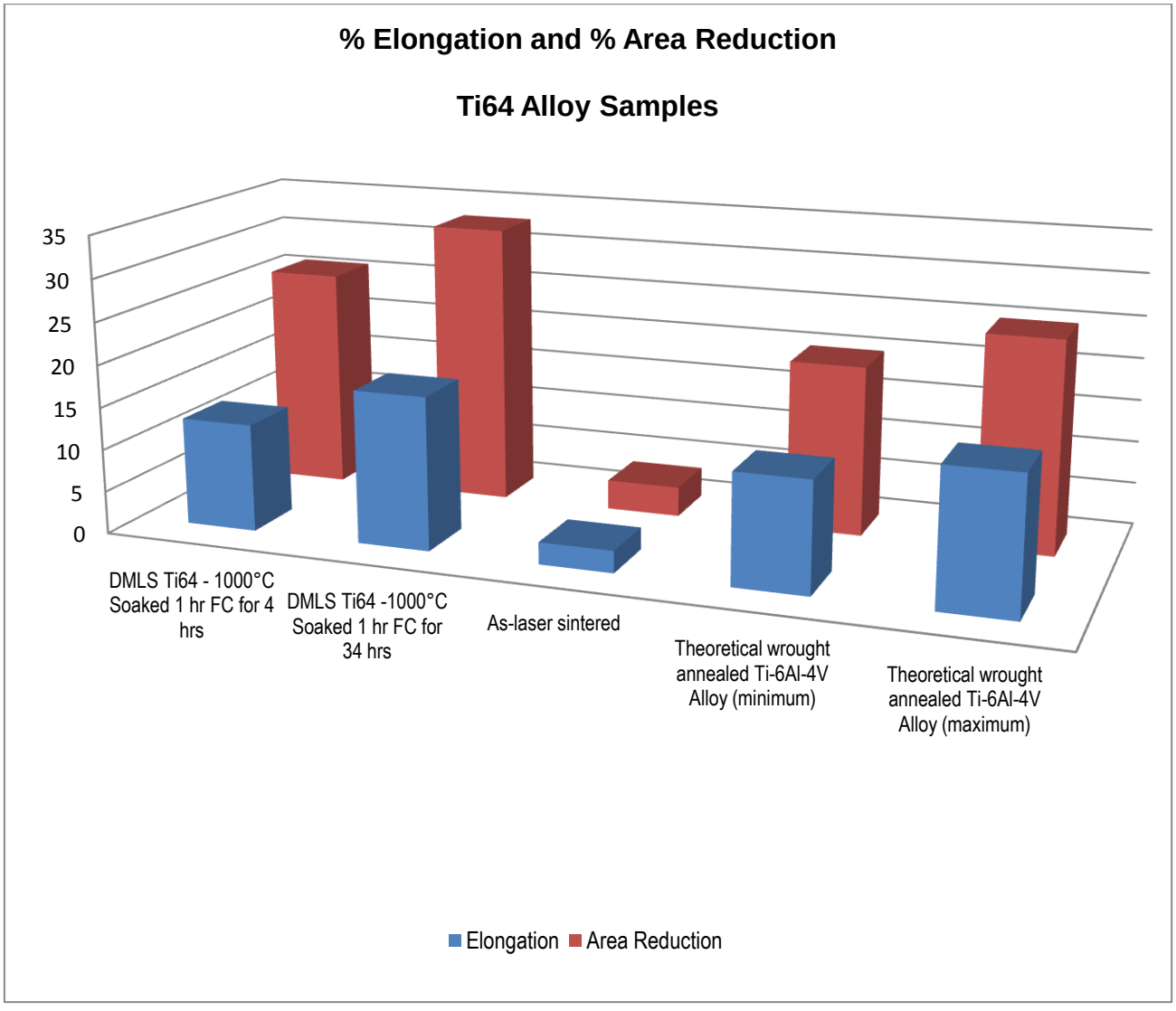

Figure 5.3 Comparison of the Ti64 alloy elongation and area reduction

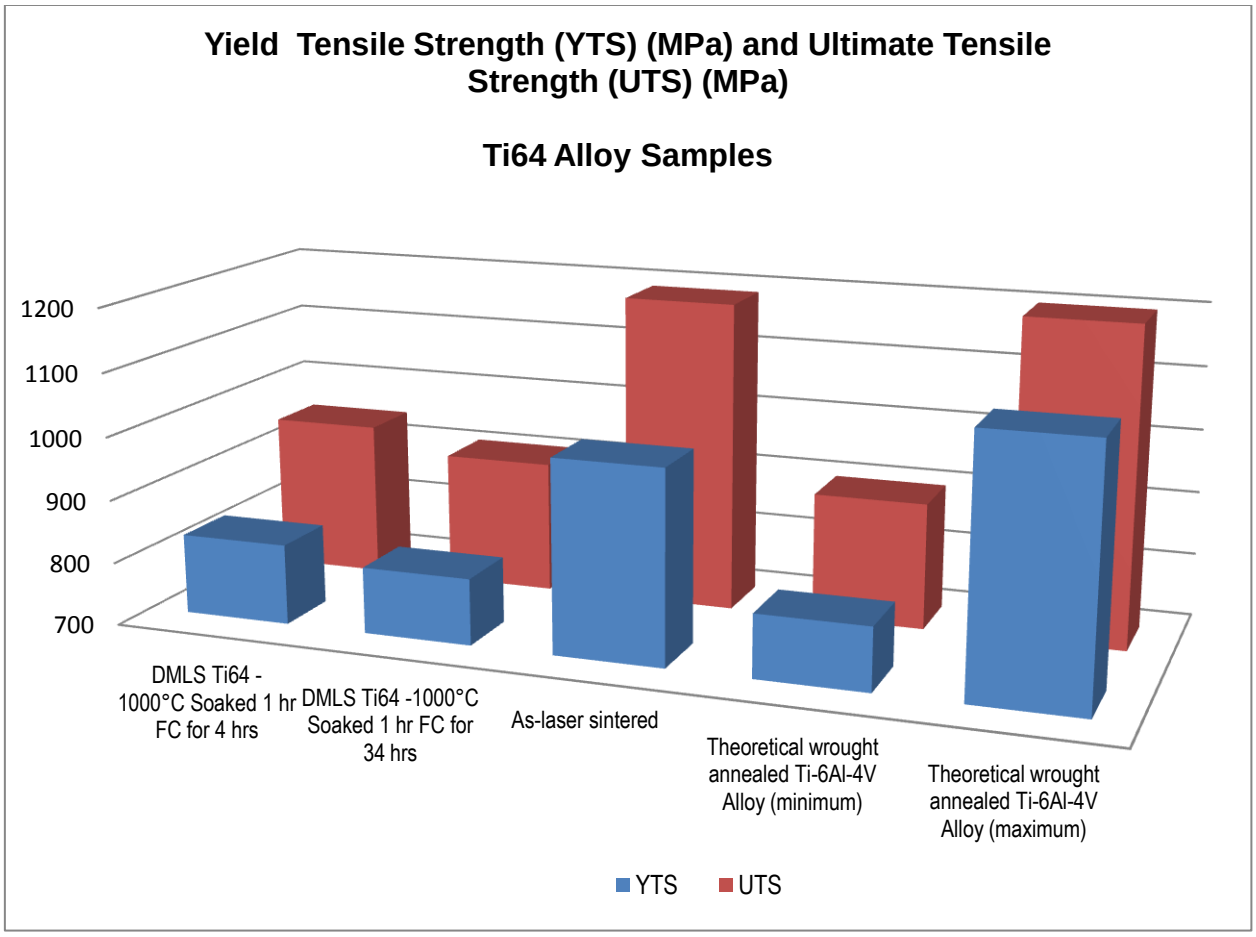

Figure 5.4 Comparison of the Ti64 alloy yield tensile strength (YTS) and ultimate tensile strength (UTS)

The obtained tensile properties of the DMLS Ti64 samples are compared to those from the literature review, and are shown in Table 5.1 and in Appendix F. The tensile properties of the DMLS Ti64 samples are similar to those of the wrought annealed titanium Ti-6Al-4V alloy and of the DMLS Ti64 samples according to the EOS material data sheet of DMLS EOSINT M 270 machine.

Table 5.1 Comparison of Ti64 alloy tensile properties

	THEORETICAL VALUES			EXPERIMENTAL VALUES		
PROPERTIES	Wrought Annealed Ti-6Al-4V Alloy *[ASTM F1472-08$^{\varepsilon 1}$ Standard]*	EOS As-laser Sintered Ti64 samples *[EOS Gmbh-Material Data Sheet 2011: 3]*	EOS DMLS Annealed Ti64 samples *[EOS Gmbh-Material Data Sheet 2011: 3-4]*	As-laser sintered Ti64 samples *[As-laser sintered Samples]*	DMLS Ti64 samples *[Samples were heat treated at 1000ºC soaked for 1 hour and furnace cooled for 4 hours]*	DMLS Ti64 samples *[Samples were heat treated at 1000ºC soaked for 1 hour and furnace cooled for 34 hours]*
TENSILE PROPERTIES						
2% Proof Stress [MPa]	800-1100	1070 ± 50	860	1005	827	805
Ultimate Tensile Strength [MPa]	900-1200	1200 ± 50	930	1190	946	909
% Elongation	6-10	11 ± 3	15±1	2.6	12.67	18.11
% Area Reduction	15-25	-	-	3.51	25.94	33.39

The calculated maximum Von Mises stresses found were similar to the FEA interpreted results. The average percentage error without the stress concentration factor was approximately 8.29%, while with the stress concentration factor included, was 0.07%. The small reaction forces induced in both x-axis and z-axis contributed to this error of 0.07% between the hand calculations and the ABAQUS^{TM} FEA results.

The 2% proof Von Mises Stress of both samples heat treated at 1000°C soaked for 1 hour and furnace cooled for 4 hours and 34 hours were within the theoretical range of 800 – 1120 MPa; whereas, the samples that were not heat treated indicated the highest 2% proof Von Mises Stress of 1184 MPa which falls outside the theoretical range (see Figure 5.5).

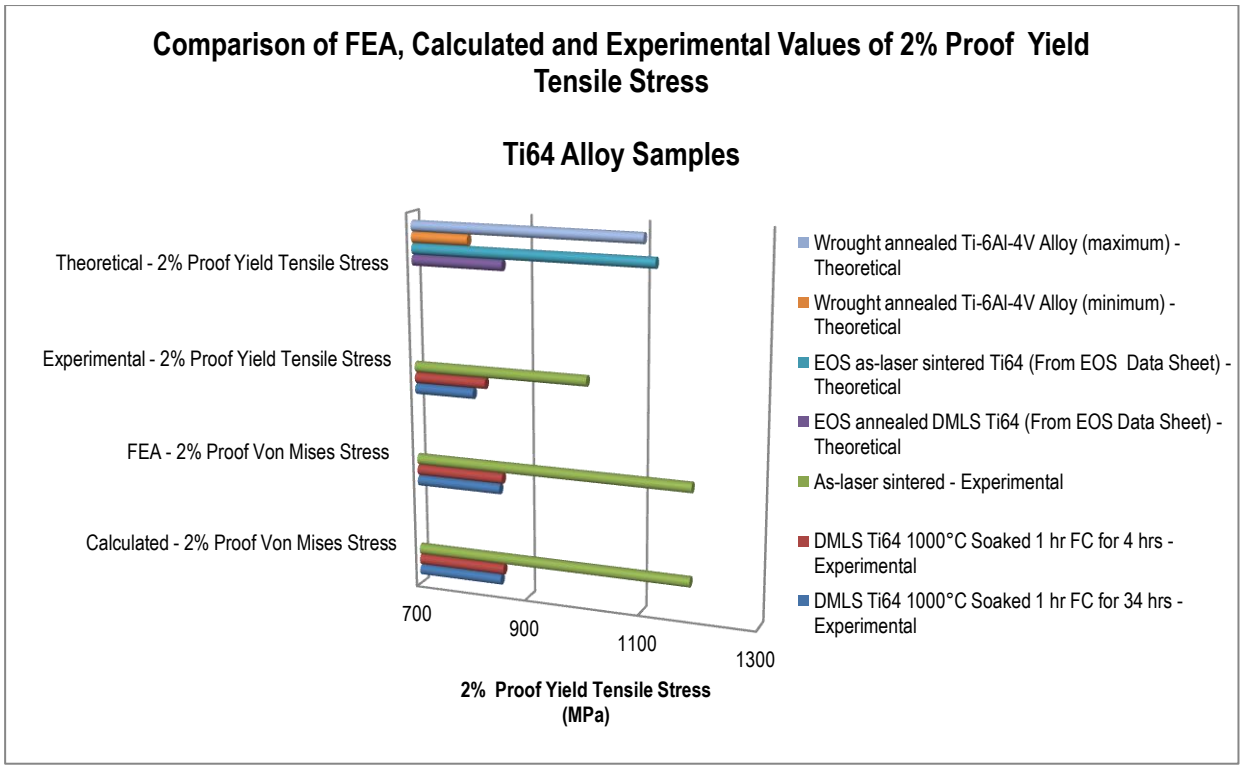

Figure 5.5 Comparison of FEA, calculated and experimental values of 2% proof yield tensile stress

Chapter 6. CONCLUSION AND RECOMMENDATIONS

6.1 Conclusion

The mechanical properties of unpolished DMLS Ti64 samples built on a vertical position, such as elastic constants, tensile and hardness results have fulfilled the standard specification for wrought annealed Ti-6Al-4V alloy for surgical implant application requirements (ASTM F1472-08$^{\varepsilon 1}$ standards).

However, the mechanical properties of materials are often limited by their imperfection due to either the design and/or the manufacturing process. According to the investigations done, the DMLS Ti64 samples inherited imperfections in the form of voids. Even though they are not quantified, the voids are possible initiation sites for cracks; thus, more research should be done on the possible effects of surface roughness on the strength of the unpolished DMLS Ti64 samples.

Extreme care should be taken whenever heat treatment is applied to the DMLS Ti64 samples. Heat treatment atmosphere plays a major role. The reaction of interstitial elements to titanium affects the mechanical properties.

The objectives of this study were achieved. The following were the major findings from the project:

- SEM-EDX and XRD analyses results for the powder identified major phases as the alpha + beta; thus, the alloy powder was confirmed to be Ti-6Al-4V. The powder particles are spherical in shape. The sizes of particles are within the range as they are less than 60µm. These results confirm that the EOS Ti64 powder is suitable for the DMLS process.

- The hardness, yield and ultimate tensile stresses were higher than those of standard specification for wrought annealed Ti-6Al-4V alloy for surgical implant application requirements. As-laser sintered samples failed, based on the Von Mises Criterion. Both the elongation and area reduction for as-laser sintered samples were very low, therefore, were found to be brittle. Thus the samples failed without yielding or warning.

- There is a relationship between the microstructure and the mechanical properties. However, this relationship should extend to other mechanical properties, such as fracture toughness, and high and low cycle fatigue. Tensile test results confirm the improvement of the ductility. The DMLS Ti64 samples that were beta annealed fell within the Von Mises Criterion; therefore, they did not fail due to yielding. Thus, the parts produced by the DMLS process should be heat treated whenever ductility is an important factor for the end user.

- The recommended heat treatment is beta annealing at 1000ºC and soaked for one hour. Thereafter, the parts should be cooled with the slowest cooling rate, such as furnace cooled so as to allow alpha grain growth. It is evident that increasing the alpha grain size increases ductility but decreases the hardness of the parts produced by the DMLS process. A vacuum furnace should be used to control the heat treatment atmosphere in order to avoid the contamination of interstitial elements, especially when the samples are being cooled in the furnace.

- The prediction of the DMLS Ti64 samples behaviour under static tensile load, up to a yield point using the ABAQUS^{TM} Finite Element Analysis program was accurate.

6.2 Recommendations

- The results of the characterisation of the EOS Ti64 powder indicate that more work needs to be done to establish the relationship between the density of the components built from the above powder and powder characteristics, such as chemical composition, particle shape, size and distribution.

- All tensile testing was performed on samples grown in a vertical orientation. More tests should be done on samples grown in both a horizontal and a diagonal

orientation so as to establish further the orientation effects on the ductility and the other tensile properties, such as yield stress and ultimate tensile strength.

- It is recommended that further tests should be conducted to establish if the similarities extend to other properties, such as compression, shear, torsion, fracture toughness, creep and fatigue. Heat treatment should also be included in the samples to be tested.

- This research was based on static conditions. Dynamic conditions should also be studied.

- The interstitial elements and/or impurities should be investigated in future as their quantities can affect the physical properties of the pure metal.

- Further studies should be done on stress concentration, looking particularly at the surface roughness of the DMLS Ti64 samples.

- The stress-strain curve relationship studies should extend to other aspects, such as stress-strain gradient and stress-strain rate over a larger range of strain. Further studies should be done to investigate the exact necking point in both experimental and FEA tensile tests. These studies can also extend to a compression test.

REFERENCES

Amstutz, H. C. & Grigoris P. 1996. Metal on Metal Bearings in Hip Arthroplasty. Clinical Orthopaedics and Related Research. 329:11-34.

Armstrong, R.W. 1987. The (cleavage) strength of pre-cracked polycrystals. Engineering Fracture Mechanics. 28 (5-6): 529–538.

ASM Aerospace Specification Metals Inc, version 10.12. 2011. Titanium Ti-6Al-4V - AMS 4911. [Online]. Available: http://www.aerospacemetals.com/titanium- Ti-6Al-4V-ams-4911.html. [Accessed on the 12 March 2011].

ASTM B 265-13ae1 Grade 1 Standard Specification for Titanium and Titanium Alloy Strip, Sheet, and Plate.

ASTM E 494 Standard practice for measuring ultrasonic velocity in materials. Annual book of ASTM standards.

ASTM E8 / E8M - 11 Standard Test Methods for Tension Testing of Metallic Materials. Annual book of ASTM standards.

ASTM E 385-11e1 Standard practice for Knoop and Vickers hardness of materials. Annual book of ASTM standards.

ASTM F136 - 12 Standard Specification for Wrought Ti-6Al-4V ELI (Extra Low Interstitial) Alloy for Surgical Implant Applications (UNS R56401) Annual book of ASTM standards.

ASTM F 1472-08$^{\varepsilon 1}$ Standard Specification for Wrought Annealed Titanium Ti-6Al-4V Alloy for Surgical Implants Application (UNS R56400).

Bao, J. 2003. Prediction of Ductile crack formation in uncracked Bodies. Massachusetts Institute of Technology. Cambridge. [Online]. Available: http://dspace.mit.edu/handle/1721.1/17634. [Accessed on the 22 June 2011].

Baufeld, B. & van der Biest, O. 2009. Mechanical properties of Ti-6Al-4V specimens produced by shaped metal deposition. *Journal of Science and Technology of Advanced Materials*. 10 (1): 1-10.

Bertol L. S., Kindlen Jnr W., Da Silva F. P., Aumund-Koop C. 2010. Medical Design; Direct Metal Laser Sintering of Ti-6Al-4V. *Materials and Design* 31(8): 3982–3988.

Boyer R., Collings, E.W., Welsch, G (eds.). 1994. Materials Properties Handbook: Titanium Alloys ASM International.

Callister W. D. Jr. 2006. Materials Science and Engineering: An introduction, Material Selection and Design Consideration, 7th Edition. John Wiley & Sons, Inc.

Carpenter technology. 2011. *Technical datasheet: titanium alloy Ti-6Al-4V*. [Online]. Available: http://cartech.ides.com/datasheet.aspx?i=101&E=269. [Accessed on the 12 March 2011].

Chao I., Pinkall U., Sanan P., Schröder P. 2010. A Simple Geometric Model for Elastic Deformations. Caltech, TU Munchen Germany. 29 (4):38.

Charnley, J. 1970. Total hip replacement by low-friction arthroplasty. *Clinical Orthopaedics and Related Research*. 72: 7-21.

Cook R. D., Malkus D. S., Plesha M. E., Witt R. J., 2002. Concepts and Applications of Finite Element Analysis. University of Wisconsin–Madison, 4th Edition John Wiley & son, Inc.

da Rocha, S. S., Adabo, G. L., Henriques, G. E. P. & Nóbilo, M. A. 2006. Vickers hardness of cast commercially pure titanium and Ti-6Al-4V alloy submitted to heat treatments. *Brazillan Dental Journal*. 1 (2): 126-129.

Drotsky, J. G. 1994. Strength of Materials for Technicians. 2nd Edition.

Eisen, W.B., Ferguson, B.L., German, R.M., Lacocca, R., Lee, P.W., Madan, D., Moyer, K., Sanderow, H. & Trudel Y. (Eds). 1998. *Powder Metal Technologies and Applications Volume 07*. ASM International Handbook.

Engh, C. A., Bobyn, J. D. & Glassman, A. H.1987. Porous-coated hip replacement: the factors governing bone in-growth, stress shielding and clinical results. *Journal of Bone and Joint Surgery*. 69(1):45-54.

EOS GmbH-Electro Optical System. 2011. Material data sheet: EOS Titanium Ti64 for EOSINT M 270. [Online]. Available: http://www.detekt.com.tw/download/eos/4%E6%9D%90%E6%96%99%E7%A8%AE%E9%A1%9E/Metal/Ti-Ti64-M270_Material_data_sheet_05-11_en.pdf. [Accessed on the 10 December 2011].

Filip, R., Kubiak, K., Ziaja, W. & Sieniawski, J. 2003. The effect of microstructure on the mechanical properties of two-phase titanium alloys. *Journal of Material Processing Technology.* 133(1-2): 84-89.

Finlay W. L. & Snyder J. A. 1950. Effects of three interstitial solutes (Nitrogen, Oxygen and Carbon) on the mechanical properties of high-purity alpha titanium. *Journal of Metals*. 188: 277-286.

Gilbert R., IMI Titanium, Shannon, C. R. & Allvac, T.(Eds) 1990. ASM Handbook Volume 4, Heat Treating. ASM International.

Ghany, K. A. & Moustafa, S. F. 2006. Comparison between the products of four RPM systems for metals. *Rapid Prototyping Journal*. 12 (2): 86-94.

Grote Karl-H. & Antonsson Erik K. 2009. Springer Handbook of Mechanical Engineering, Technology and Engineering. Springer. 10: 737- 750.

Hall, E.O. 1951.The Deformation and Ageing of Mild Steel. Discussion of Results. *Proceedings of the Physical Society London.* 64 (9): 747-753. [Online] Available: http://iopscience.iop.org/0370-1301/64/9/303. [Accessed on the 22 April 2012].

Hänninen, J. 2002. Direct metal laser sintering. *Advanced Materials & Processes. 160(5):* 33-36.

Hausmann, J., Baumann, K., Lenser, S., Kelm, K., Chernova, L., Weber, K. & Reh, S. 2009. Processing of (α/β) and (α2/γ) titanium alloys to tailor microstructure for performance, *Aeromat Presentation* June 9 2009, Deutsches Zentrum für Luft- und Raumfahrt [Online] Available: http://www.mtu.de/en/technologies/engineering_news/others/Smarsly_Processing_en.pdf. [Accessed on the 4 October 2010].

He G., Liu P. & Tan Q. 2012. Porous titanium materials with entangled wire structure for load-bearing biomedical applications. *Journal of Mechanical Behaviour of Biomedical Materials*. 5(1): 16-31.

Huiskes, R. 1993. Stress shielding and bone resorption in THA: clinical versus computer-simulation studies. *Acta Orthopaedic Belgica*. 59(1):118-129. International Titanium Association 2005. Specifications Book. 4th Edition.

Joshi, M. G., Advani, S. G., Miller, F. & Santare, M. H. 2000. Analysis of a femoral hip prosthesis designed to reduce stress shielding. Journal of Bio-Mechanics. 33(12): 1655-62.

Joshi, V. A. 2006. *Titanium alloys - an atlas of structures and fracture features. Defense Metallurgical Research Lab, Hyderabad, India.* CRC Taylor & Francis Group.

Joun, M., Choi, I., Eom, J. & Lee, M. 2007. Finite element analysis of tensile testing with emphasis on necking. *Computational Material Science*. 41 (1):63-69.

Jovanović M.T., Tadić S., Zec S., Mišković Z. & Bobić I. 2006. The Effect of Annealing Temperatures and Cooling Rates on Microstructure and Mechanical Properties of Investment Cast Ti-6Al-4V Alloy. *Materials & Design*. 27:192-199.

Kao, Y. L., Tu, G. C., Huang C. A. & Liu, T.T. 2005. A study on the hardness variation of α- and β-pure titanium with different grain sizes. Journal of Materials Science and Engineering. 398 (1-2): 93-98.

Krishna, B. V., Bose, S. & Bandyopadhyay, A. 2007. Low stiffness porous Ti structure for load-bearing implants. *Acta Biomaterialia*. 3 (6): 997-1006.

Kruth, J., Leu M.C. & Nakagawa, T. 1998. Progress in Additive Manufacturing and Rapid Prototyping. CIRP Annals - Manufacturing Technology. 47 (2): 525-540.

Lee TY, Peters M, Welsch G. 1991. Elastic Moduli and Tensile and Physical Properties of Heat-Treated and Quenched Powder Metallurgical Ti-6Al-4V Alloy; *Metallurgical Transactions A.* 22 (3): 709-713.

Leyens, C. & Peters, M. (Eds). 2003. *Titanium and Titanium Alloys: Fundamentals and Applications*. WILEY-VCH GmbH & Co. KGaA.

Liu X., Chu P.K., & Ding C. 2004. Surface Modification of Titanium, Titanium Alloys and Related Materials for Biomedical Applications. *Materials Science and Engineering.* 47: 49-121.

Long, M. & Rack, H. J. 1998. Titanium alloys in total joint replacement - a materials science perspective. *Biomaterials. 19 (18): 1621-1639.*

Lütjering, G 1998. Influence of processing on microstructure and mechanical properties of (α+β) titanium alloys. *Journal of Materials Science and Engineering*. 243 (1-2): 32-45.

Mahesh, M., Wong, Y. S., H. Fuh, F.Y. & Loh, H.T. 2004. Benchmarking for comparative evaluation of RP systems and processes. *Rapid Prototyping Journal*. 10(2): 123-135.

Matthew, J. & Donachie Jr. (Eds). 2000. *Titanium: A technical Guide*. 2nd Edition. ASM international.

McClintick, R. J., Bauer, W.C. & Busch L. S. 1955. *Physical* Metallurgy *and Heat treatment of Titanium Alloys.* Niles Ohio. Mallory-Sharon Titanium Corporation.

Meyers, M. C. & Chawla, K. K. 1999. *Mechanical behavior of materials, 2nd edition.* Cambridge University Press.

Murr, L. E., Gaytan, S. M., Medina, F., Lopez, M. I., Martinez, E & Wicker, R.B. 2009. Additive layered manufacturing of reticulated Ti-6Al-4V biomedical mesh structures by electron beam melting. 25th Southern Biomedical Engineering Conference IFMBE Proceedings. 24 (3): 23-28.

Murra, L.E., Quinonesb, S.A., Gaytana, S.M., Lopeza, M.I., Rodelaa, A., Martineza, E.Y., Hernandeza, D.H., Martineza, E., Medinac, F. & Wickerc R.B. 2009. Microstructure and mechanical behaviour of Ti-6Al-4V produced by rapid-layer

manufacturing, for biomedical applications. *Journal of Mechanical Behaviour of Biomedical Materials*, 2 (1): 20-32.

Nalla R.K., Boyce B.L., Campbell J.P., Peters J.O. & Ritchie R.O. 2002. Influence of Microstructure on High Cycle Fatigue of Ti6Al4V Bimodal vs. Lamellar Structures: *Metallurgical and Materials Transactions A*, 33 (13): 899-918.

Ning, Y., Fuh, J.Y.F., Wong, Y. S. & Loh, H.T.2004. An intelligent parameter selection system for direct metal laser sintering process. *International Journal of Production Research*. 42 (1): 183-199.

Ning, Y., Wong, Y. S. & Fuh, J. Y. H. 2005. Effect and control of hatch length on material properties in the direct metal laser sintering process. *Part B: J. Engineering manufacturing*. 219 (1): 15-25.

Parthasarathy. J., Starly, B., Raman, S. & Christensen, A. 2010. Mechanical Evaluation of Porous Titanium (Ti-6Al-4V) Structures with Electron Beam Melting (EBM). *Journal of Mechanical Behaviour of Biomedical Materials.* 3 (3): 249–259.

Petch N.J. 1953. The Cleavage Strength of Polycrystals. Journal of the Iron and Steel institute 174(): 25-28. [Online] Available: https://www.zotero.org/vayardley/items/itemKey/V8T44E77. [Accessed on the 22 April 2012].

Philpot T., 2000. MDSolids: Software to Bridge the Gap between Lectures and Homework in Mechanics of Materials. University of Missouri-Rolla. Tempus Publications. 16 (5): 401-407.

Philpot, T. A. 2010. Mechanics of materials: an integrated learning system. Wiley.

Pilkey, W. D. & Pilkey, D. F. 2008. Peterson's Stress Concentration Factors. 3rd Edition. John Wiley & Sons, Inc

Poondla, N., Srivatsan, T.S., Patnaik, A. & Petraroli, M. 2009. A study of the microstructure and hardness of two titanium alloys: commercially pure and Ti-6Al-4V. *Journal of Alloys and Compounds*. 486 (1-2): 162-167.

Pottier, T., Toussaint, F. & Vacher, P. 2007. An inverse method for material parameters determination of titanium samples under tensile loading. *International Journal of Material Forming*.1 (1): 21-24.

Queheillalt, D. T. & Wadley, H. N. G. 2005. Cellular metal lattices with hollow trusses. *Acta Materialia*. 53: 303-313. [Online] Available: http://www.ipm.virginia.edu/newpeople/wadley/PDF/Cellular_Metal_Lattice_with_Hollow Trusses.pdf. [Accessed on the 22 April 2010].

Rehme, O. & Emmelmann, C. 2006. *Rapid manufacturing of lattice structures with selective laser melting*. Conference Proceedings. Volume 6107, Laser-based Micropackaging CA January 21, 2006. [Online]. Available: http://dx.doi.org/10.1117/12.645848. [Accessed on the 20 March 2011].

Rocha, S., Adabo, G. L., Henriques, G. E. P. & Nóbilo, M. A. (2006). Vickers hardness of cast commercially pure titanium and Ti-6Al-4V alloy submitted to heat treatments. *Brazillan Dental Journal*. 17 (2): 126-129.

Rosen, D., Johnston, S. & Reed, M. 2006. *Design of general lattice structures for lightweight and compliance applications*. Rapid Manufacturing Conference Loughborough University July 5-6, 2006. Atlanta. [Online] Available:

http://www.srl.gatech.edu/publications/2006/LatticeAnl_DWR_RM2006.pdf.

[Accessed on the 13 October 2007].

Roylance, D. 2001. Stress-strain curve. *Department of Material Science and Engineering, Massachusetts Institute of Technology Cambridge MA 02139.* 23 August 23 2001: 1-14. [Online] Available: http://ocw.mit.edu/courses/materials-science-and-engineering/3-11-mechanics-of-materials-fall-1999/modules/ss.pdf. [Accessed on the 04 April 2011].

Sander, B.R. & Weintraub, T.L. (eds) 2000. *Mechanical Testing and Evaluation Volume 8, 9th edition*. ASM International handbook.

Semiatin, S.L., Knisley, S.L., Fagin, P.N., Barker, D. R. & Zhang, F. 2003. Microstructure Evolution during Alpha-Beta Heat Treatment of Ti-6Al-4V. *Metallurgical and Material Transactions*, 34 (10): 2377-2386.

Sharma A., Junaidh M. I., Purushothana K. K., Kotval C. P., Paul J., Tripathi S., Pant B. & Sandaranarayan A. S. 2006. Acoustic Emissions Response of Ti6Al4VV in Different Heat Treatment conditions during tensile Testing. Chapter published in National Seminar proceeding at Hyderabad, 7-9 December 2006: 1-12. [Online] Available: http://www.ndt.net/article/nde-india2006/files/tp-15-pap.pdf. [Accessed on the 20 April 2010].

Shigley, J. E. & Mischke, C. R. 2003. *Mechanical Engineering Design, 6th metric edition*. New York. McGraw Hill.

Simachi, A. & Pohl, H. 2003. Effects of laser sintering processing parameters on the microstructure and densification of iron powder. *Journal of Materials and Engineering*, 359 (1-2): 119-128.

Simchi A. 2006. Direct Laser Sintering of Metal Powders, Mechanism, Kinetics, and Microstructural Features. *Material Science and Engineering.* 428 (1-2): 148–158.

Smith, W. F. 1981. Structure and properties of engineering alloys. New York. McGraw-Hill.

Sustarsic B., Dolinsek S., Jenko M., Leskovšek V. 2009. Microstructure and Mechanical Characteristics of DMLS Tool-Inserts. *Materials and Manufacturing Processes*. 24: 837- 841.

Timoshenko, S. P. & Krieger, S. W. 1970. *Theory of Plates and Shells, 2nd edition*. New York. Mc Graw Hill.

Tabor, D. 1947. *A Simple Theory of Static and Dynamic Hardness.* Proceedings of the Royal Society of London Series A: Mathematical and Physical Sciences 4 February 1948. 192 (1029): 247-274 [Online] Available: http://www.jstor.org/stable/98140. [Accessed on the 20 March 2009].

Tabor, D. 1951. *The Hardness and Strength of Metals*. Oxford: Clarendon Press.

Vail, N. K., Swain, L. D., Fox, W. C., Aufdlemorte, T. B., Lee, G. & Barlow, J. W. 1999. Materials for biomedical applications. *Materials & Design*. 20 (2): 123-132.

Vandenbroucke, B. & Kruth, J. P. 2007. Selective laser melting of biocompatible metals for rapid manufacturing of medical parts. *Rapid Prototyping Journal.* 13 (4): 196-203

Van Hengel C., 2001. Fiber Metal Laminates: An Introduction, *Academic Publisher*. 1 (1):15-16.

Van Lenthe, G. H., De Waal Malefijt, M. C. & Huiskes, R. 1997. Stress shielding after total knee replacement may cause bone re-sorption in the distal femur. *The Journal of Bone and Joint Jurgery*, 79-B (1):117-122.

Vicatos, G. & Hosking, K. 2003. Engineering and surgical techniques combine in cost-effective titanium implants that are bringing patients new hope page 82-85. December 2003. University of Cape Town S A.

Voort, G.V. (ed). 2004. *Metallography and Microstructures Volume 09.* ASM international Handbook.

Wallach, J. C. & Gibson, L. J. 2001. Mechanical behaviour of three-dimensional truss material. *International Journal of Solids and Structures.* 38 (40-41): 7181-7196.

Wallach, J. C. & Gibson, L. J. 2001. Defect sensitivity of a 3D truss material. *Scripta Materialia*. 45 (6): 639-644.

Yingbin, B., 2003. Prediction of Ductile Crack formation in Uncracked bodies. *Massachusette Institute of Technology. Department of Ocean Engineering*. [Online] Available: http://dspace.mit.edu/handle/1721.1/17634. [Accessed on the 4 September 2010].

Zheng,Y., Rong,Y. & Hou, Z. 2008. The study of fixture stiffness part I: A finite element analysis for stiffness of fixture units. The International Journal of Advanced Manufacturing Technology. 36 (9-10): 865-876.

Zhou, J., Shrotriya, P. & Soboyejo, W. O. 2004. On the deformation of aluminium lattice block structures: from struts to structures. *Mechanics of Materials.* 36 (8): 723-737.

Yuehuei H., M.D., Robert A. & Draughn, D.Sc (Eds) 1999. *Mechanical testing of bone and the bone-implant interface.* London. C CRC Press.

Žitňanský,M. & Čaplovič, Ľ. 2004. The preparation of Ti-6Al-4V alloy in laboratory conditions. *Journal of Material Processing Technology*, 157-158 (December 20, 2004): 781-787.

APPENDICES

Appendices are presented in chart format and are written in CD disc. This CD disc will be handed in together with the dissertation book. Below is the list of appendices:

Appendix A

Density and Elastic Constants of As-laser Sintered Ti64 Samples.

Appendix B

Optical Microscope (OM), Scanning Electron Microscope (SEM) & Chemical Analysis of As-laser Sintered Ti64 Samples.

Appendix C

Optical Microscope (OM), Scanning Electron Microscope (SEM) & Chemical Analysis of DMLS Ti64 Samples; Heat treated at 700°C Soaked for 1 hour then cooled at different medium.

Appendix D

Optical Microscope (OM), Scanning Electron Microscope (SEM) & Chemical Analysis of DMLS Ti64 Samples; Heat treated at 1000°C Soaked for 1 hour then cooled at different medium.

Appendix E

Optical Microscope (OM), Scanning Electron Microscope (SEM) & Chemical Analysis of DMLS Ti64 Samples; Heat treated at 1100°C Soaked for 1 hour then cooled at different medium.

Appendix F

Optical Microscope (OM) & Scanning Electron Microscope (SEM), Chemical Analysis of DMLS Ti64 Samples; Heat treated at 1000°C Soaked for 1 hour then vacuum furnace cooled at different times.

Appendix G

Macro Hardness of DMLS Ti64 Samples.

Appendix H

Tensile Properties of DMLS Ti64 Samples.

Appendix I

Chemical Composition, Elastic Constants and Mechanical Properties of Ti64 Alloy

Appendix J

Ramosoeu, M. E., Booysen, G. & Ngonda, T. N. 2009. Mechanical Characteristics of Direct Laser Sintered Titanium (Ti64) Built on EOSINT M270 Sintering Machine. Paper

presented at the RAPDASA 2009 Conference held at Mpekwini Beach Resort in East London on the 04-06 November 2009.

Appendix K

Ramosoeu, M. E., Chikwanda, H. K., Bolokang, A. S., Booysen, G. & Ngonda T. N. 2010. Additive Manufacturing: Characterisation Of Ti-6Al-4V Alloy Intended for Biomedical Application. *Southern African Institute of Mining and Metallurgy, published in Conference Proceedings.* ISBN Number 978-1-920410-10-0:337-344.

[Online]. Available:

http://researchspace.csir.co.za/dspace/bitstream/10204/4617/1/Ramosoeu1_2010.pdf.

[Accessed on the 05 January 2011].

Paper also presented at Light Metal Conference on the 27-29 October 2010 held at Misty Hills Muldersdrift.

Appendix L

Ramosoeu, M. K. E., Booysen, G., Ngonda, T. N. & Chikwanda, H. K. 2011. Mechanical Properties of Direct Laser Sintered Ti-6Al-4V. *ASM International 2011, published in Conference Proceedings*. ISBN Number 978-1-1183-0502-7:1460-1468.

[Online]. Available:

http://www.asminternational.org/portal/site/www/AsmStore/ProductDetails/?vgnextoid=d1bf6a4a56944310VgnVCM100000621e010aRCRD.

[Accessed on the 05 January 2011].

Paper also presented at MS&T 2011, Materials Science & Technology 2011 Conference and Exhibition (MS&T Partner Societies) on the 16-20 October 2011 held at Columbus, OHIO.

APPENDIX A

DENSITY AND ELASTIC CONSTANTS AS-LASER SINTERED Ti64 SAMPLES

	Method:	Archimedes principle										
	Liquid:	Water										
	Material	DMLS Ti-6Al-4V										
Sample no	A	B	C	D	E	F	G	H	I	J	K	L
Mass dry 1 (g)	0.8878	0.949	0.9608	0.7283	1.7755	1.8981	2.8033	2.8823	1.4526	1.4566	3.7959	3.8431
Mass dry 2 (g)	0.8879	0.949	0.9608	0.7284	1.7755	1.8983	2.8031	2.8823	1.4526	1.4567	3.796	3.8433
Average dry (g)	**0.8879**	**0.949**	**0.9608**	**0.7284**	**1.7755**	**1.8982**	**2.8032**	**2.8823**	**1.4526**	**1.4567**	**3.796**	**3.8432**
Mass wet 1 (g)	0.6855	0.7321	0.7421	0.5621	1.3711	1.4683	2.1694	2.226	1.1185	1.1241	2.9368	2.9681
Mass wet 2 (g)	0.6846	0.7323	0.7419	0.5616	1.3712	1.4692	2.1692	2.2258	1.1181	1.1231	2.9372	2.9683
average wet (g)	**0.6851**	**0.7322**	**0.742**	**0.5619**	**1.3712**	**1.4688**	**2.1693**	**2.2259**	**1.1183**	**1.1236**	**2.937**	**2.9682**
Volume (cm3)	**0.2028**	**0.2168**	**0.2188**	**0.1665**	**0.4044**	**0.4295**	**0.6339**	**0.6564**	**0.3343**	**0.3331**	**0.859**	**0.875**
Density (g/cm3)	**4.378**	**4.3773**	**4.3912**	**4.3745**	**4.391**	**4.4201**	**4.4221**	**4.3911**	**4.3452**	**4.3737**	**4.4193**	**4.3922**

DENSITY

MEASURED AND CALCULATED VALUES

	Method:	Pulse echo ultrasonic													
	Equipment:	Krautkramer USIP 12													
	Longitudinal probe:	50MHz													
	Transverse probe:	20MHz													
	Material:	DMLS Ti-6Al-4V													
Sample no	A	B	C	D	E	F	G	H	I	J	K	L				
Sample Thickness (mm)	0.77	0.75	0.83	1.51	1.54	1.55	2.32	2.49	3	3.02	3.11	3.33				
2T (µs)	0.255	0.245	0.268	0.491	0.509	0.501	0.746	0.804	0.97	0.98	1.002	1.072				
4T (µs)	0.512	0.492	0.536	0.983	1.023	1.004	1.5	1.607	1.942	1.966	2.008	2.144				
Average time one way (µs)	0.127833333	0.122833333	0.134	0.245666667	0.255333333	0.250833333	0.374333333	0.401833333	0.485333333	0.491	0.501666667	0.536				
Longitudinal Speed of sound (I	6023.468057	6105.834464	6194.029851	6146.540027	6031.331593	6179.401993	6197.684773	6196.598922	6181.318681	6150.712831	6199.335548	6212.686567				
2T (µs)	0.487	0.479	0.531	0.958	0.974	0.987	1.474	1.59	1.906	1.916	1.976	2.124				
4T (µs)	0.974	0.959	1.057	1.918	1.948	1.974	2.944	3.17	3.823	3.835	3.948	4.228				
Average time one way (µs)	0.2435	0.239666667	0.264666667	0.479333333	0.487	0.4935	0.736333333	0.793333333	0.954833333	0.9585	0.987333333	1.058666667				
Transverse Speed of sound (m	3162.217659	3129.346314	3136.020151	3150.208623	3162.217659	3140.8308	3150.746944	3138.655462	3141.909583	3150.75639	3149.898717	3145.465995				
Density (g/cm3)	**4.377959**	**4.427306**	**4.391225**	**4.374474**	**4.390998**	**4.420072**	**4.422149**	**4.391073**	**4.425199**	**4.373668**	**4.419291**	**4.392229**	average	4.4004703	S.D.	0.02082925
Poisson's ratio	3.10E-01	3.22E-01	3.28E-01	3.22E-01	3.10E-01	3.26E-01	3.26E-01	3.27E-01	3.26E-01	3.22E-01	3.26E-01	3.28E-01	average	3.23E-01	S.D	0.00625462
Shear modulus, G, (Gpa)	4.3778E+10	4.3356E+10	4.3186E+10	4.3411E+10	4.3908E+10	4.3603E+10	4.39E+10	4.3257E+10	4.3684E+10	4.3419E+10	4.3848E+10	4.3457E+10	average	4.357E+10	S.D	253962458
Young's modulus, E, (Gpa)	1.15E+11	1.15E+11	1.15E+11	1.15E+11	1.15E+11	1.16E+11	1.16E+11	1.15E+11	1.16E+11	1.15E+11	1.16E+11	1.15E+11	average	1.15E+11	S.D	643981785
Bulk modulus, B, (Gpa)	1.00E+11	1.07E+11	1.11E+11	1.07E+11	1.01E+11	1.11E+11	1.11E+11	1.11E+11	1.11E+11	1.08E+11	1.11E+11	1.12E+11	average	1.08E+11	S.D	320642469

ELASTIC CONSTANTS

MEASURED AND CALCULATED VALUES

MAKHABO KHABISO ELLEN RAMOSOEU
20203047

APPENDIX B

OPTICAL MICROSCOPE (OM), SCANNING ELECTRON MICROSCOPE (SEM) & CHEMICAL ANALYSIS AS-LASER SINTERED Ti64 SAMPLES

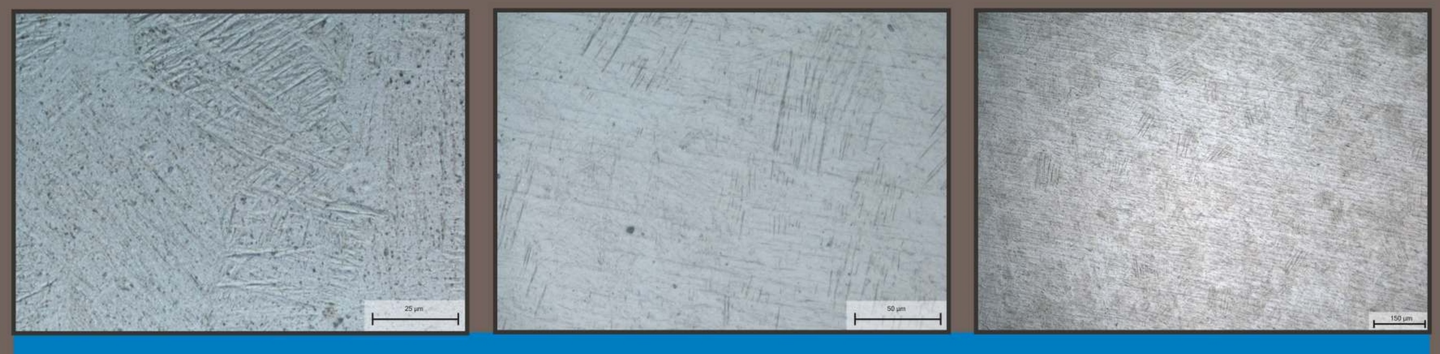

OM MICROGRAPHS (SAMPLES CUT LONGITUDINAL)

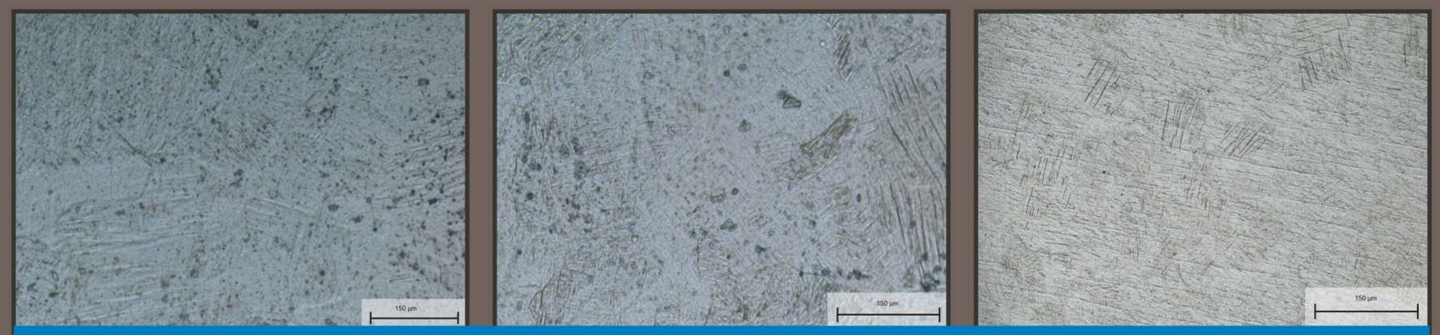

OM MICROGRAPHS (SAMPLES CUT TRANSVERSE)

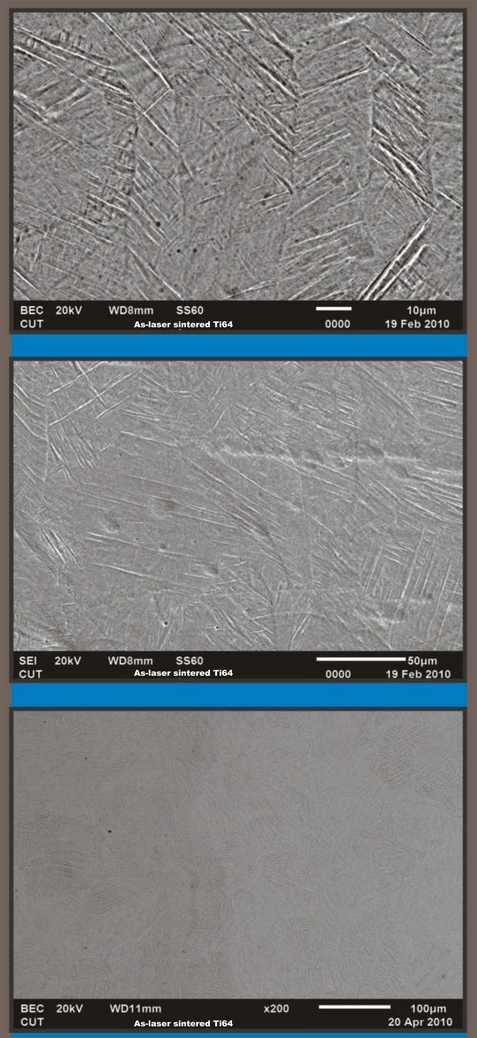

SEM MICROGRAPHS

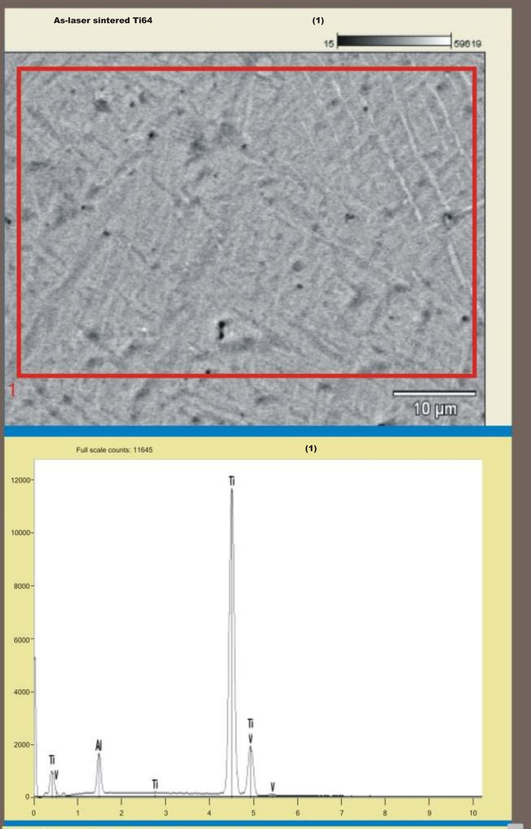

Wed Nov 17 14:51:49 2010
Filter Fit Chi-squared value: 9.741 Errors:+/-1 Sigma
Correction Method: Proza[Phi-Rho-Z]
Acc Voltage: 20.0 kV Take Off Angle:35.3 deg

Element Line	Element Wt%	Wt% Error	Atom%	Atom% Error
AlK	5.33	+/-0.07	9.10	+/-0.12
TiK	90.823	+/-0.34	87.41	+/-0.32
VK	3.86	+/-0.12	3.49	+/-0.11
Total	100.00		100.00	

CHEMICAL ANALYSIS

MAKHABO KHABISO ELLEN RAMOSOEU
20203047

APPENDIX C

OPTICAL MICROSCOPE (OM), SCANNING ELECTRON MICROSCOPE (SEM) & CHEMICAL ANALYSIS
DMLS Ti64 SAMPLES
HEAT TREATED AT 700°C SOAKED FOR 1 HOUR THEN COOLED AT DIFFERENT MEDIUM

OM MICROGRAPHS - FURNACE COOLED (SAMPLES CUT LONGITUDINAL)

OM MICROGRAPHS - FURNACE COOLED (SAMPLES CUT TRANSVERSE)

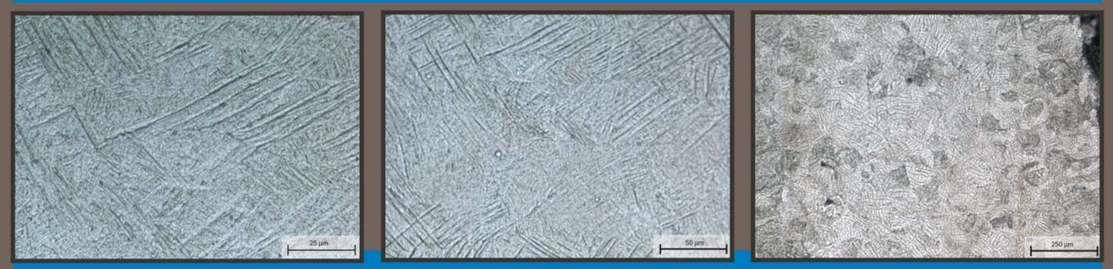

OM MICROGRAPHS - WATER QUENCHED (SAMPLES CUT LONGITUDINAL)

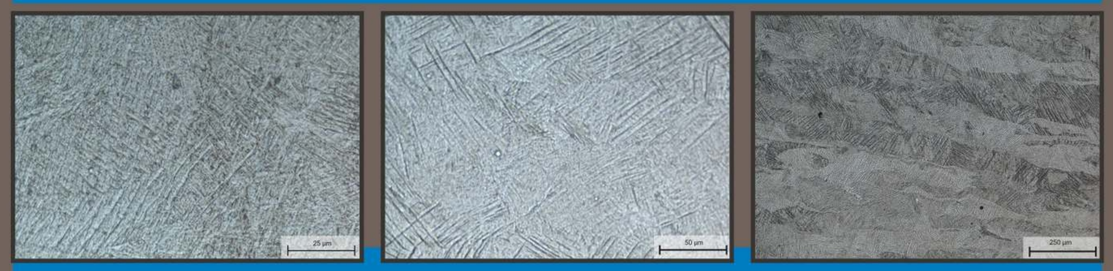

OM MICROGRAPHS - WATER QUENCHED (SAMPLES CUT TRANSVERSE)

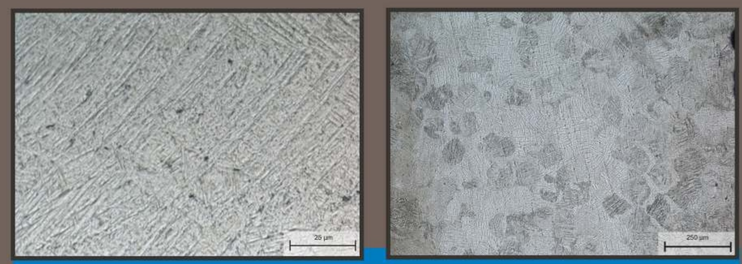

OM MICROGRAPHS - AIR QUENCHED
(SAMPLES CUT LONGITUDINAL)

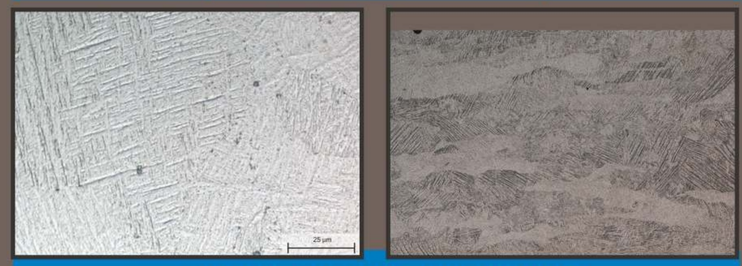

OM MICROGRAPHS - AIR QUENCHED
(SAMPLES CUT TRANSVERSE)

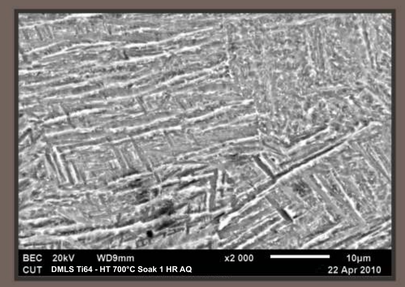

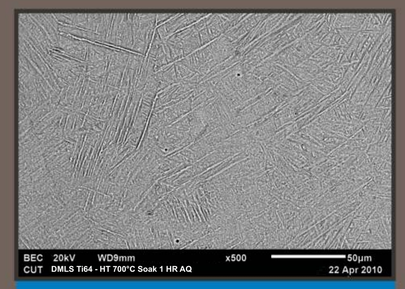

SEM PHOTO MICROGRAPHS - AIR QUENCHED

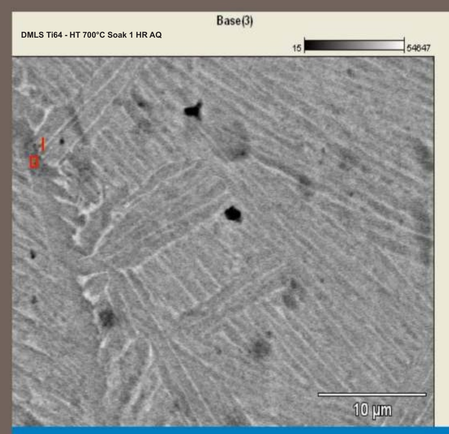

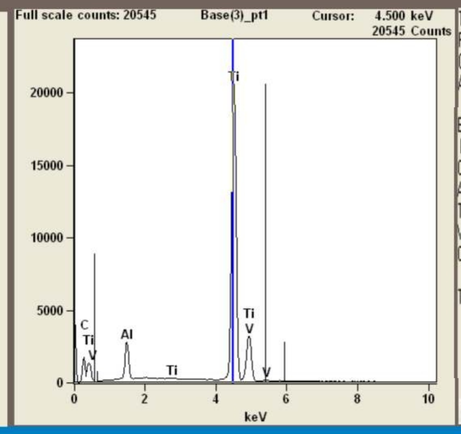

Thu Apr 22 10:59:37 2010
Filter Fit Chi-squared value: 20.478 Errors:+/-1 Sigma
Correction Method: Proza (Phi-Rho-Z)
Acc.Voltage: 20.0 kV Take Off Angle: 34.8 deg

Element Line	Element Wt.%	Wt.% Error	Atom %	Atom % Error
C K	1.88	+/-0.26	40.20	+/-0.71
Al K	5.26	+/-0.05	5.12	+/-0.05
Ti K	88.98	+/-0.20	52.84	+/-0.14
V K	3.88	+/-0.08	1.83	+/-0.05
Cr K	0.00	+/-0.00	0.00	+/-0.02
Total	100.00		100.00	

CHEMICAL ANALYSIS

MAKHABO KHABISO ELLEN RAMOSOEU
20203047

APPENDIX D

OPTICAL MICROSCOPE (OM), SCANNING ELECTRON MICROSCOPE (SEM) & CHEMICAL ANALYSIS
DMLS Ti64 SAMPLES
HEAT TREATED AT 1000°C SOAKED FOR 1 HOUR THEN COOLED AT DIFFERENT MEDIUM

OM MICROGRAPHS - FURNACE COOLED (SAMPLES CUT LONGITUDINAL)

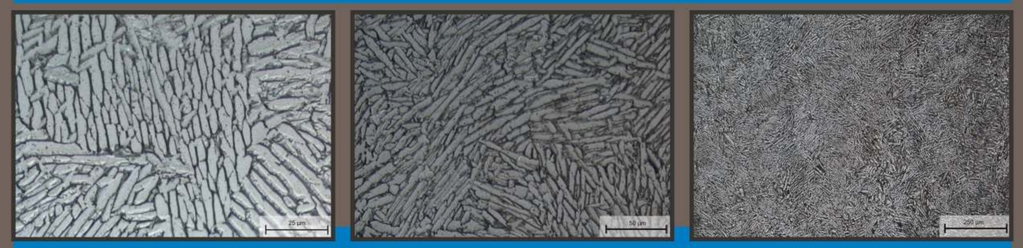

OM MICROGRAPHS - FURNACE COOLED (SAMPLES CUT TRANSVERSE)

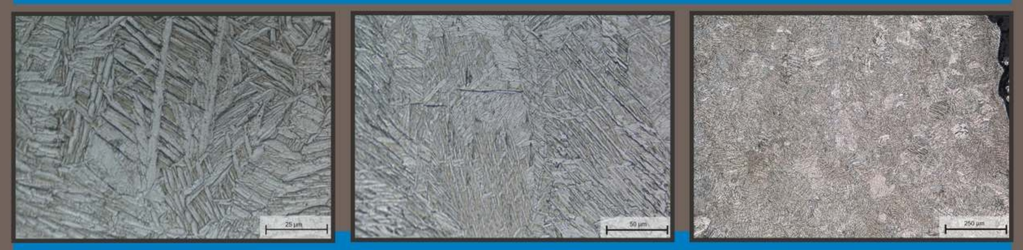

OM MICROGRAPHS - WATER QUENCHED (SAMPLES CUT LONGITUDINAL)

OM MICROGRAPHS - WATER QUENCHED (SAMPLES CUT TRANSVERSE)

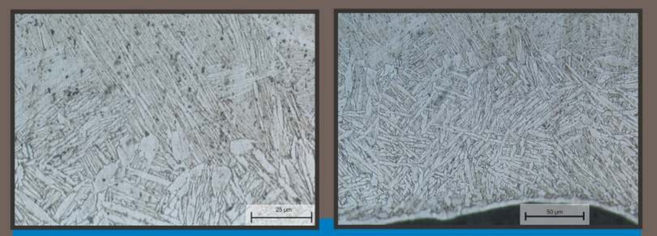

OM MICROGRAPHS - AIR QUENCHED (SAMPLES CUT LONGITUDINAL)

OM MICROGRAPHS - AIR QUENCHED (SAMPLES CUT TRANSVERSE)

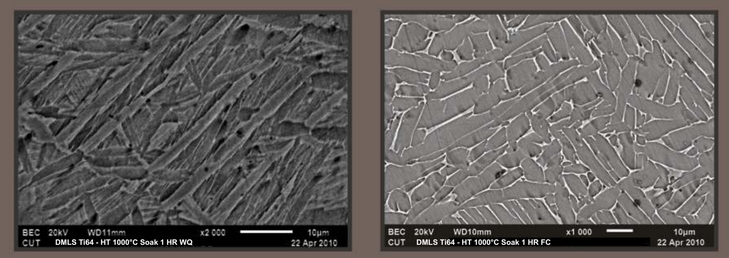

SEM MICROGRAPHS - WATER QUENCHED

SEM MICROGRAPHS - FURNACE COOLED

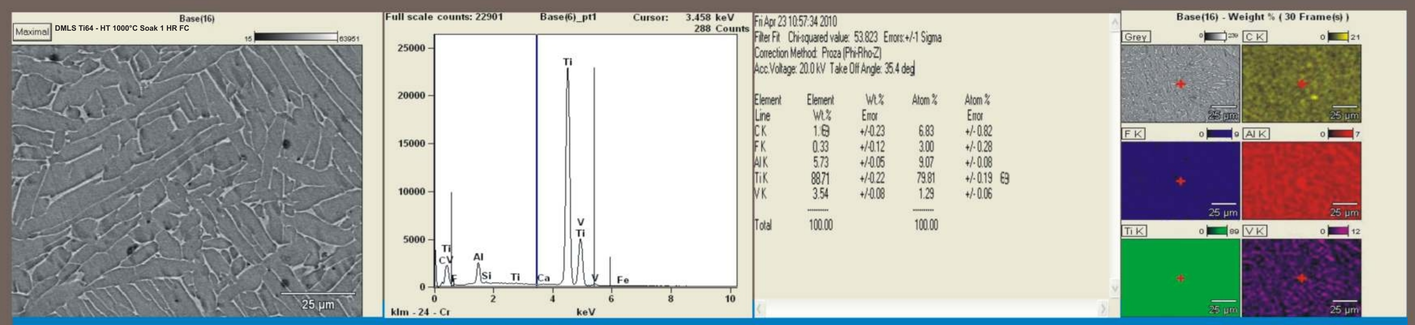

CHEMICAL ANALYSIS

MAKHABO KHABISO ELLEN RAMOSOEU
20203047

APPENDIX E

OPTICAL MICROSCOPE (OM), SCANNING ELECTRON MICROSCOPE (SEM) & CHEMICAL ANALYSIS
DMLS Ti64 SAMPLES
HEAT TREATED AT 1100°C SOAKED FOR 1 HOUR THEN COOLED AT DIFFERENT MEDIUM

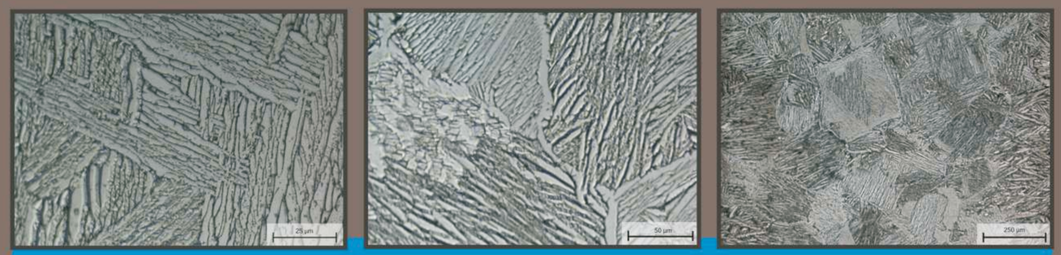

OM MICROGRAPHS - FURNACE COOLED (SAMPLES CUT LONGITUDINAL)

OM MICROGRAPHS - AIR QUENCHED (SAMPLES CUT LONGITUDINAL)

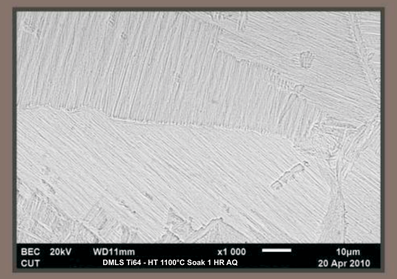

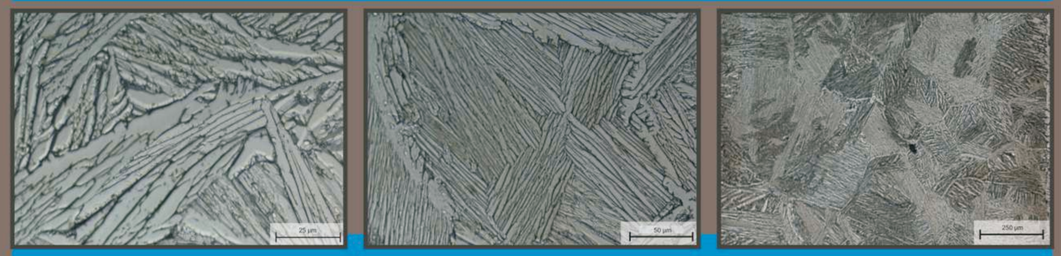

OM MICROGRAPHS - FURNACE COOLED (SAMPLES CUT TRANSVERSE)

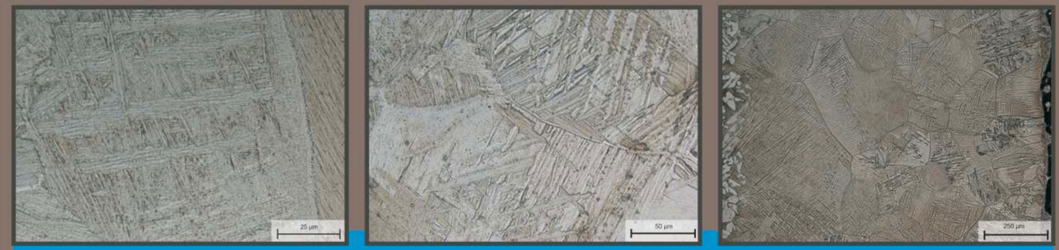

OM MICROGRAPHS - AIR QUENCHED (SAMPLES CUT TRANSVERSE)

SEM MICROGRAPHS - AIR QUENCHED

OM MICROGRAPHS - WATER QUENCHED (SAMPLES CUT LONGITUDINAL)

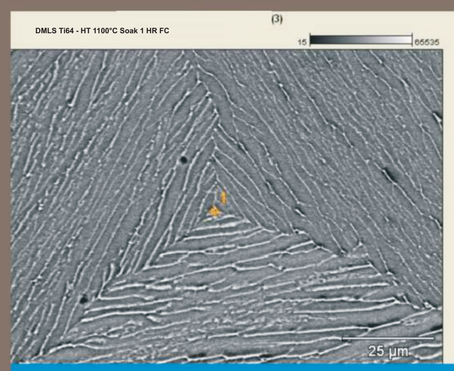

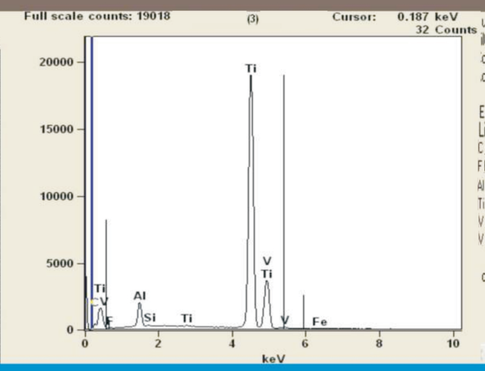

ue Apr 20 12:52:40 2010
ilter Fit Chi-squared value: 37.476 Errors:+/-1 Sigma
orrection Method: Proza (Phi-Rho-Z)
cc.Voltage: 20.0 kV Take Off Angle: 34.7 deg

Element Line	Element Wt.%	Wt.% Error	Atom %	Atom % Error
C K	1.60	+/-0.24	5.68	+/- 0.85
F K	0.32	+/-0.15	5.75	+/- 0.32
Al K	5.77	+/-0.05	7.54	+/- 0.08
Ti K	87.92	+/-0.28	78.19	+/- 0.25
V K	4.30	+/-0.14	2.76	+/- 0.12
V K	0.09	+/-0.04	0.08	+/- 0.04
otal	100.00		100.00	

CHEMICAL ANALYSIS

MAKHABO KHABISO ELLEN RAMOSOEU
20203047

APPENDIX F

OPTICAL MICROSCOPE (OM) & SCANNING ELECTRON MICROSCOPE (SEM), CHEMICAL ANALYSIS
DMLS Ti64 SAMPLES
HEAT TREATED AT 1000°C SOAKED FOR 1 HOUR, VACUUM FURNACE COOLED AT DIFFERENT TIMES

NECKING OF DMLS TI-6AL-4V TENSILE SPECIMEN - FURNACE COOLED FOR 4 HOURS

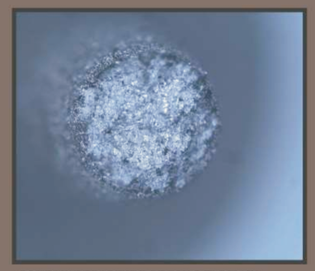

CONE LIKE FRACTURE OF DMLS TI-6AL-4V TENSILE SPECIMEN - FURNACE COOLED FOR 4 HOURS

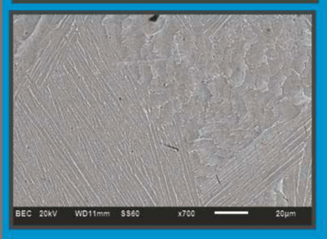

OM MICROGRAPHS
- FURNACE COOLED FOR 4 HOURS

SEM MICROGRAPHS
- FURNACE COOLED FOR 4 HOURS

Ground and Etched DMLS Ti-6Al-4V specimens

DMLS Ti-6Al-4V tensile specimens.

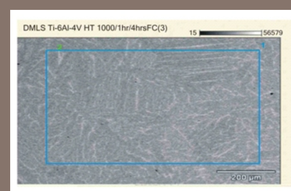

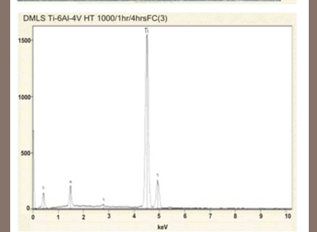

Thu Nov 11 15:17:30 2010
Filter Fit Chi-squared value: 4.650 Errors:+/-1 Sigma
Correction Method: Proza[Phi-Rho-Z]
Acc Voltage: 20.0 kV Take Off Angle:36.1 deg

Element Line	Element Wt%	Wt% Error	Atom%	Atom% Error
AlK	5.54	+/-0.14	8.31	+/-0.23
TiK	90.02	+/-0.38	88.88	+/-0.61
VK	4.44	+/-0.02	4.01	+/-0.12
Total	100.00		100.00	

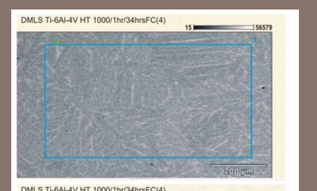

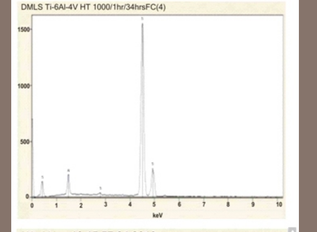

Wed Nov 10 15:57:34 2010
Filter Fit Chi-squared value: 2.096 Errors:+/-1 Sigma
Correction Method: Proza[Phi-Rho-Z]
Acc Voltage: 20.0 kV Take Off Angle:36.3 deg

Element Line	Element Wt%	Wt% Error	Atom%	Atom% Error
AlK	6.14	+/-0.07	8.10	+/-0.12
TiK	90.14	+/-0.28	89.88	+/-0.27
VK	3.72	+/-0.15	3.54	+/-0.22
Total	100.00		100.00	

CHEMICAL ANALYSIS

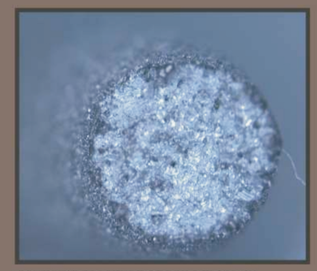

CONE LIKE FRACTURE OF DMLS TI-6AL-4V TENSILE SPECIMEN - FURNACE COOLED FOR 34 HOURS

NECKING OF DMLS TI-6AL-4V TENSILE SPECIMEN - FURNACE COOLED FOR 34 HOURS

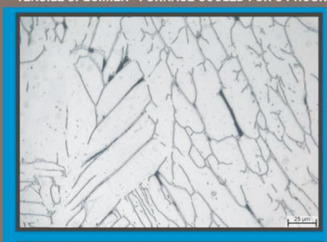

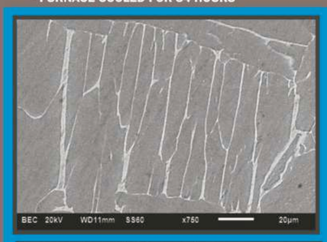

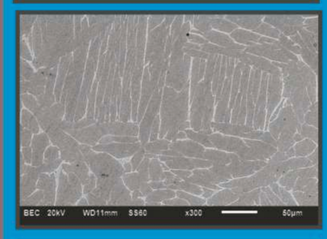

OM MICROGRAPHS
- FURNACE COOLED FOR 34 HOURS

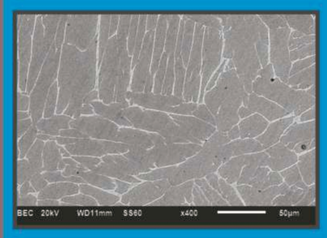

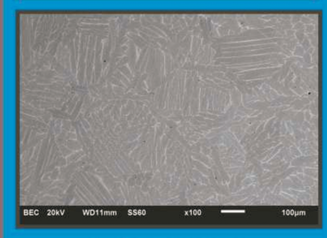

SEM MICROGRAPHS
- FURNACE COOLED FOR 34 HOURS

MAKHABO KHABISO ELLEN RAMOSOEU
20203047

APPENDIX G

MACRO HARDNESS
DMLS Ti64 SAMPLES

			Hardness Measure: Hardness Vickers (HV)							
			Load: 10Kg f							
			Material: DMLS Ti-6Al-4V							
			o			o			o	
	As-laser sintered	HT at 700 C 1hr			HT at 1000 C 1hr			HT at 1100 C 1hr		
		WQ	AC	FC	WQ	AC	FC	WQ	AC	FC
	342.9	359.7	341.1	339.5	341.9	315.3	301.1	361.0	346.7	313.2
	344.4	363.4	324.2	329.9	340.9	296.6	300.2	351.2	346.2	315.4
	345.4	342.0	341.7	335.5	339.7	312.3	300.8	353.5	356.3	312.4
	341.9	358.1	343.3	333.7	340.9	312.0	296.6	367.1	357.9	313.2
	345.1	347.1	361.5	337.2	338.9	318.4	303.3	353.3	356.2	312.9
	345.8	354.5	343.9	340.1	339.8	307.2	301.1	356.4	355.6	311.5
	344.5	334.2	333.0	338.4	340.2	309.9	302.2	360.5	355.3	312.4
	343.3	353.3	347.2	333.1	337.4	321.8	302.3	361.8	358.2	313.6
	345.9	355.5	332.7	345.6	338.9	302.7	301.5	351.3	349.3	312.2
	342.5	357.7	347.7	340.4	339.9	323	300.5	358.1	357.7	312.1
Averange	344.2	352.6	341.6	337.3	339.9	311.9	301.0	357.4	353.9	312.9
Standard deviation	1.4	8.9	10.2	4.5	1.3	8.3	1.8	5.2	4.7	1.1

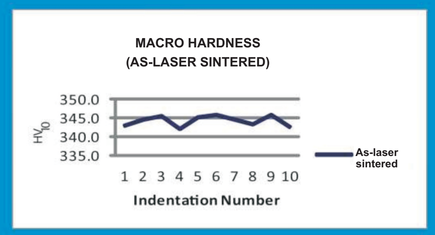

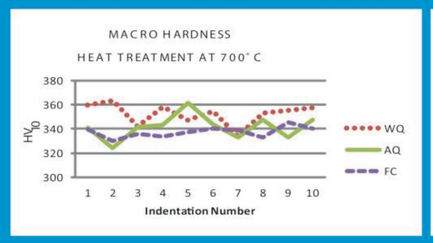

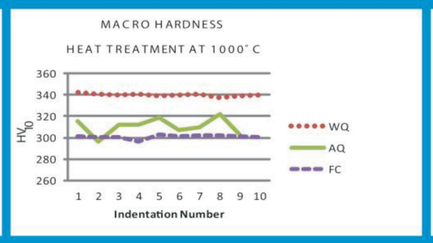

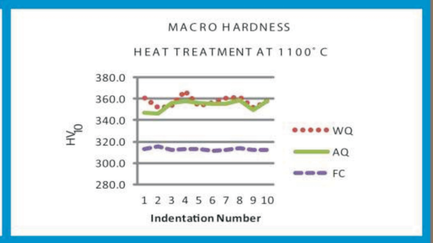

MACRO HARDNESS
OF THE DMLS TI-6AL-4V SAMPLES;
HEAT TREATED AT 700°C, 1000°C, 1100°C SOAKED 1 HOUR THEN COOLED AT DIFFERENT MEDIUM

	Hardness Measure: Hardness Vickers (HV)		
	Load: 10Kg f		
	Material: DMLS Ti-6Al-4V		
	As- laser sintered	1000°C/1hr/4hrs FC	1000°C/1hr/ 34hrs FC
	344.2	304.3	296.8
	344.3	304.1	297.2
	343.5	304.8	296.8
	345.7	309.1	295.1
	345.5	304.1	295.8
	344.5	303.2	294.5
	343.7	302.8	297.2
	343.1	306.2	296.7
	346.2	301.5	296
	342.4	300.9	294.8
Averange	344.3	304.1	296.09
Standard deviation	1.2	2.3	1.0

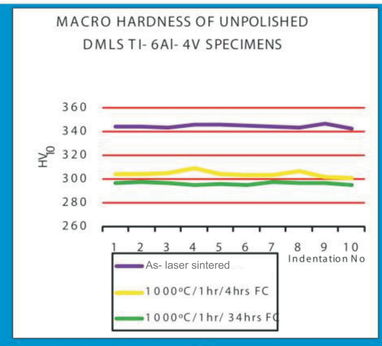

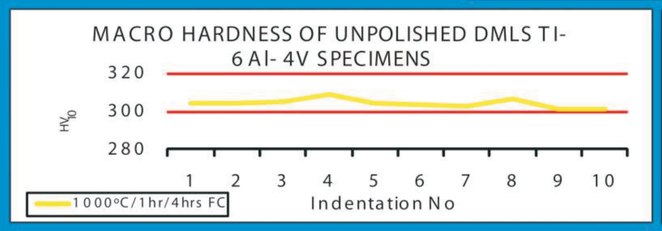

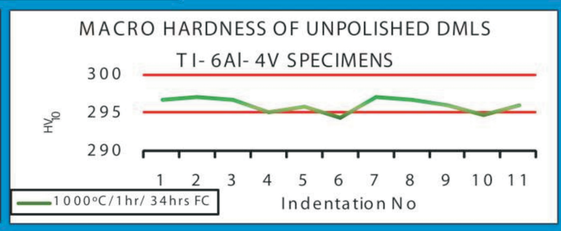

MACRO HARDNESS
OF THE DMLS TI-6AL-4V SAMPLES;
HEAT TREATED AT 1000°C SOAKED 1 HOUR THEN FURNACE COOLED AT DIFFERENT TIMES

MAKHABO KHABISO ELLEN RAMOSOEU
20203047

APPENDIX H

TENSILE PROPERTIES
DMLS Ti64 SAMPLES

H1-Tensile Properties (As- laser sintered)

Laboratory Name	CSIR Materials Testing Laboratory
Company	Makhabo - CUT
Operator ID	203406
Method description	ASTM E8 M
Sample description	Titanium TI-6AL-4V
Test Date	25/10/2010

	Specimen label	Area (mm^2)	Maximum Load (kN)	Tensile stress at Yield (Offset 0.2 %) (MPa)	Modulus (Chord 200 MPa - 600 MPa) (GPa)	UTS (MPa)	Elongation(%) 4.D	Area Reduction (%)
	2344-B1	14.19	16.99	982.93	91.74	1197.42	3.11	2.34
	2345-C1	14.05	16.84	1021.02	94.14	1198.37	2.83	2.82
	2347-B2	13.99	15.93	998.16	93.52	1139.07	2.61	6.07
	2348-C2	13.99	17.15	1016.06	95.44	1226.17	1.83	2.82
Coefficient of Variation		0.66944	3.25946	1.73558	1.64072	3.07816	21.13033	48.93449
Mean		14.05	16.73	1004.54	93.71	1190.26	2.60	3.51
Range		0.20	1.22	38.09	3.70	87.10	1.28	3.73
Standard Deviation		0.09408	0.54522	17.43462	1.53747	36.63812	0.54880	1.71827
Minimum		13.99	15.93	982.93	91.74	1139.07	1.83	2.34
Maximum		14.19	17.15	1021.02	95.44	1226.17	3.11	6.07
Median		14.02	16.91	1007.11	93.83	1197.90	2.72	2.82

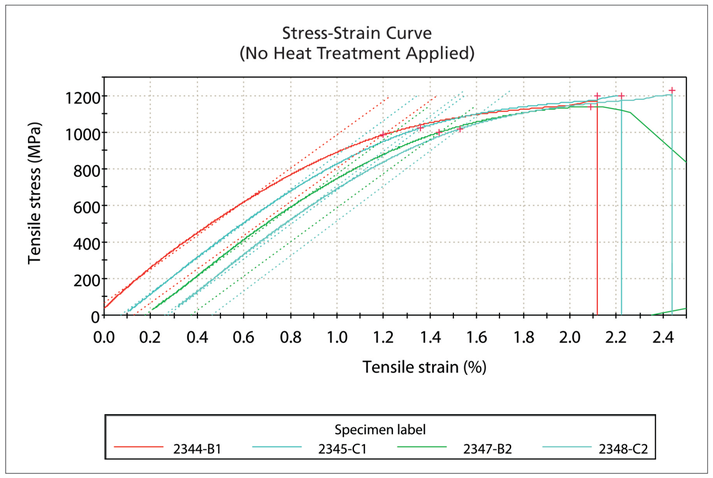

H2- Tensile Properties (Heat Treated at 1000°C/1hr/FC-4hrs)

Laboratory Name	CSIR Materials Testing Laboratory
Company	Makhabo - CUT
Operator ID	203406
Method description	ASTM E8 M
Sample description	Titanium TI-6AL-4V
Test Date	3/11/2010

	Specimen label	Area (mm^2)	Maximum Load (kN)	Tensile stress at Yield (Offset 0.2 %) (MPa)	Modulus (Chord 200 MPa - 600 MPa) (GPa)	UTS (MPa)	Elongation(%) 4.D	Area Reduction (%)
	B4-FC	14.25	13.52	829.02	111.24	948.67	12.22	30.56
	B5-FC	14.25	13.58	834.28	116.68	952.65	14.44	31.34
	C4-FC	14.25	13.46	817.48	103.60	944.09	14.22	30.95
	C5-FC	14.32	13.43	826.87	111.51	937.98	9.78	10.93
Coefficient of Variation		0.23474	0.48911	0.84867	4.86548	0.66616	17.12961	38.60859
Mean		14.27	13.50	826.91	110.76	945.85	12.67	25.94
Range		0.07	0.15	16.80	13.08	14.66	4.67	20.41
Standard Deviation		0.03350	0.06602	7.01776	5.38902	6.30085	2.16975	10.01535
Minimum		14.25	13.43	817.48	103.60	937.98	9.78	10.93
Maximum		14.32	13.58	834.28	116.68	952.65	14.44	31.34
Median		14.25	13.49	827.94	111.38	946.38	13.22	30.75

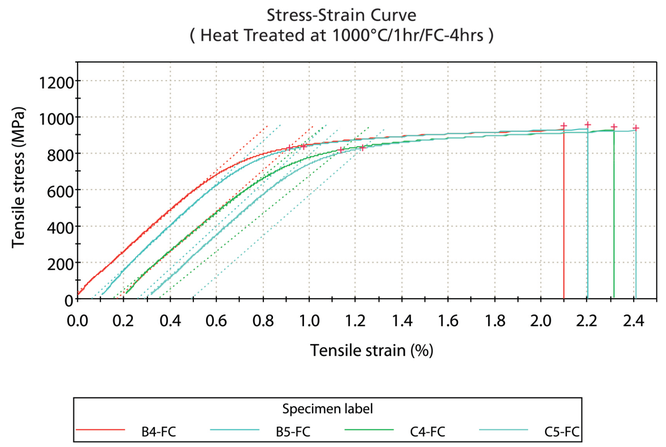

H3- Tensile Properties (Heat Treated at 1000°C/1hr/FC-34hrs)

Laboratory Name	CSIR Materials Testing Laboratory
Company	Makhabo - CUT
Operator ID	203406
Method description	ASTM E8 M
Sample description	Titanium TI-6AL-4V
Test Date	3/11/2010

	Specimen label	Area (mm^2)	Maximum Load (kN)	Tensile stress at Yield (Offset 0.2 %) (MPa)	Modulus (Chord 200 MPa - 600 MPa) (GPa)	UTS (MPa)	Elongation(%) 4.D	Area Reduction (%)
	D4-34HRS	14.25	12.98	807.13	109.64	910.88	16.72	32.88
	D5-34HRS	14.32	12.95	803.92	112.02	904.50	18.78	34.72
	E1-34HRS	14.32	13.14	808.21	107.97	917.72	20.28	32.81
	E5-34HRS	14.39	12.97	799.84	105.29	901.43	16.67	33.13
Coefficient of Variation		0.38243	0.67405	0.46704	2.60579	0.79500	9.64511	2.69345
Mean		14.32	13.01	804.77	108.73	908.63	18.11	33.39
Range		0.13	0.19	8.36	6.73	16.29	3.61	1.91
Standard Deviation		0.05476	0.08770	3.75858	2.83330	7.22364	1.74684	0.89923
Minimum		14.25	12.95	799.84	105.29	901.43	16.67	32.81
Maximum		14.39	13.14	808.21	112.02	917.72	20.28	34.72
Median		14.32	12.98	805.52	108.81	907.69	17.75	33.01

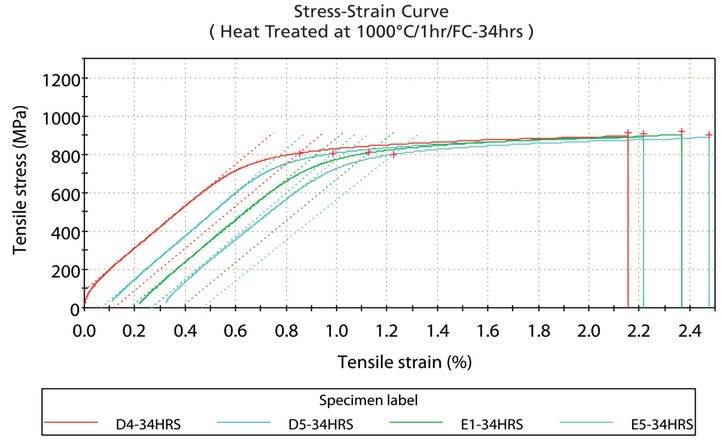

APPENDIX I

CHEMICAL COMPOSITION, DENSITY, ELASTIC CONSTANTS AND MECHANICAL PROPERTIES TITANIUM Ti-6Al-4V ALLOY

CHEMICAL COMPOSITION

	Ti	Al	V	FE	C	O	N	H	Ultimate Tensile Strength (MPa)
THEORETICAL VALUES									
Grade 1 (CP Ti) *[ASTM B 265-13ae1 Grade 1 Standards]*	balance	-	-	0.2	0.1	0.18	0.03	0.015	240
Wrought annealed Ti-6Al-4V alloy *[ASTM F 1472-08$^{\varepsilon 1}$Standard]*	balance	5.5-6.75	3.5-4.5	0.3	0.08	0.2	0.05	0.015	930
EOS as- laser sintered Ti-6Al-4V alloy parts *[EOS GmbH-Electro Optical System 2011: 3-4]*	balance	5.5-6.75	3.5-4.5	0.3	0.08	0.2	0.05	0.015	1200
EOS DMLS annealed Ti-6Al-4V alloy parts *[EOS GmbH-Electro Optical System 2011: 3-4]*	balance	5.5-6.75	3.5-4.5	0.3	0.08	0.2	0.05	0.015	930
EXPERIMENTAL VALUES									
As-laser sintered Ti-6Al-4V alloy parts *[As-laser sintered]*	90.823	5.33	3.86	-	-	-	-	-	1190
DMLS Beta annealed Ti-6Al-4V alloy parts *[HT 1000°C Soak 1 HR 4HRS FC]*	90.02	5.54	4.44	--	-	-	-	-	949
DMLS Beta annealed Ti-6Al-4V alloy parts *[HT 1000°C Soak 1 HR 34HRS FC]*	90.14	6.14	3.72	-	-	-	-	-	909

DENSITY AND ELASTIC CONSTANTS

Density and Elastic Constants		
PROPERTY	**THEORETICAL VALUES**	**EXPERIMENTAL VALUES**
	Wrought annealed Ti-6Al-4V Alloy *[ASTM F 1472-08$^{\varepsilon 1}$ Standard]*	**EOS as-laser sintered Ti-6Al-4V Alloy** *[As-laser sintered Sample]*
Density (g/cm^3)	4,49	4,4005
Poisson's Ratio	0,321	0.324
Shear Modulus, G, (GPa)	43	43.357
Young's Modulus, E, (GPa)	114	115
Bulk Modulus, K, (GPa)	106	108

CHEMICAL COMPOSITION, ELASTIC CONSTANTS, AND MECHANICAL PROPERTIES
TITANIUM TI-6AL-4V ALLOY SAMPLES

MECHANICAL PROPERTIES

	THEORETICAL VALUES			EXPERIMENTAL VALUES		
PROPERTIES	**Wrought Annealed Ti-6Al-4V Alloy** [ASTM F1472-08$^{\varepsilon 1}$ Standard]	**EOS As-laser Sintered Ti-6Al-V4 Alloy** *[EOS GmbH-Electro Optical System. 2011: 3]*	**EOS DMLS Annealed Ti-6Al-4V Alloy** [EOS GmbH-Electro Optical System. 2011: 3]	**As-laser Sintered Ti-6Al-V4 Alloy** *[As-laser sintered Samples]*	**DMLS Ti-6Al-V4 Alloy** *[Samples were heat treated at 1000°C soaked for 1 hour and furnace cooled for 4 hours]*	**DMLS Ti-6Al-V4 Alloy** *[Samples were heat treated at 1000°C soaked for 1 hour and furnace cooled for 34 hours]*
TENSILE PROPERTIES						
2% Proof Stress [MPa]	800-1100	1070 ± 50	860	1005	827	805
Ultimate Tensile Strength [MPa]	900-1200	1200 ± 50	930	1190	946	909
% Elongation	6-10	11 ± 3	15±1	2.6	12.67	18.11
% Area Reduction	15-25	-	-	3.51	25.94	33.39
OTHER MECHANICAL PROPERTIES						

MAKHABO KHABISO ELLEN RAMOSOEU
20203047

MECHANICAL CHARACTERISTICS OF DIRECT LASER SINTERED TITANIUM (TI64) BUILT ON EOSINT M270 SINTERING MACHINE

M E Ramosoeu[1], T N Ngonda[2] and G Booysen[3]
School of Mechanical Engineering & Applied Mathematics
Central University Technology, Free State
Private Bag X 20539, Bloemfontein, 9300, RSA,
mramosoeu@cut.ac.za[1], tngonda@cut.ac.za[2], and gbooysen@cut.ac.za[3]

Abstract: The Center for Rapid Prototyping and Manufacturing (CRPM) is mainly using DMLS EOSINT M270 machine to manufacture Titanium (Ti64) products. The need to acquire knowledge of the fundamental characteristics of sintered Ti64 under different mechanical loading is ultimately for these reasons; to provide sustainable empirical data to CRPM in order to know the accuracy, behaviour and performance of Ti64 built on DMLS EOSINT M270 machine and also to use these data to predict deformation and or failure for a given application. Preliminary analyses on sintered Ti64 specimens built in a horizontal orientation on DMLS EOSINT M270 machine set at standard building parameters has been conducted. Visual and Macroscopic examination of sintered Ti64 studs reveal that there are voids even though they are not quantified. SEM examination reveals a dimple type of fracture. Ultrasonic test shows that sintered Ti64 has Young's modulus of 114, 6 GPa, Shear modulus of 43 GPa bulk modulus of 109 GPa, Poisson's ratio of 0, 3246 while the density was 4, 34 g/cm^3. Yield stress of 839 MPa, ultimate stress of 983 MPa, were also found in tensile test. The preliminary results indicate similarities between solution treatment aged (STA) wrought Ti-6Al V4 and polished DMLS Ti64.

Key words: Sintered Ti64, DMLS ESOINT M270, Mechanical Properties

I BACKGROUND

Direct Metal Laser Sintering (DMLS) is one of the Additive Manufacturing technologies developed by EOS GmbH of Munich, Germany. The Center for Rapid Prototyping and Manufacturing (CRPM) at Central University of Technology, Free State (CUT, FS) manufacture Titanium Ti64 parts directly from 3D CAD data using DMLS EOSINT M270 machine for both medical and aerospace industry.

DMLS EOSINT M270 machine is based on a solid-state, dual focus 200Watts ytterbium fiber laser. It has the speed scan of up to 7.0 meters per second, and the available focus diameter of 100-500 micro-meters. The layer thickness depends on material and ranges from 20-60 micro-meter [2, 3, 4]. DMLS works by sintering together very fine layers of metal powder layer by layer along a stalking axis from the bottom to until the three dimensional component is built. Each layer is scanned by laser beam of high intensity as to provide thermal energy to the bonding of adjacent surfaces of particles in a powder until they adhere to each other. Parts are heated in a protective atmosphere chamber to a high relative temperature below the melting points of the particular metal or alloy. Sintering process strengths powder mass and usually increase density therefore; parts manufactured by DMLS process do not require post-sintering and /or infiltrating process [2, 3, 4]. Figure 1 below shows the basic components of DMLS system. The finished part will go through support removal and if required, shot peening and polishing.

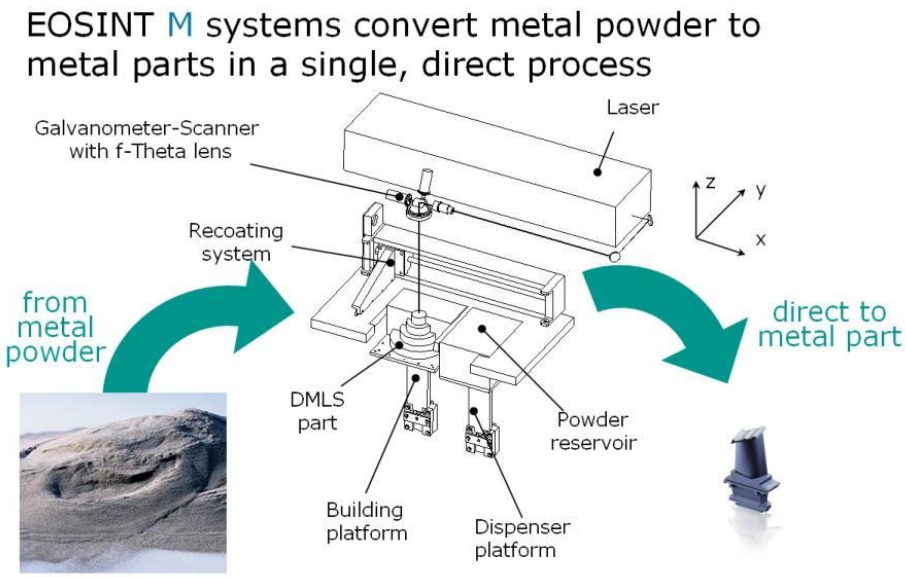

Figure 1: *Schematic diagram showing DLMS process on EOSINT M270 machine*

[Courtesy to EOS GmbH*]*

In the medical application, bone prosthesis are generalized and made for any individual, hence in such manner many implants are been manufactured in mass production using Subtractive manufacturing technology like Milling process or Casting technology. However, the disadvantage of generalizing the shape is that, human anatomy is not uniform. All individuals require customized shapes for their implants, especially on the complex topographies such as bones in knee, elbow or hip joints. Using Subtractive manufacturing technology and Casting technology to produce an individual prosthesis is time consuming, expensive and complex. These methods require artisans with extraordinary skills. DMLS method can be used in manufacturing bone prosthesis. Therefore it is very advantageous to choose DMLS process as it enables the designer to produce part geometries that have complex shapes and allows for the fabrication of parts with high degree of geometric freedom, high individuality as well as few processing steps. [2,3,4] DMLS process produces parts directly from 3D CAD data, no tooling is required and can combine what would have been several parts into one hence saving manufacturing costs, and reducing assembly time.

The shape and topology of the prosthesis to be designed is mostly based on the CT scan data. CT scan data will eventually be translated to the computer aided design data. Once the data is in the computer then it is easy to work on, thus modify the design. From the computer, the data will be translated to the machine data so that the design can be manufactured [2, 3, 4.] (See figure 2 below).

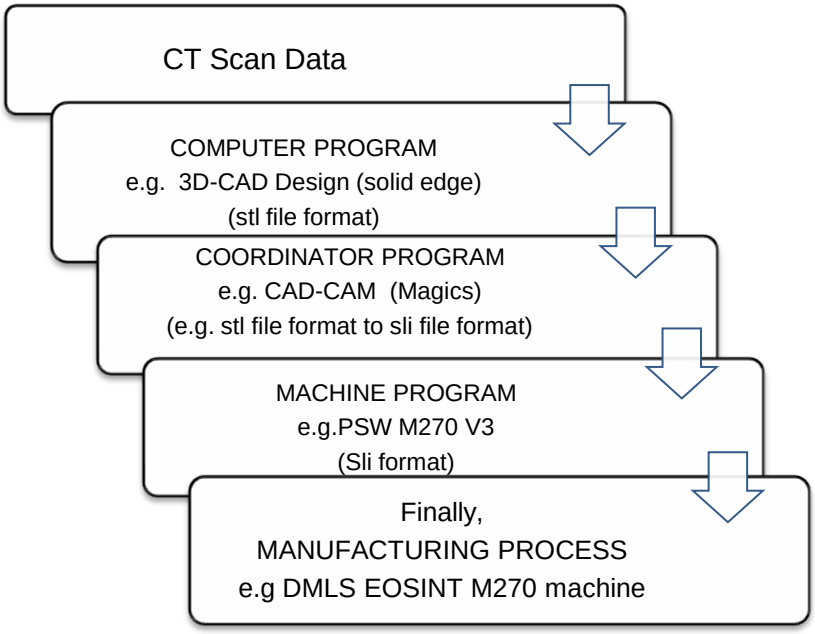

Figure 2: Steps from CT scan Data to Manufacturing

Different materials have been used in bone prosthesis. Titanium is one of the preferred biomaterials as it is strong, light in weight, good in resisting corrosion and has the closest elasticity to bone hence it is highly recommended in the medical environment. [1, 6, 7] From Figure 1 below, titanium has elastic modulus of 110 GPa and an ultimate strength of 1250 MPa which is about 10 times the ultimate strength of bone tissue.

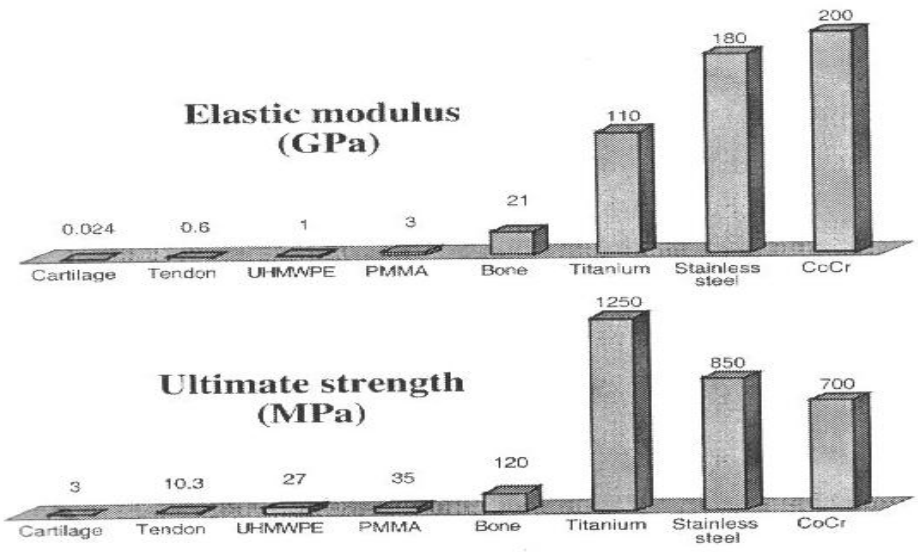

Figure 3: Some Mechanical Properties of Tissues and Biomaterials [7]

CRPM uses Titanium Ti64 in the form of power which is formed into functional parts by DMLS process. Titanium Ti64 is pre-alloyed Ti 6AlV4 powder. The microstructure of this Titanium alloy is described by the size and arrangement of the two phases' (α) and (β). Titanium Ti 64 exits in three types of microstructures namely Lamellar, equiaxed and bimodal and have strong influence on the mechanical behavior [6]. The microstructure is influenced by the manufacturing process and /or any post process (for example heat treatment) applied to the alloy hence it is of high importance to determine the microstructure of parts built on DMLS ESOINT M270.

Mechanical properties are empirical data used to predict the response of materials under mechanical loads. They are expressed in terms of forces which may deform materials or even cause them to fail completely. The geometry of the loaded component can be designed to deal with applicable loading. The physical nature of the material has to ensure that the component can survive in service. The performance of such component during usage is limited by properties of material depending on the application. These limitations are based on the mechanical properties such as elastic constants (young's modulus, shear modulus, Poisson's ratio and bulk modulus), yield stress, ultimate stress and physical properties such as density.

Deformations can be produced by forces which cause a body to be stretched, compressed, twisted or sheared. These forces can also be combined to produce more complex types of deformation (for example, flexure). Figure 3 below shows the reaction of an object under different forces.

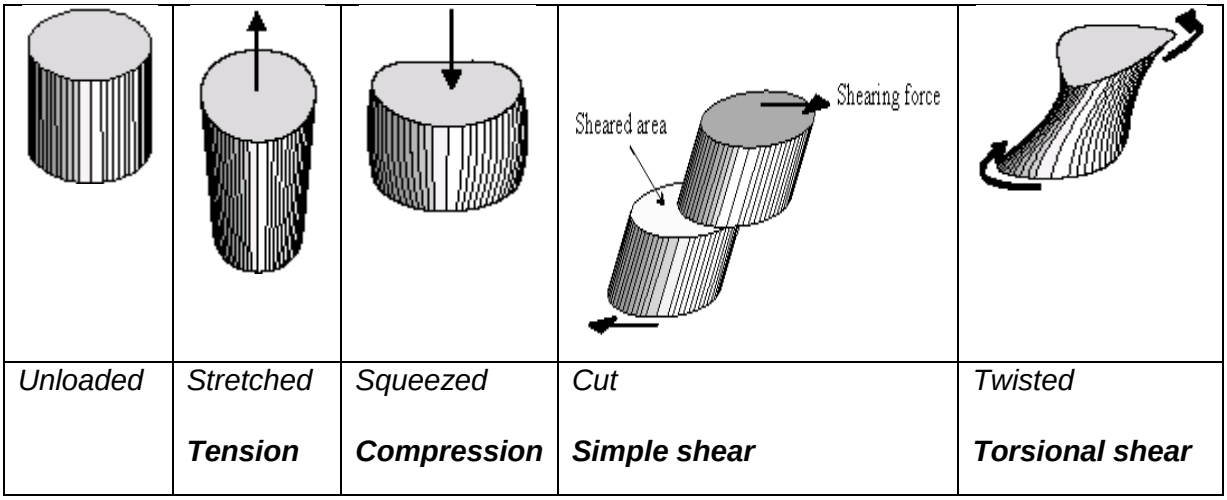

Unloaded	*Stretched* ***Tension***	*Squeezed* ***Compression***	*Cut* ***Simple shear***	*Twisted* ***Torsional shear***

Figure 4: Typical Loading Conditions for Implants

Stress is the force exerted on a body per unit cross sectional area. When considering tensile stress the weight is applied in the direction of elongation. If the same weight was placed on the rectangular specimens to cause a contraction in the longitudinal direction, the resulting stress would be called compressive stress. Shear stress relates to the force which distorts rather than extends a body. Shear forces can also result in failure [8].

Strength is defined as the highest stress that a material can withstand before it completely fails to perform structurally. If the applied force is tensile (stretch), the ultimate stress is known as

tensile strength (i.e., maximum tensile stress that the material can tolerate). Other types of strength are related to the mode of the applied force, i.e. compressive, shear, torsional and flexural [8].

Strain is the change in one dimension produced as a result of an applied force and it is expressed as the ratio of the amount of deformation to the sample's original dimension.

Stress-strain relationships (below failure conditions); Materials deform elastically or inelastically. During elastic deformation, the stress in a body is directly related to the strain, and vice-versa. Therefore, when the force is removed (i.e. when stress becomes zero) then strain returns to zero. The plot of stress against strain produces a straight line; the stress can be increased or decreased, and stress and strain are always proportional to each other [8].

Modulus is the relationship between stress and strain and is expressed in terms of a property called the Young Modulus. The linear portion of the stress-strain curve can be used to determine the modulus which corresponds to the slope of the curve before the yield point, up to which all deformation is elastic. The Modulus of Elasticity is the modulus which has been determined for materials deformed in tension or compression. The Modulus of Rigidity is used to express the resistance to shear or torsion [8].

In practice in the medical environment it is very important to know what happens to the bone deformation and/or failure. For example Compressive loading in vivo creates a shortening and widening of the bone and is commonly seen in human vertebra while tensile loading creates fractures and they are seen in cancellous bone [7]. In these case properties such as yield stress, ultimate stress, and young's modulus are of high importance in choosing the correct material for bone prosthesis and will lead the designer to choose the correct limiting properties as well.

II THE NEED FOR CHARACTERIZATION OF DIRECT SINTERED TITANIUM TI64

Ti64 is highly recommended as a structural material and have been determined to possess high specific strength [6]. Its application is mostly in the medical environment for bone implants and in the field of aerospace engineering. During these applications titanium structures are exposed to different forms of loading which can lead to material failure for example, fracture behavior which could be in the form of fatigue, thus failure due to cyclic loading and what can happen is; where there is void there is possibility for initiation of a crack, with time followed by crack growth then the material will failure. However, information regarding mechanical properties of this titanium alloy is still limited.

The need for CRPM to acquire knowledge of the fundamental characteristics of laser sintered Titanium (Ti64) under different mechanical loading is ultimately for these reasons: To provide sustainable empirical data to CRPM in order to know the accuracy, behaviour and performance of sintered Ti64 built on DMLS EOSINT M270 sintering machine. To create phenomenological model that relates the microstructure and mechanical properties in order to inspect, predict deformation and/or failure of the component built.

III METHOD OF APPROACH

The sample were built at CRPM and microstructure examination and elastic property determination was done at VUT and AEROSUD AVIATION (PTY) LTD. Design of phenomenological model will be done once the full set of empirical data of laser sintered Ti64 becomes available.

The following steps will be done in order get empirical data:

Theory

Investigate information Based on mechanical properties of Titanium Ti64 and its microstructure, DMLS process, mechanical loading and failure modes, mechanical and physical tests.

Processing

Manufacture Ti64 part samples using DMLS process on ESOINT M270 machine.

Characterization

Perform physical and Mechanical tests in order to get empirical data. Figure 4 below shows tests that have been done and those that will be performed.

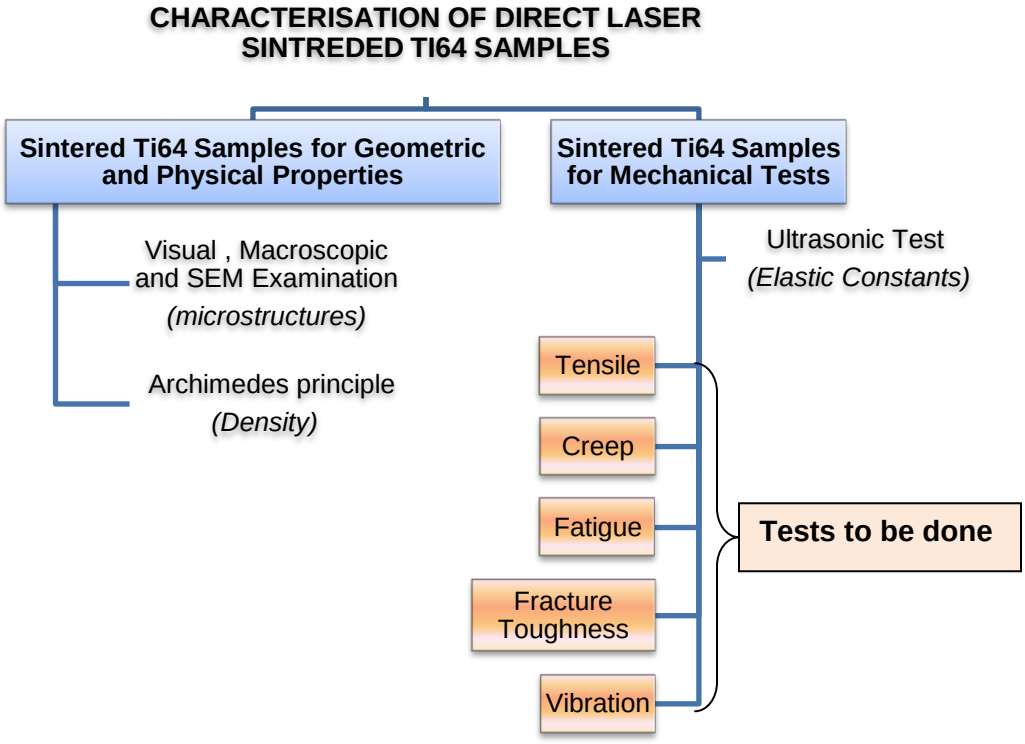

Figure 5: The testing regime

IV PRELIMINARY WORK DONE

1. Investigation of Sintered Titanium Studs

Specimens of sintered Titanium studs were supplied with the request to determine the soundness (void content) of the material. The following examinations were done at Vaal University of Technology (VUT):

1.1. Visual and Macroscopic Examination

Samples were sectioned longitudinally along the middle position. One half of each specimen was ground and polished with alumina suspension to a surface finish of 3 microns. The samples were examined visually and at low magnification. Samples showed marked amounts of voids, visible to the naked eye, to a length of ±1 mm long. These voids occurred mainly at the specimen centre, and at the outer surface of the circular section. (See figure 6 and 7 shown at low magnification)

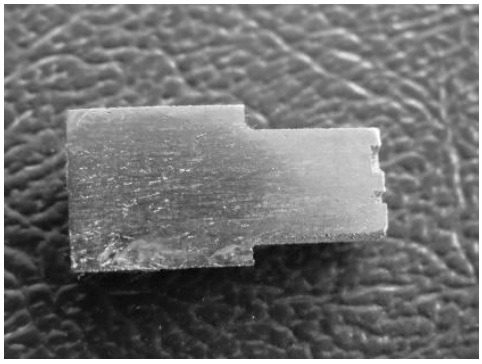

Figure 6 longitudinal section of stud

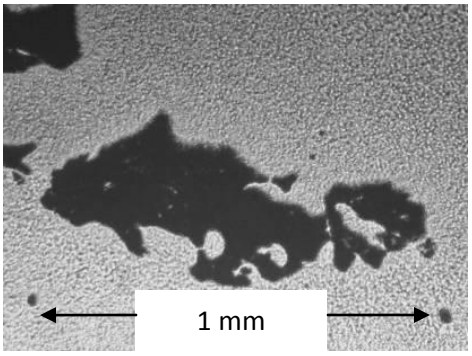

Figure 7 void of about 1 mm

1.2. Scan Electron Microscopy (SEM) Examination

The other half of each specimens obtained from sectioning, were fractured by impact loading, in such a way that facture occurred in the onset of the square section. It should be bared in mind that this fractured surface is not at the same position were the high concentrating of voids were recorded during the visual examination. The fractured surfaces were examined with a Joel 35 scanning electron microscope at 20 kV at 180X, and 1000X magnification. The fractured surfaces revealed in all the specimens a dominantly ductile dimple type of fracture. The dimples varied in size. (See figure 8 and 9 below)All sample showed evidence of voids, especially specimen A4 and A5 in which voids were visible during visual inspection. The dimples occur in a circular manner. (See figure 9)

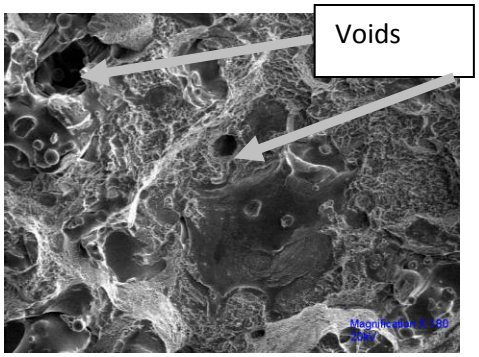

Figure 8 voids at magnification X180 20KV)

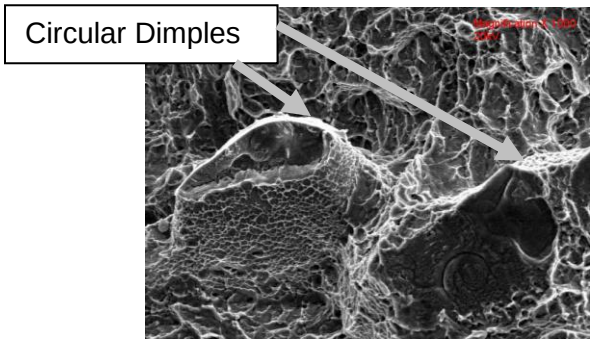

Figure 9 dimples at magnification X1000 20KV

1.3. Microscopic Examination

Sintered Ti64 specimen were polished firstly with water cooled grinding on SiC-paper from grit 240 up to 1200 grit then followed polishing with diamond grit 5 µm and lastly 3 µm. After polishing the specimen were etched in a Hydrogen peroxide/ hydrofluoric acid / Nitric acid solution. Then the specimens were viewed using microscope at magnification of X500. Microstructure of the direct laser sintered Ti64 indicates that it is in the form of fine lamellar α phase and β phase. (See figure 6).

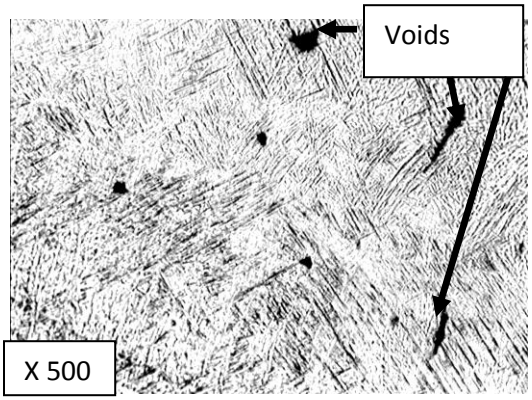

Figure 10 microstructure of sintered Ti64 at magnification X500

2. Measurement of Elastic Constants Using Ultrasonic Pulse-Echo Technique

Elastic parameters of sintered Ti64 were measured according to ASTM E494-48 using an ultrasonic pulse echo technique as show in figure 7 below. The equipment used was Krautkramer USIP12 and was done at Diamond Research Laboratory in collaboration with VUT. Table 1 below show mean results

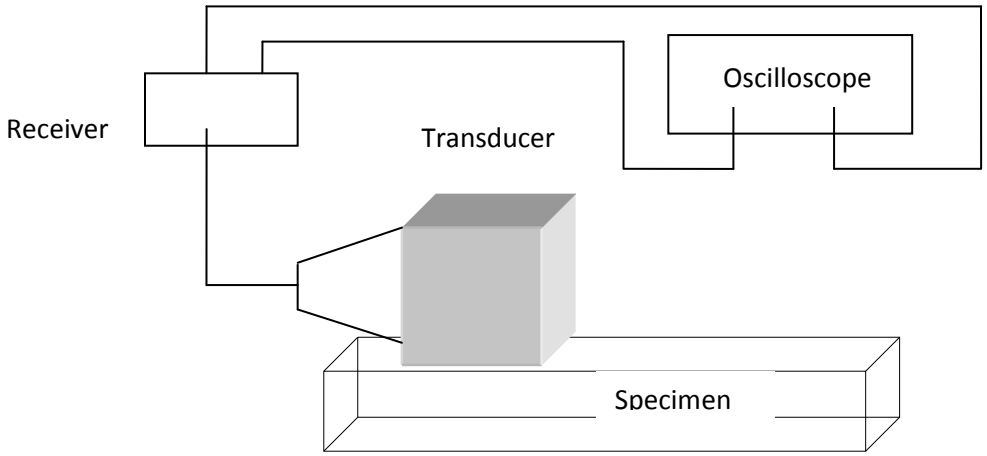

Figure 11 schematic of an ultrasonic pulse echo technique

Table 1 Results from Ultrasonic test and Archimedes principle (for determining density)

	Density (g/cm^3)	Poison's ratio	Shear modulars G (GPa)	Young's modulas E (GPa	Bulk modulus K (GPa)
mean	4,34	0,3246	43	114,6	109

3. Tensile Test

The test was done at Aerosud Aviation (PTY) LTD using Instron Tensile Tester (AS09) & Extensometer (AS648) at 25% humidity and 21ºC of temperature. 3 sintered Ti64 samples of gauge length 50 mm mean with of 12, 63 mm and mean thickness of 3,072 mm were tested. See tensile specimen figure 7. Table 2 below shows mean and standard deviation (S.D) results

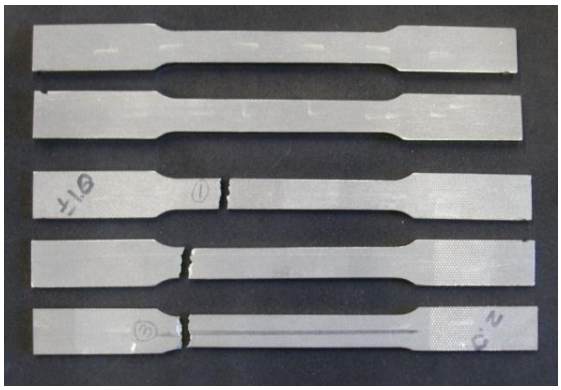

Figure 12 sintered Ti64 samples for tensile test

Table 2 Tensile Properties of Titanium Ti64test

	Max load (KN)	0,2% yield stress(MPa)	Ultimate Stress (MPa)
mean	38,207	839	983

V AVAILABLE DATA AND EXISTING GAPS AFTER PRELIMINARY TESTS

Table 3 Mechanical Property Data for Wrought (STA) and Laser Sintered Ti 64

PROPERTIES	**Ti 6Al V4 (STA)**	**Ti 6Al V4 DMLS (Polished)**
Densityg/cm3	4,49	4,34
2% proof stress (MPa)	800-1100	839
Ultimate strength (MPa)	900-1200	983
% elongation	13-16	11
%reduction	25	**?**
Young's modulus (GPa)	114	114,6
Shear modulus (GPa)	43	43
Shear strength (MPa)	760	**?**
Poisson's ratio	0,321	0.3246
Bulk modulus K (GPa)	106	109
Fracture toughness K1e (MPa. $m^{½}$)	33-110	**?**
Fatigue strength (smooth) (MPa)	700	**?**
Fatigue strength (notched) (MPa)	160	**?**

The empirical data shown in Table 3 above indicate similarities between wrought Titanium Ti64 and polished sintered Titanium Ti64. But there are still gaps that needed to be filled; nothing is known about the characteristics of unpolished Titanium Ti64. Not all medical implants can be polished for example lattice structure applied in the hip joint. The competitive advantage of DMLS is lost if the components cannot be used straight from the machine without applying any other post processes. Therefore there is a need as well to have empirical data on unpolished laser sintered Ti64.

VI DISCUSSION

The mechanical properties of materials are often limited by their imperfection due to either the design and/or manufacturing process. According to the investigations done, laser sintered Ti64 inherited imperfection in the form of voids. Even though they are not quantified; the voids are possible initiation sites for cracks hence more investigations must be done on the possible effects to the mechanical failure and or strength of sintered Ti64.

More investigations using highly resolution cameras must also be done as it is very important to exactly know the microstructure of sintered Titanium Ti64 built on DMLS EOSINT M270.

VII FURTHER WORK

Further work will focus on the tests such as tensile, creep, fatigue, fracture toughness, vibration in order to fill the gaps in Table 3 and once the empirical data is available, phenomenological models encompassing both polished and unpolished Ti64 will be developed.

VIII CONCLUSION

The preliminary results indicate similarities between solution treatment aged (STA) wrought Ti-6Al V4 and polished DMLS Ti-6Al V4. However, more work needs to be done before generalized trends are noted. The authors will conduct more tests to see if the similarities extend to other properties such as creep and fatigue.

IX ACKNOWLEDGEMENTS

The authors acknowledge the support of Mr. Kobus Dippenaar and his colleagues at Vaal University of Technology. Mr. Andries Uys of Aerosud Aviation (PTY) LTD and EOS GmbH.

X REFERENCES

1. EOS GmbH, " EOS Titanium and EOS Titanium Ti64 ELI for EOSINT M270 system, Titanium version", 05-07

2. Juha Kotila, Tatu Syvanen, Jouni Hanninen, Maria Latikka and Olli Nyrhila, "Direct Metal Laser Sintering in Rapid Manufacturing**",** Proceedings of PM2Tech Conference, Montreal, June 19-23, 2005

3. K. Abdel Ghany and S.F. Moustafa, "Comparison Between the Products of Four RPM Systems for Metals", Rapid Prototyping Journal, 2 December 2006, 86-94.

4. Y. NING, J.Y.H. FUH, Y. S WONG and H.T LOH, "An Intelligent Parameter Selection System for Direct Metal Laser Sintering Process", International Journal of Production Research, 2004, Vol. 42, No. 1, 183-199.

5. A. Simahi and H. Pohl "Effects of Laser Sintering Processing Parameters on the Microstructure and Densification of Iron Powder", Material and Engineering A 359, 2003 119-128.

6. C. Leyens and M.Peters, "Titanium and Titanium Alloys: Fundamentals and Applications", WILEY-VCH Verlag GmbH & Co., 2003

7. Yuehuei H. An Robert A. Draughn, "Mechanical testing of bone and the bone-implant interface", CRC Press, 2000

8. Marc Andre Meyers and Krishan Kumar Chawla, "Mechanical Behaviour of Materials", Cambridge University Press, 2009

ADDITIVE MANUFACTURING: CHARACTERIZATION OF TI-6AI-4V ALLOY INTENDED FOR BIOMEDICAL APPLICATION

M E Ramosoeu, H K Chikwanda, A S Bolokang, G Booysen and T N Ngonda
CUT and CSIR

Abstract

Direct Metal Laser Sintering (DMLS) is one of the new Laser Additive Manufacturing (LAM) techniques used for producing complex topology components mostly found in medical applications. The work presented in this paper focuses on metallographic analyses of laser sintered Ti-6Al-4V samples. The samples were built by DMLS process from EOSINT Ti-6Al-4V powder. They were then heat treated at temperatures of 1000 and 1100°C and subsequently either cooled with the furnace or water quenched. Slow cooling of Ti-6Al-4V samples from 1000 and 1100°C resulted in a microstructure constituted more by the alpha phase of lower hardness than the laser-sintered material. High hardness was obtained by water quenching. The water quenched evidenced martensitic transformation and high hardness when compared to furnace cooled samples.

Background

Ti-6Al-4V has found application as a bio-alloy and is widely used as an implant material due to its corrosion resistance and high strength to weight ratio [1]. The alloy has a two-phase (α-β) microstructure [2]. Titanium (Ti) undergoes α to β-transformation. Aluminium (Al~ 6 at. %) and vanadium (V~4 at. %) stabilise the alpha and the β-phases, respectively [2]. These phases can exist as lamellar, equi-axed or bimodal see Figure 1 below [3]. These microstructures have a strong influence on the mechanical behavior of the alloy.

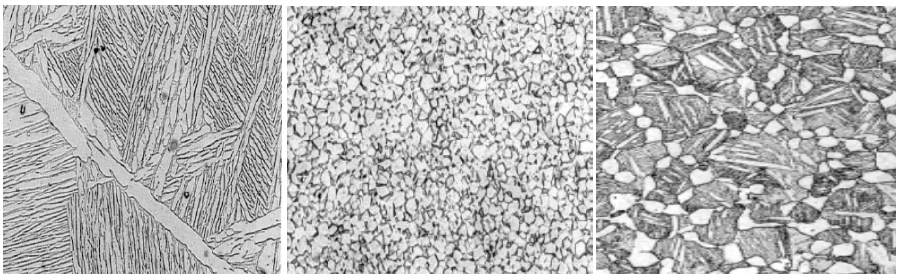

(a) (b) (c)

Figure 1: Microstructures of Ti-6Al-4V (a): an example of a lamellar structure; (b) an example of equi-axed structure; (c) an example of a bimodal structure [3].

Ti6Al4V components may be produced by a variety of methods such as casting [3], or sintering of powders among others [1]. There in turn, is a variety of powder methods such as injection moulding, hot and cold compaction and additive or direct laser sintering. Direct Metal Laser Sintering (DMLS) is one of the latest additive technologies used in manufacturing implants. This technology is capable of producing intricate customised biomaterial implants parts [1]. DMLS works by sintering very fine layers of metal powder layer by layer from the bottom up into a three dimensional component. Figure 2 below shows the schematic diagram of the DMLS process.

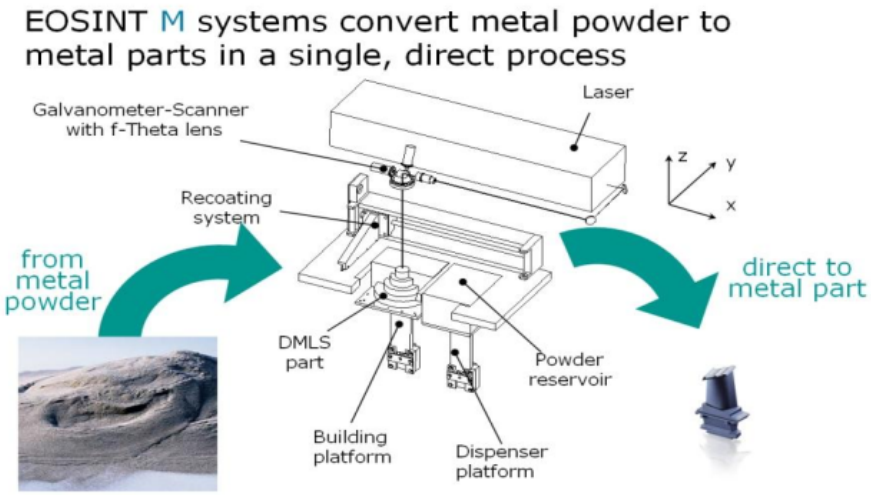

Figure 2: Schematic Diagram Showing DLMS Process on EOSINT M270 Machine [Courtesy to EOS GmbH]

The microstructure of Ti-6Al-4V alloy is influenced by the manufacturing process and /or any post-manufacturing process such as heat treatment. Figure 3 below illustrates pseudo-binary phase diagram of Ti-6Al-4V alloy at 4% per weight of vanadium together with a section on heating temperatures and cooling rates which results in different microstructures as shown.

Direct Metal Laser Sintering (DMLS) is capable of producing customised biomaterial implants parts using EOSINT M270 machine. The main purpose of this work to evaluate the microstructural characteristics of a direct laser sintered Ti-6Al-4V alloy after various heat treatments. An understanding of the relationship of microstructures and hardness is of high importance since it is a fundamental mechanical property of the material. Hardness test in most cases is regarded as a non-destructive test that often indicates tensile and wear properties of a material [6]. It is expected that the results will aid in creating phenomenological model that relates microstructure and mechanical properties in order to tailor-make, inspect, predict deformation and/or failure of the components build at Centre for Rapid Prototyping and Manufacturing (CRPM).

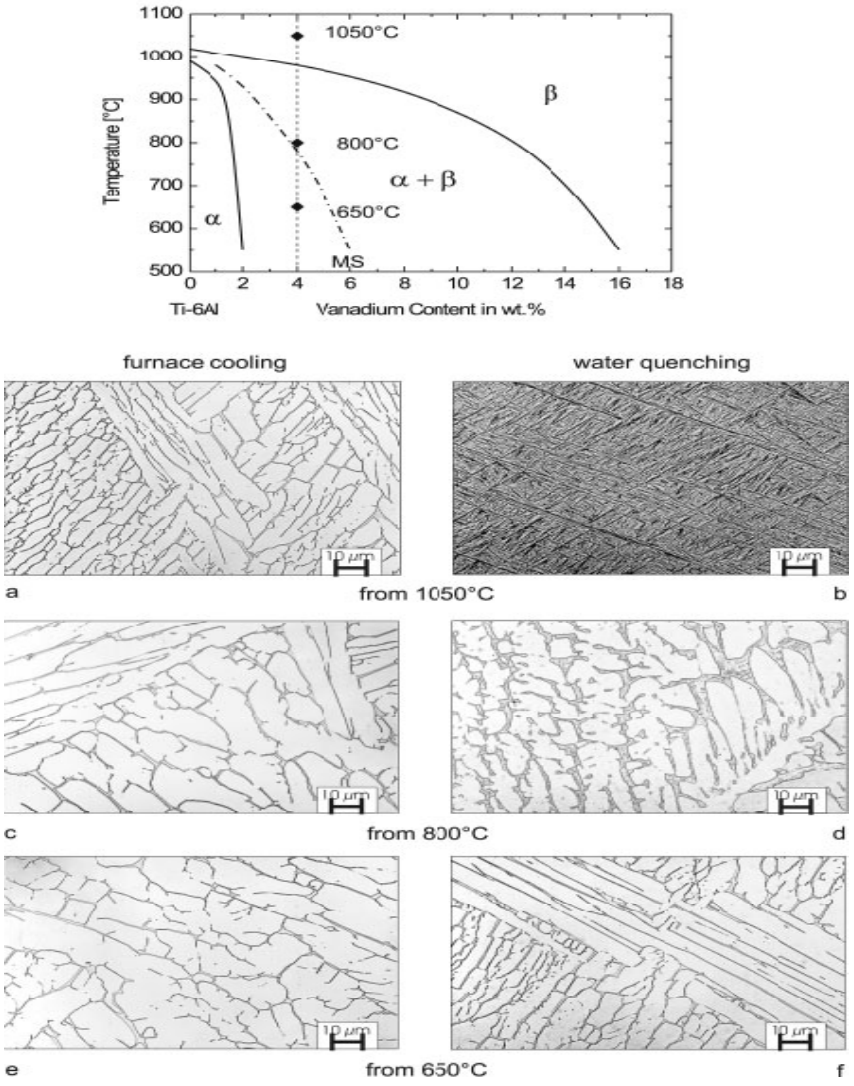

Figure 3: Schematic ternary phase diagram Ti-6Al-V (MS: martensite start temperature); microstructure of Ti-6Al-4V after slow cooling (50ºC/h) and water quenching from 1050ºC, 800ºC, and 650º[3].

Experimental Work

The Ti6Al4V alloy powder used for this work was supplied by EOS GmbH. Samples were manufactured at CRPM in Bloemfontein using the DMLS process on EOSINT M270 machine set at standard building parameters. The samples were built to represent the alloy in order to study the mechanical properties, but no specific implant was produced. Some of the directly sintered samples were heat treated at temperatures of 1000ºC and 1100ºC and others were left

untreated. All the heat treated samples were soaked at the set temperature for an hour, after which some were quenched in water and others were slowly cooled with the furnace. Soaking temperatures were selected based on pseudo-binary phase diagram (figure 3) whereby 1000ºC is just above the β-transus temperature while 1100ºC is a high temperature in the β phase-field [2-5]. A carbolite tube furnace was used. The heat treatments were done in an atmosphere with a protective argon gas. Samples were prepared for metallographic analyses using standard methods and etched using Keller's reagent. Metallographic analyses was performed on optical microscope (OM) and scanning electron microscope (SEM) to reveal phases of the microstructure on both the as-sintered and the heat treated samples. Macro hardness measurements were taken using a digital low load tester for Vickers.

Results and Discussions

The photomicrographs of microstructures captured from an OM are shown in figure 4 b, c, e, and f. There is evidence of martensite laths in water-quenched samples as compared to furnace-cooled samples. Slow cooling or equilibrium cooling rates result in the formation of more alpha (α) phase with a lamellae microstructure. This phase dominates as observed in figure 4 (b and e). Fast cooling, as performed by water quenching, results in a martensitic transformation in agreement with Filip et al studies [2]. By furnace cooling, materials follow equilibrium while fast cooling disturbs the thermodynamic path. The fast cooling processes such as quenching in either water or air induces metastable phases with good mechanical properties.

The SEM micrographs in figure 5 a, b, c, d and e show martensitic laths of the Ti-6Al-4V alloy in the as sintered and heat treated states, respectively. It follows that the cooling rate induced during laser sintering promoted the martensitic transformation. This implies that the cooling was fast enough (air quenching) to induce the martensitic transformation. Since the process involves melting of thin layers approximately 10 μm, high cooling rates enables martensitic transformation. Subsequent deposition of layers also provide the stress release on previously deposited layers and this is evidenced by the varying contrast in figure 5 a. Titanium metal show a polymorphic transformation from low temperature alpha to high temperature beta phase. In order to exploit this behavior and to improve the mechanical properties, aluminium (Al) and vanadium (V) are added. It has been found that Al in 6 wt% stabilized the low temperature while 4 wt% V promote the existence of the high temperature beta phase. Among other properties Al increase chances of martensite formation while V is responsible for corrosion resistance and strength. It then follow that for beta alloys, Al amount will be decreased while beta-stabilizing elements such as V, and Nb are added.

Macro Hardness Results and Optical Microscope Pictures of Direct Laser Sintered Ti-6al-4v Samples

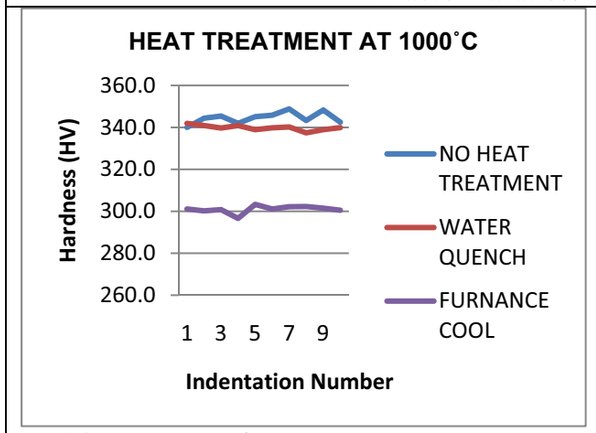

(a) Macro Hardness 1000ºC

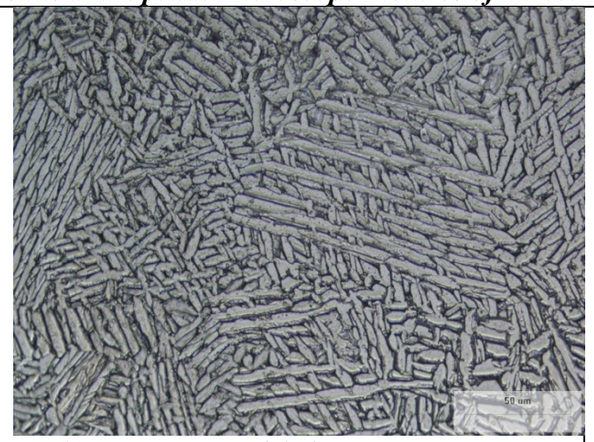

(b) HT at 1000ºC/1hr/ FC

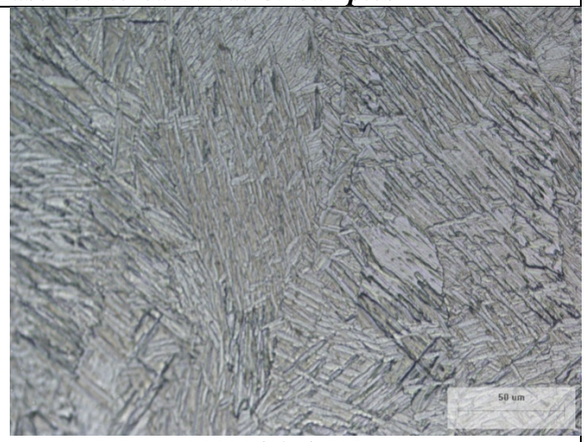

(c) HT at 1000ºC/1hr/ WQ

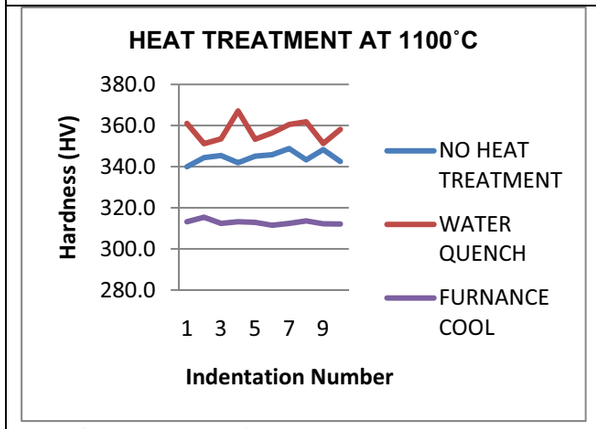

(d) Macro Hardness at 1100ºC

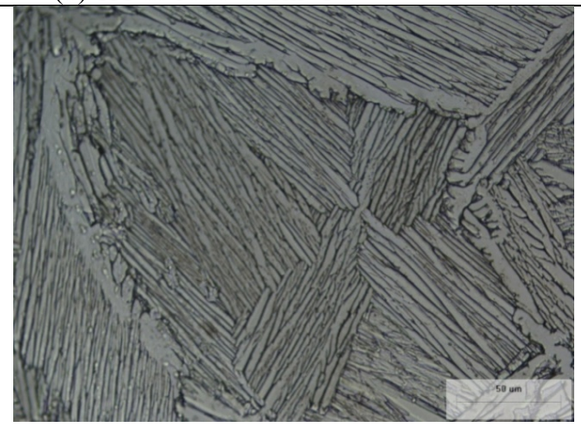

(e) HT at 1100ºC/1hr/ FC

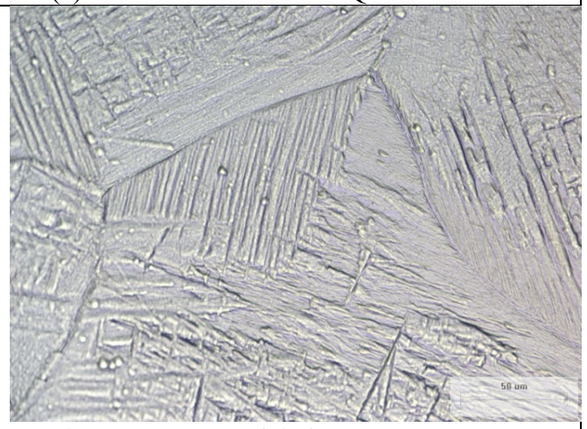

(f) HT at 1100ºC/1hr/ WQ

Figure 4: Optical Microscope of Both Un-Heat Treated and Heat Treated Direct Laser Sintered Ti-6Al-4V Samples

SEM micrograph of Direct Laser Sintered Ti-6Al-4V Samples

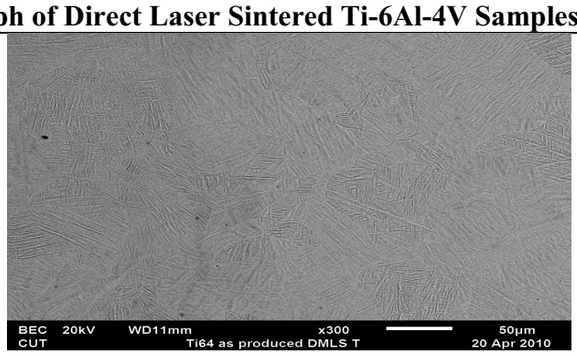

(a) No heat treatment

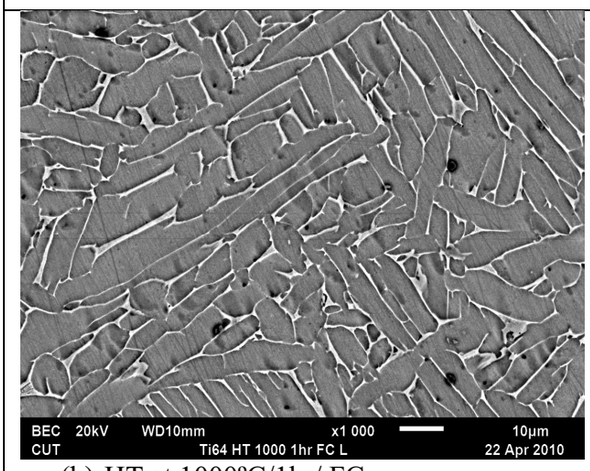

(b) HT at 1000ºC/1hr/ FC

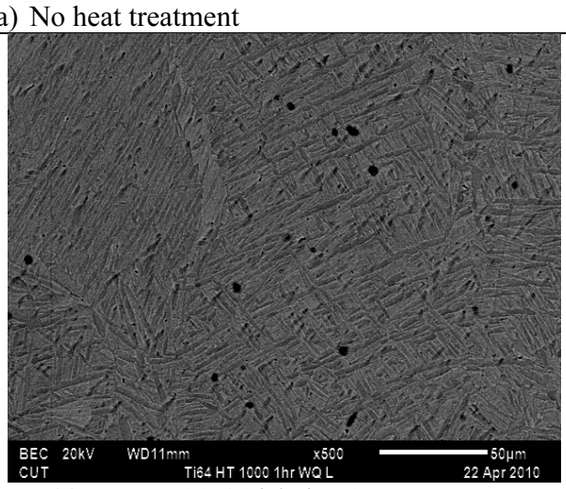

(c) HT at 1000ºC/1hr/ WQ

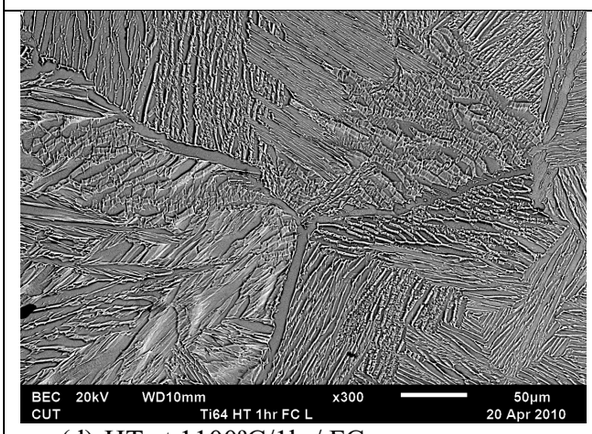

(d) HT at 1100ºC/1hr/ FC

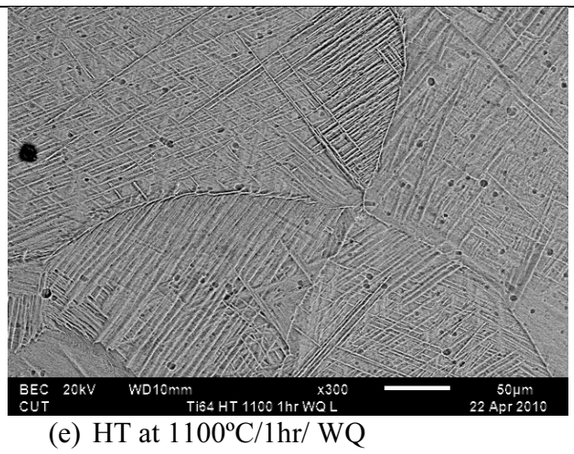

(e) HT at 1100ºC/1hr/ WQ

Figure 5: SEM micrograph of both un-heat treated and heat-treated Direct Laser Sintered Ti-6Al-4V Samples

An average hardness of 345 HV_{10} was obtained as laser-sintered was comparable to the hardness of the as-casted Ti-6Al-4V alloy after solution treated at 800ºC/1hr/water quenched as reported in literature [7]. The comparable hardness values suggest that the additive process by direct laser

sintering has achieved competitive hardness value both the powder sintering and the sintered part quench-treatment.

Volume fraction of α and β phase can be predicted by the hardness values presented in table 1. It is documented that β possesses high hardness than α-phase [2-5]. Water quenched samples (from 1000 and 1100^{o}C) are harder than furnace cooled, but not entirely surpassing the laser sintered material. Quenching from 1000 and 1100^{o}C above β-transus temperatures resulted in harder alloy with 339 and 357 hardness, respectively, although the former is softer than the latter. The amount of beta phase trapped during quenching increase the hardness. Therefore, the presence of α/β beta lamellae is higher than in furnace-cooled samples. The beta transus temperatature is ~1000^{o}C, hence quenching at this temperature may induce the alpha phase since the sample is slightly exposed to the atmosphere before the operation. It should be noted that on pure Ti the beta transus occur at 882^{o}C indicating that in Ti6Al4V, Al has increased this temperature. At 1100^{o}C, the alloy has completely transformed to beta phase, hence higher residual beta in martesitic structure after quenching. The furnace cooled samples from 1000 and 1100^{o}C have 301 and 312 HV_{10} and are softer than as-sintered samples due to high alpha phase with small amount of intergranular beta. In this instance the transformation β→α follow a thermodynamic route.

***Table 1**: The influence of heat treatment on the hardness of the Ti-6Al-4V alloy*

Heat treatment	As-Sintered	1000 ºC/ FC	1000 ºC/ WQ	1100 ºC/ FC	1100 ºC/ WQ
Hardness HV_{10} (average)	345	301	339	312	357

Conclusion

Slow cooling of Ti-6Al-4V samples from 1000ºC and 1100^{o}C resulted in more alpha than beta phases of lower hardness than untreated (as-sintered) material. The highest hardness was obtained by water quenching hence the hardness increases with higher β-phase in the alloy. Quenching from 1000ºC allowed small fraction of alpha phase, probably due to decrease in sample temperature prior to cooling process. The samples quenched from 1100^{o}C illustrated martensitic structure as well as higher hardness than annealed samples.

Further Work

The authors seek to create a phenomenological model that relates to microstructure and mechanical properties in order to tailor-make, inspect, predict deformation and/or failure of Ti6Al4V components built at the CRPM. Therefore other relations between microstructure and mechanical properties such as tensile properties (yield strength, ductility), fracture toughness, low cycles fatigue as well as creep will be established.

Acknowledgements

The authors express gratitude the CRPM for supplying Titanium samples, especially to Mr. J. Els (CRPM) for the hard work in building the samples. It has been a great pleasure collaborating with CSIR team. Miss G. Lesejane and Dr. S. Chikosha (CSIR) are acknowledged for assistance with metallographic analysis and hardness testing.

References

1. EOS GmgH, EOS Titanium and EOS Titanium Ti64 ELI for EOSINT M270 system, Titanium version, 05-07

2. Filip R, Kubiak K, Ziaja W, Sieniawski J The effect of microstructure on mechanical proerties of two-phase titanium alloys, Journal of Materials Processing and Technology, 133:84 2003

3. C. Leyens and M.Peters, Titanium and Titanium Alloys: Fundamentals and Applications, WILEY-VCH Verlag GmbH & Co., 2003

4. Marc Andre Meyers and Krishan Kumar Chawla, Mechanical Behaviour of Materials, Cambridge University Press, 2009

5. Gerhard Welsch, Rodney Boyer, E W Coolings, Materials Properties Handbook; Titanium alloys, Technology and Engineering, 1994, pp 483 – 641

6. Kao Y.L, Tu G.C, Huang C.A, Liu T.T A study on the hardness variation of α- and β-pure titanium with different grain sizes, Materials and Engineering A, 398, 93-98, 2005

The Author

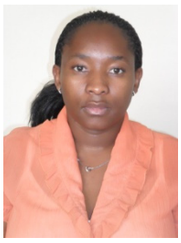

Makhabo Ellen Ramosoeu, Central University of Technology, (CUT)

I have registered with Engineering Council of South Africa (ECSA) as a candidate engineering technologist. I worked for Product Development Technology Station (PDTS) CUT from 2006 to 2008 then changed to the school of mechanical engineering where I am presently a junior lecturer. I am currently pursuing M-tech in mechanical engineering. My research work focuses on characterization of Ti-6Al-4V components particularly for biomedical application. I specialize on Ti-6Al-4V components that are manufactured by Direct Metal Laser Sintering (DMLS) process on EOSINT M270 machine. The work done so far has been well received and was presented at RAPDASA 2009 and CUT 2010 conferences. I was attached for two weeks at CSIR in the department of materials science and manufacturing under supervision of Dr. Hilda Chikwanda whereby I did a metallographic analysis work.

MECHANICAL PROPERTIES OF DIRECT LASER SINTERED Ti-6Al-V4

M K E Ramosoeu, G Booysen, T N Ngonda
CUT, Bloemfontein, Free state, South Africa

H K Chikwanda
CSIR, Pretoria, Gauteng, South Africa

Keywords: Direct metal laser sintering, Ti-6Al-V4, Laser-based additive manufacturing, Mechanical Properties, Heat treatment

Abstract

Mechanical properties of samples made by the Laser-based Additive Manufacturing technique have been determined. The specimens were manufactured using a direct metal laser sintering EOSINT M270 machine. All samples were built in a vertical orientation. Property tests included tensile, hardness, determination of elastic constants and metallographic examinations. Some porosity was observed. Elastic constants of the laser sintered samples were similar to those of solution treated and aged wrought Ti-6Al-V4. However, the ductility showed significant differences. As sintered samples were brittle: with average elongation of 2.6% and area reduction of 3.51%. Annealing increased elongation to 18% and area reduction to 33.39%. Annealing conversely reduced yield strength by 19.89% and ultimate tensile strength was reduced by 23.66 %.

Introduction

Direct metal laser sintering (DMLS) is a Laser-based Additive Manufacturing technique used to fabricate biomedical and aerospace parts. Knowledge of mechanical properties of DMLS Ti-6Al-4V is currently limited. The Center for Rapid Prototyping and Manufacturing (CRPM) uses DMLS process to manufacture parts from EOSINT Ti-6Al-4V powder. This technology is capable of producing intricate customised biomaterial implants parts [1]. DMLS works by sintering very fine layers of metal powder layer by layer from the bottom up into a three dimensional component [1,2]. Titanium alloys are generally classified into three main categories; Alpha (α) alloys, Beta (β) alloys and alpha + beta (α + β) alloys. Ti-6Al-V4 is an (α + β) alloy with Aluminum as the alpha stabilizer and Vanadium as the beta stabilizer [3, 4]. Titanium alloys have received most attention in recent times this is due to inherent properties of titanium that are very attractive to orthopaedic surgery applications. High chemical reactivity has delayed the development of titanium due to the difficulty associated with melting, casting into ingots and hot working of this metal [3,4]. Ti-6Al-V4 offers a combination of high strength, lightweight and resistance to corrosion. Mechanical properties depend on the phases present in the material. Changing the physical properties such as grain size, grain shape, grain texture and/or arrangement of the phases strongly influences mechanical properties [6]. Ti-6Al-V4 can be heat treated to achieve desired mechanical properties. It is through heat treatment that two famously known microstructures that exists in (α + β) type can be produced and altered. In the Ti 6AL-4V microstructure the size of alpha colony plays a major role in controlling the maximum dislocation slip length. Thus, the bigger the size of alpha colony, the softer the material can be as

alpha colony is the soft phase [3, 4, 5, and 7]. The softer the material can be the more ductile it becomes.

The Need for Characterization of DMLS Ti-6Al-4V

Ti-6Al-V4 is highly recommended as a structural material and has been determined to possess high specific strength [3, 5]. During application, titanium structures are exposed to different forms of loading which can lead to material failure. For example, fracture behavior which could be in the form of fatigue, thus failure due to cyclic loading and what can happen is; where there is a void there is a possibility for initiation of cracks, with time, followed by crack growth, then the material will eventually fail. However, information regarding mechanical properties of this titanium alloy is still limited. The need for CRPM to acquire knowledge of the fundamental characteristics of laser sintered Ti-6Al-4V under different mechanical loading is ultimately for these reasons: To provide sustainable empirical data to CRPM in order to know the accuracy, behaviour and performance of Ti-6Al-V4 built on DMLS EOSINT M270 sintering machine. To create phenomenological model that relates the microstructure and mechanical properties in order to inspect, predict deformation and/or failure of the components built.

Experimental Procedures

Ti-6Al-4V samples were manufactured at CRPM in Bloemfontein using the DMLS process on EOSINT M270 machine set at standard building parameters according to the manufacturer of the machine. All samples were built in a vertical orientation. They were built in order to study the mechanical properties. EOSINT Ti-6Al-4V powder was submitted for characterization in order to study its properties prior to using it in experimental work. Powder particle size distribution analyses were done using a Microtac Bluewave particle analyzer. The powder morphological features were studied using a Leica optical microscope and a LEO 1525 Field-Emission Scanning Electron Microscope (FE-SEM) coupled with a Robinson Backscatter Electron Detector (RBSD). EDX analyses were performed using SEM. To study the phases present and their evolution, a Phillips PW 1830 X-ray diffraction (XRD) machine fitted with Cu Kα radiation was used. A step size of 0.02 was used to scan the samples from 20 to 90 (2θ) Elastic constants of specimens were measured according to ASTM E494-48 using an ultrasonic pulse echo technique on Krautkramer USIP12 machine. Density was measured based on Archimedes principle and the liquid used was water at room temperature. Tension tests were performed according to ASTM 8 in order to evaluate tensile properties of specimen such as strength and ductility. Standard tensile specimens (both as-sintered and heat-treated) were mounted in a instron 50 kN tension testing machine. Specimens were pulled at constant rate until fracture occurs. The tensile test measured the load (force) against the elongation (displacement) and then converted to an engineering stress-strain curve for determining valuable tensile properties. Heat treatment was employed because the as-sintered specimens were brittle. Heat treatments were conducted, as indicated on table 1. The temperature selected was 1000 ^{o}C which is just below the tranus temperature of 1050 ^{o}C. Temperature selection was done using a schematic ternary phase diagram (figure 1). To minimize contamination during the heat treatment processes, a vacuum furnace was used. Titanium has a strong tendency to react with oxygen and nitrogen [3, 4]. Specimens were also cleaned using methanol, in an ultrasonic cleaner in order to get rid of all impurities such as oil.

Table 1 Post heat treatment conditions applied to second experiment

Temperature (^{o}C)	Soaking time (Hrs)	Cooling media and time taken
1000	1	Furnace cool/ 4 hrs
1000	1	Furnace cool/ 34 hrs

After heat treatment, specimens were prepared for metallographic analyses using standard methods. They were subsequently etched using Keller's reagent. Optical Microscopy (OM) and Scanning Electron Microscopy (SEM) were performed to reveal microstructures and phases in both the as-sintered and the heat treated samples. Macro hardness measurements were taken using a digital low load tester for Vickers.

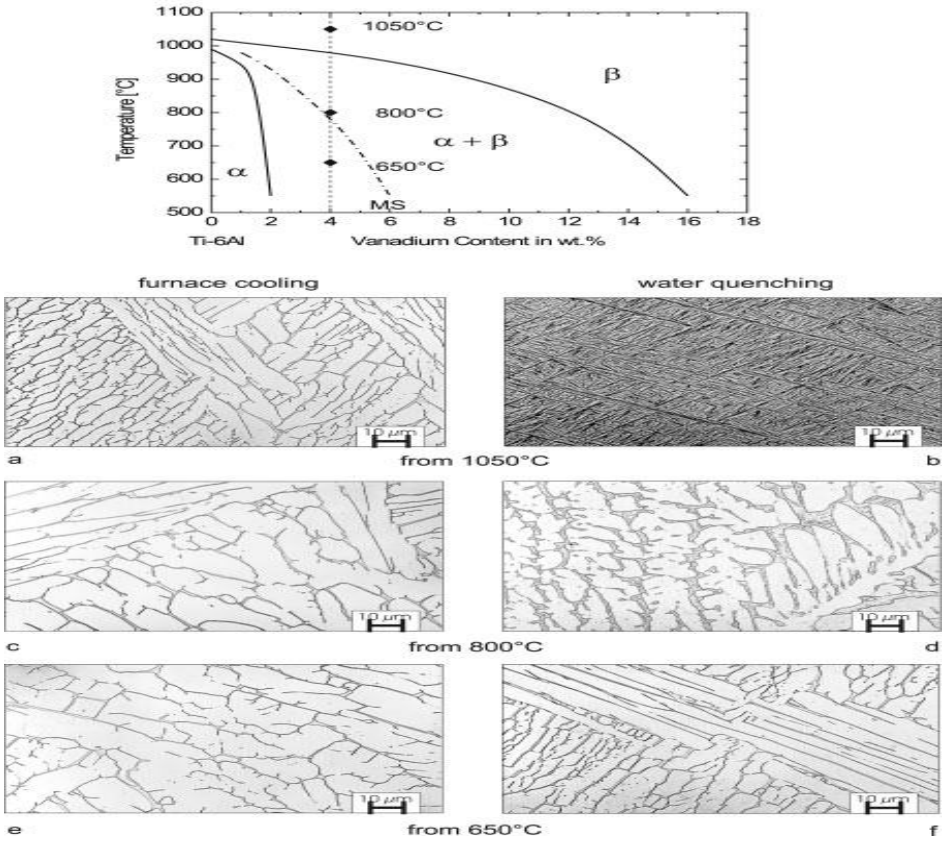

Figure 1: Schematic ternary phase diagram Ti-6Al-V (MS: martensite start temperature);microstructure of Ti-6Al-4V after slow cooling (50ºC/h) and water quenching from 1050ºC, 800ºC, and 650º[3].

Results and Discussions

Characterization of EOSINT Ti-6Al-4V Powder

The morphology of the EOSINT Ti-6Al-4V powder particles were found to be spherical in shape (figure 2). This is typical of powders produced by the atomization process [3, 4, 5].

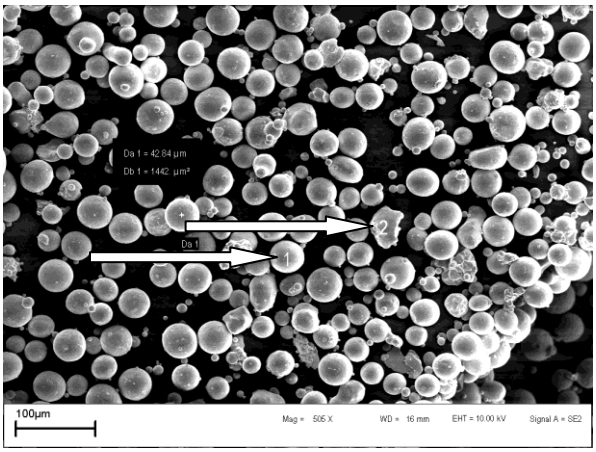

Figure 2 SEM-EDX Spot analyses

Figure 3 shows the powder particle size distribution. The average particle sizes obtained were: D10 - 22.20 µm D50 - 32.64 µm and D90 -48.74 µm.

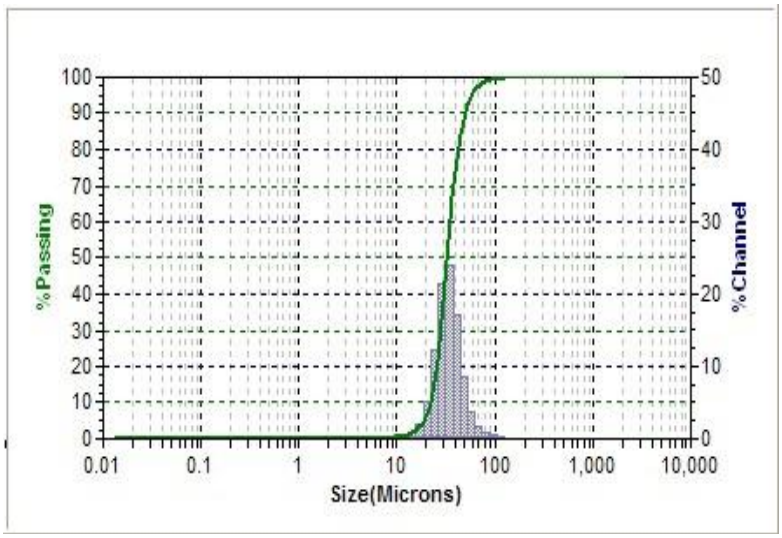

Figure 3 Particle size distribution of EOSINT Ti-6Al-4V powder

SEM-EDX spot analyses results are presented in table 2. The powder had about 2,5 % carbon. The carbon was picked up from the graphite tape that was used to hold the powders. Titanium, aluminium and vanadium were in their expected quantities. Figure 3 presents the microstructural and the morphological features of the starting powders. XRD analyses results for the powders are shown in figure 4. Major phases identified were the alpha (⇨) and alpha +beta (⇨+⇦) phases. The alloy powder was thus, confirmed to be Ti-6Al-4V.

Table 2 SEM-EDX Spot analyses

Spectrum	C	Al	Ti	V
spot 1	2.44	5.75	88.09	3.71
spot 2	2.62	5.52	87.67	4.19

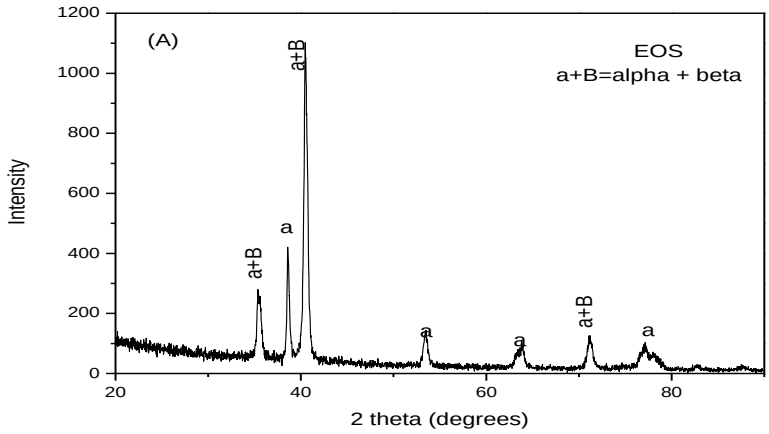

Figure 4 XRD pattern of EOSINT Ti-6Al-4V powder

Characterization results of DMLS Ti-6Al-4V Specimens

Elastic Constants DMLS Ti-6Al-4V Specimens

Elastic constants of specimens obtained are shown in table 3. They are similar to those of solution treatment aged (STA) wrought Ti-6Al-4V. The density of these samples was determined to be 4,34 g/cm^3. This value is comparable to that of the STA (4,349 g/cm^3) which shows that the DMLS process produces dense parts hence there is no need for post sintering densification.

Table 3 Elastic constants of the DMLS TI-6AL-4V SPECIMENS

Elastic constant	DMLS Ti6Al4V	STA) Wrought Ti-6Al-V4 *[www.cartech.com]*
Poison's Ratio	0,323	0,321
Shear Modulus G (GPa)	43.57	43
Young's Modulus E (GPa	115.0	114
Bulk Modulus K (GPa	108	106

Metallographic Analyses

Microstructures studied using OM and SEM revealed presence fabrication imperfections such as voids and/or inclusions even though they are not quantified. Figure 5a shows islands martensitic plates. These have also been previously reported to be observed in a uniform alpha case [3, 4, 5]. Fine plates of martensite with an average lath size in the nano-range (known as alpha prime) are clearly seen in SEM photomicrograph in figure 5b. These fine microstructural features are consider to be due to the high cooling rates experienced during laser sintering. During DMLS process, layers of powder are heated up to melting temperatures by the laser and then quickly cooled. As more powder layers are added and immediately sintered the resulting part/component has an as quenched microstructure. Therefore, the DMLS process results in a martensitic non-equilibrium structure. Figures 6 and 7 show that heat treating the samples at 1000°C and cooling them at different rates coarsens the obtained microstructures. This is expected. Coarse alpha phase and grain boundaries decorated with beta phase are clearly visible.

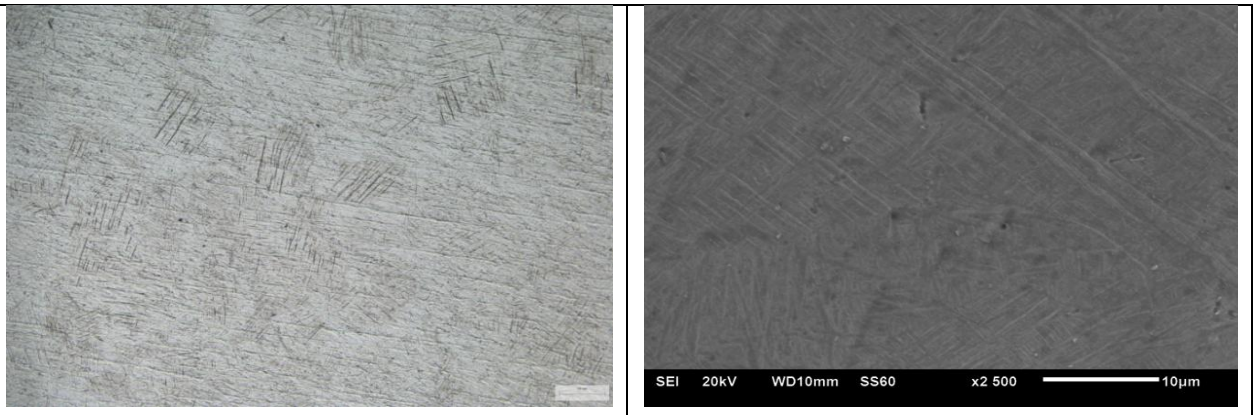

a) Optical Microscopy b) SEM

Figure 5: OM and SEM Photomicrographs of as-sintered DMLS Ti-6Al-4V specimens

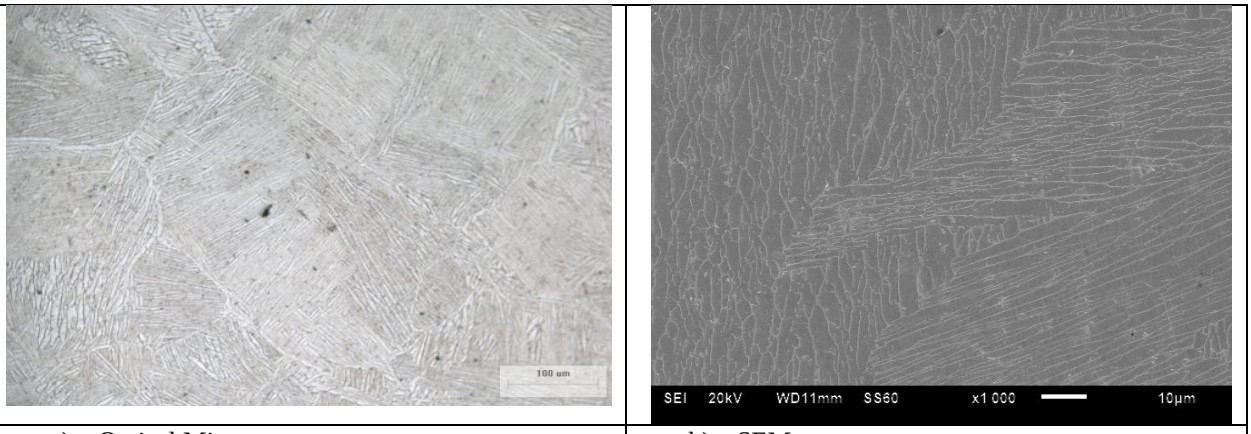

a) Optical Microscopy b) SEM

Figure 6: OM and SEM Photomicrographs of heat treated samples (1000°C/1hr/ FC4hrs)

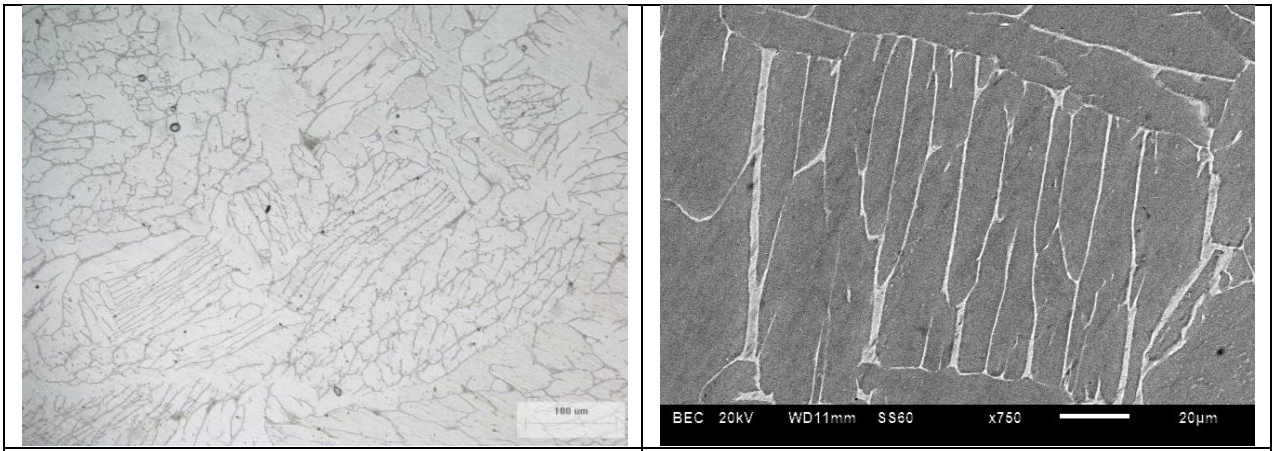

a) Optical Microscopy b) SEM

Figure 7: OM and SEM Photomicrographs of heat treated specimens (1000C/1hr/ FC34hrs)

EDX Analyses

The EDX results of the as-sintered and the samples heat treated at 1000ºC for 1 hour and the furnace cooled for 4hrs are presented in figures 8 and 9 respectively. Those for the samples heat treated at 1000ºC for 1 hour and then furnace cooled for 34hrs are in figure 10. The EDX results confirm the Ti6Al4V composition. This indicates that there is basically no significant contamination during the DMLS process,

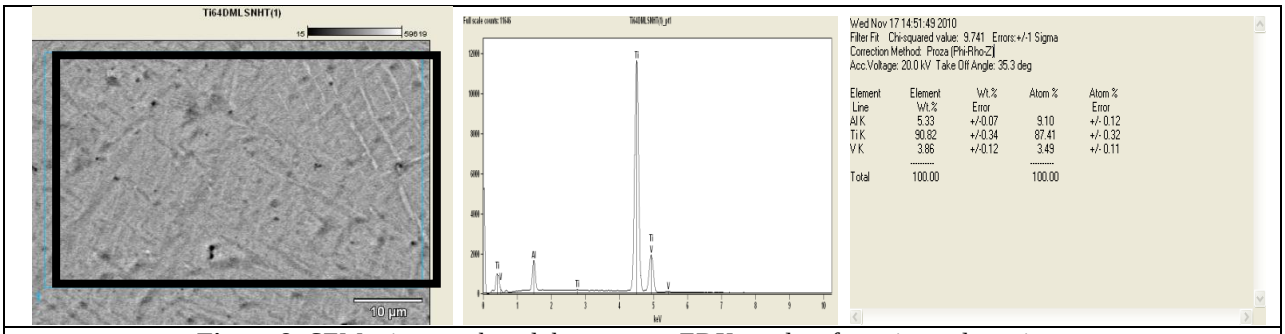

Figure 8: SEM micrograph and the average EDX results of as-sintered specimens

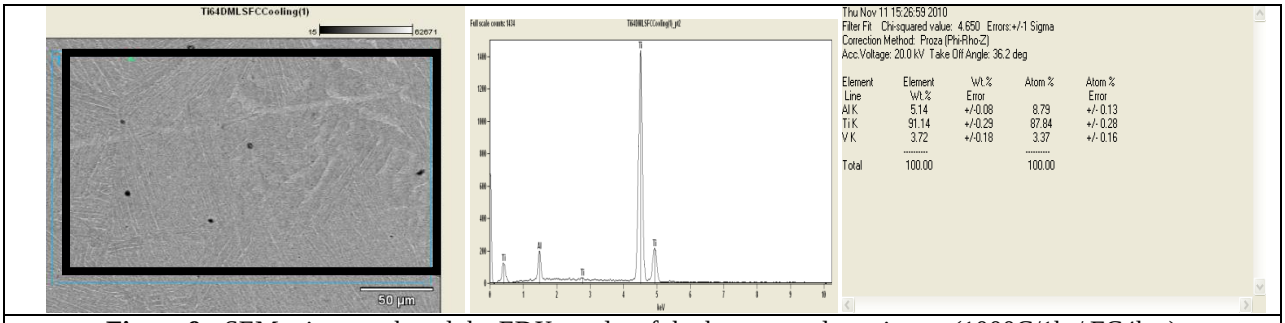

Figure 9: SEM micrograph and the EDX results of the heat treated specimens (1000C/1hr/ FC4hrs)

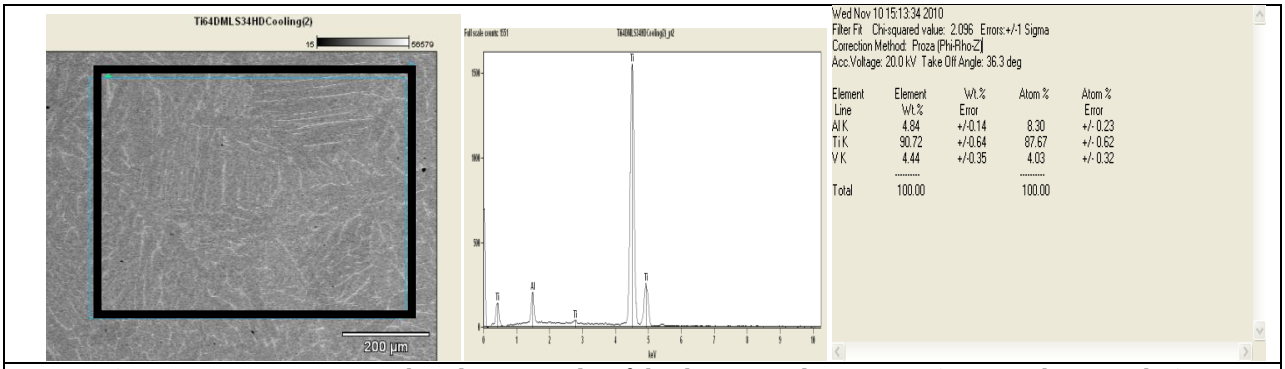

Figure 10: SEM micrograph and EDX results of the heat treated specimens (1000ºC/1hr/ FC 34hrs)

Macro Hardness

Macro Hardness measurements obtained are in table 4. The hardness value of 344.2 HV_{10} obtained for the as-sintered samples is close to that of solution heat treated (STA) wrought Ti-6Al-4V (300-400). This hardness measure can be used to predict some of mechanical properties such as wear, tensile strength [6]. A hardness of 304 HV_{10} was obtained for the

specimens that were heat treated at 1000ºC, held for 1 hour and the furnace cooled for 4 hours while that for the specimens furnace cooled for 34 hours was 296HV_{10}. These values relate to the coarsening observed.

Table 4: The influence of heat treatment on the hardness of the Ti-6Al-4V alloy

Heat treatment	As-Sintered	1000ºC/1hr/ FC4hrs	1000ºC/1hr/ FC34hrs
Hardness HV_{10} (average)	344.2	304	296

Tensile Properties

Tensile properties are shown in table 5. Yield stress (at 0.2% offset) of 1004.54 MPa and ultimate stress of 1190.26 MPa were found for the as-sintered specimens. Elongation and area reduction of 2, 6 and 3, 51% respectively were also found as both are measures of material ductility. Due to the fact that both percent elongation and area reduction are low, it is confirmed that DMLS process produces brittle parts. Thus the parts can fail without warning. However, biomedical implants needed to indicate failure hence high ductility parts are required. It is then logical to assume that a post DMLS heat treatment be conducted to improve ductility. The effect of the heat treatment can be seen on the tensile properties of the specimens. Heat treatment at 1000ºC/1hr/ FC4hrs improved the ductility from 2.61 to 12% elongation and even to a higher value of 18% when cooling time was increased to 34 hours. Area reduction increased from 3.51 to 25.95% at 1000ºC/1hr/ FC 4hrs treatment and more to 33.39% at 34 hours cooling. Conversely, both yield and ultimate strength decrease from 1004 to 826.87 and further to 804.77MPa; 1140 to 945.85 and 908.63 MPa, respectively.

The elastic constants, tensile and hardness results indicate similarities between solution treatment aged (STA) wrought Ti-6Al-V4 and unpolished DMLS Ti-6Al-V4 see table 5 below. Not all medical implants can be polished for example lattice structure applied in the hip joint. However, more work needs to be done before generalized trends are noted. The authors will conduct more tests to see if the similarities extend to other properties such as fracture toughness, creep and fatigue.

Table 5 Mechanical Property Data for Wrought (STA) and Unpolished DMLS Ti-6Al-V4

Properties	(STA) Wrought Ti-6Al-V4 [8]	DMLS Ti-6Al-V4 [as-sintered]	DMLS Ti-6Al-V4 [HT at 1000ºC/1hr/ FC 4hrs]	DMLS Ti-6Al-V4 [HT at 1000ºC/1hr/ FC 34hrs]
Tensile Properties				
2% Proof Stress (MPa)	800-1100	1004.54	826.87	804.77
Ultimate Tensile Strength (MPa)	900-1200	1190.26	945.85	908.63
% Elongation	13-16	2.6	12.67	18.11
% Area Reduction	20-25	3.51	25.94	33.39

Conclusions and Further work

The mechanical properties of materials are often limited by their imperfection due to either the design and/or manufacturing process. According to the investigations done, DMLS Ti-6Al-4V specimens inherited imperfections in the form of voids. Even though they are not quantified; the voids are possible initiation sites for cracks hence more investigations must be done on the possible effects to the mechanical failure and or strength of DMLS Ti-6Al-4V. It is

evident that increasing ductility decreases hardness of parts produced by DMLS process. Tensile results confirm the improvement of the ductility. Thus the parts produced by DMLS process must be heat treated when ever ductility is an important factor to the end user. Further work will focus on fracture toughness, fatigue and creep strength.

Acknowledgments

The authors express gratitude the CRPM for supplying Titanium samples, especially to Mr. J. Els (CRPM) for the hard work in building the samples. It has been a great pleasure collaborating with CSIR team. Miss G. Lesejane and Dr. S. Chikosha (CSIR) are acknowledged for assistance with metallographic analysis and hardness testing and also Mr. C. McDuling for his assistance in mechanical testing.

References

[1] J. -. Kruth, M. C. Leu and T. Nakagawa, Progress in Additive Manufacturing and Rapid Prototyping, *CIRP Ann. Manuf. Technol.*, vol. 47, p. 525-540, 1998.

[2] Y. NING, J.Y.H. FUH, Y. S WONG and H.T LOH, An Intelligent Parameter Selection System for Direct Metal Laser Sintering Process, International Journal of Production Research, 2004, Vol. 42, No. 1, p183-199.

[3] C. Leyens and M.Peters, Titanium and Titanium Alloys: Fundamentals and Applications, WILEY-VCH, 2003, p 1-35

[4] G. Welsch el al., Materials Properties Handbook Titanium alloys, Technology and Engineering, 1994, p 483 – 641

[5] R. Filip, K. Kubiak, W. Ziaja and J. Sieniawski, The effect of microstructure on the mechanical properties of two-phase titanium alloys, J. *Mater. Process. Technol.*, vol. 133, p 84-89, 2/1, 2003.

[6] Y. L. Kao, G. C. Tu, C. A. Huang and T. T. Liu, A study on the hardness variation of α- and β-pure titanium with different grain sizes, *Materials Science and Engineering A*, vol. 398, p. 93-98, 5/25, 2005.

[7] S. K. Kar, Modeling of mechanical properties in alpha/beta-titanium alloys, 2005.

[8] http://cartech.ides.com/datasheet.aspx?i=101&E=269 Technical Datasheet: Titanium Alloy Ti 6Al-4V accessed January 10 2011